Aus dem Deutschen Krebsforschungszentrum Heidelberg
(Wissenschaftlicher Stiftungsvorstand: Prof. Dr. med. Michael Baumann)

Abteilung für Toxikologie und Chemotherapie
(Priv. -Doz. Dr. Hassan Adwan)

Gene expression of human LS174T colorectal cancer cells implanted into the large bowel or liver of nude rats.

Inauguraldissertation
zur Erlangung des Doktor scientiarum humanarum (Dr. sc. hum.)

an der
Medizinischen Fakultät Heidelberg
der
Ruprecht-Karls-Universität

vorgelegt von
Seyedeh Maryam Kazemi

aus
Shahrekord-Iran

2024

Dekan: Prof. Dr. Michael Boutros

Doktorvater: Priv. -Doz. Dr. Hassan Adwan

TO MY PARENTS: MOJGAN AND MAHDI

TO MY SISTER: MAHSHAD

TO MY DEAREST HUSBAND: AMIN

TABLE OF CONTENTS

ABBREVIATIONS

ACS	American Cancer Society
APC	Adenomatous polyposis coli protein
BRAF	V-raf murine sarcoma viral oncogene homolog B1
CAFs	Cancer-Associated Fibroblasts
CIN	Chromosome instability
CIMP	CpG island methylator phenotype
CO2	Carbon dioxide
CRC	Colorectal cancer
DNA	Deoxyribonucleic acid
ECM	Extracellular matrix components
EDTA	Ethylenediaminetetraacetic acid
EGTA	Ethylene Glycol-Bis (β-Aminoethyl Ether)-N,N,N',N'-Tetraacetic Acid
EpCAM	Epithelial Cell Adhesion Molecule
FACS	Fluorescence-activated cell sorter
FCS	Fetal calf serum
FITC	Fluorescein Isothiocyanate
GFP	Green Fluorescent Protein
GLOBOCAN	Global Cancer Observatory
HK	Housekeeping gene
HPLC	High Performance Liquid Chromatography
IARC	International Agency for Research on Cancer
KRAS / Ki-ras2	Kirsten rat sarcoma viral oncogene homolog
IPA	Ingenuity Pathway Analysis
LOH	Loss of Heterozygosity
MAD	Median Absolute Deviation

MAPK	Mitogen-Activated Protein Kinase
MRI	Magnetic Resonance Imaging
MSI	Microsatellite Instability
NK	Natural killer cell
ORF	Open reading frame
PAG	Polyacrylamide Gel
PBS	Phosphate-buffered saline
PBCR	Population-Based Cancer Registries
PCA	Principal component analysis
PCR	Polymerase chain reaction
PET	Positron Emission Tomography
PMT	Photomultiplier Tube
PI3K	Phosphoinositide 3-Kinase
PI3KCA	Phosphatidylinositol-4,5-Bisphosphate 3-Kinase Catalytic Subunit Alpha
RAB15	Member of the RAB GTPase family
RNA	Ribonucleic acid
RISC	RNA-Induced Silencing Complex
RPLP19	Ribosomal Protein L19
RT	Room temperature
RT-PCR	Reverse Transcription Polymerase Chain Reaction
SDS	Sodium dodecyl sulfate
SMAD	SMA (small worm phenotype) and MAD family (Mothers Against Decapentaplegic)
SPF	Specific Pathogen-Free
TAE	Tris-Acetate, EDTA
TAL	Transcription activator-like
TBS	Tris-buffered saline

TBS-T	TBS with 0.05% Tween-20
TEMED	Tetramethyl ethylenediamine
TGF-β	Transforming Growth Factor-beta
USA	United States of America
UTR	Untranslated region
WNT	Wingless Related Integration site
XRS	X-ray Radiation System
XTT	2,3-Bis-(2-methoxy-4-nitro-5-sulfophenyl)-2H-tetrazolium-5-carboxanilide

1. INTRODUCTION

1.1 Cancer

Current statistics shows that cancer will be the primary cause of death worldwide with cancer cases projected to hit 16.3 million fatalities by 2040 (Sung et al., 2021) (Ferlay et al., 2021). These reports are summarized by the International Agency for Research on Cancer (IARC) and the GLOBOCAN cancer statistics for 2020 by Ferlay et al. (2021). To generate national estimates, the most accurate data on cancer fatalities came from the World Health Organization's mortality database (Ferlay et al., 2021). In contrast, the most accurate data on cancer incidence came from population-based cancer registries (PBCR). For 2020, estimates were created for 38 cancer forms across 185 nations and territories, categorized by gender and age group. Based on estimates from Figure *1* A, B the data provided an overview of the estimated global statistics regarding new cancer cases and fatalities, divided by gender and cancer type. The global distribution of cancer cases and deaths across all cancer types and geographical areas is shown in Figure 2. North America ranked second for new cases (2.6 million) but third for deaths (699,000), just behind South and Central Asia (1.3 million). Eastern Asia had the highest numbers, with 6.0 million cases and 3.6 million deaths, which is unsurprising given the region's massive 1.7 billion inhabitants. Europe had the highest figures, accounting for one-tenth of the global population despite having just one-fifth of the total deaths and 4.4 million new cases (Ferlay et al., 2021)

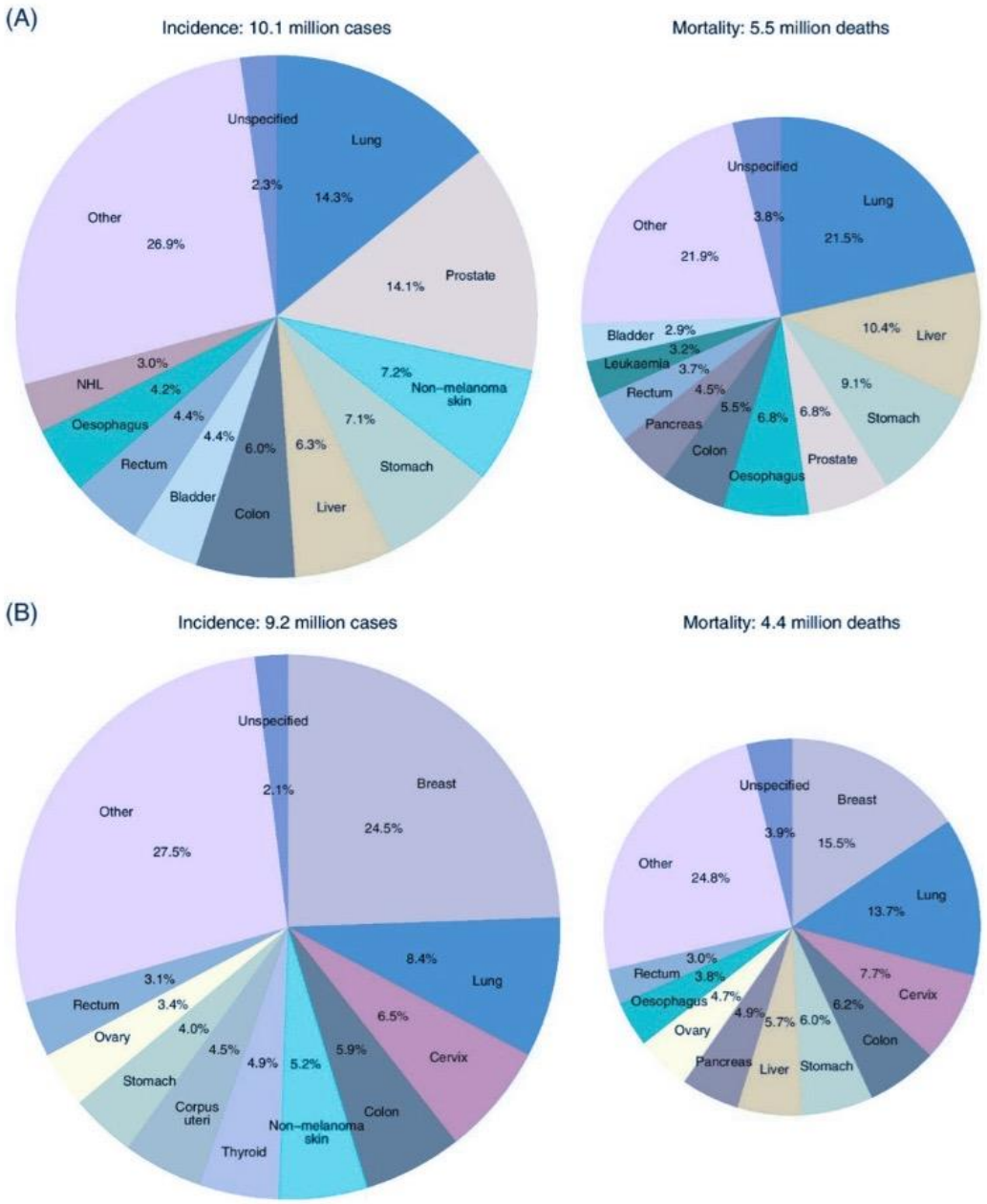

Figure 1: Predicted new cases and fatalities from the ten most frequent malignancies in 2020, broken down by sex (A-males, B- females). The area of the pie chart represents the percentage of overall cases or fatalities that may be attributed to each sex (reproduced from:(Ferlay et al., 2021) pg. 9).

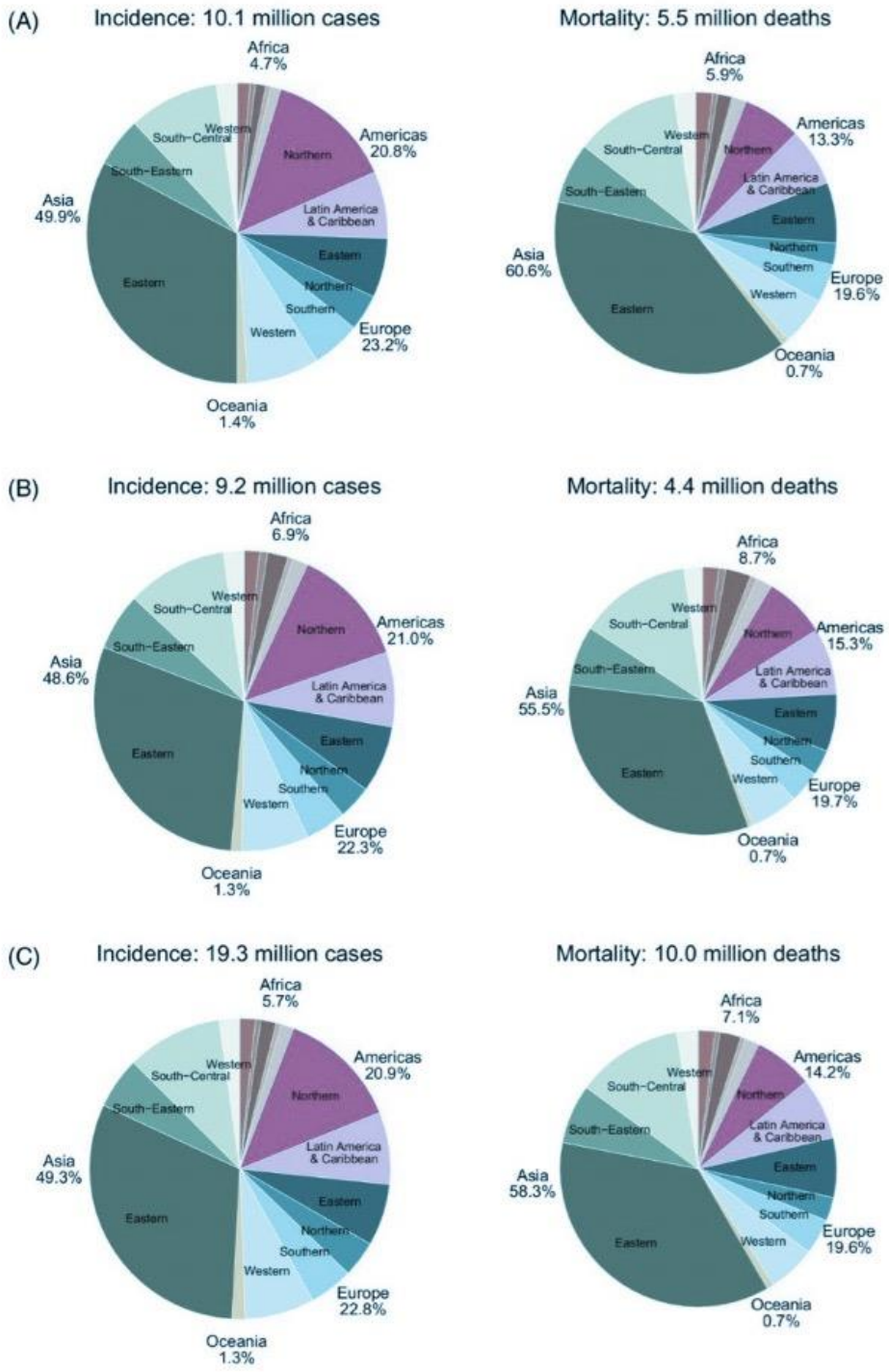

Figure 2: Approximate number of males (A), females (B), and both sexes (C), who will be affected by cancer and die from this disease worldwide in 2020 in relation to the distribution of these figures by world area (C) ((reproduced from: (Ferlay et al., 2021) pg. 10).

1.2 Colorectal Cancer: Epidemiology

Colorectal Cancer is the third most common cancer globally, with 1.9 million cases recorded in 2020 as per the World Cancer Research Fund website (https://www.wcrf.org). It is the second most prevalent cancer in women (9.2%) and the third most common disease in men (10 %) (Moridikia et al., 2018, Bray et al., 2018). It is the second most common reason for cancer deaths globally (Boakye et al., 2019). In affluent nations, colorectal cancer cases account for around 55% of all cases (Sears and Garrett, 2014). The lifetime risk of colorectal cancerin industrialized nations is up to 5%, and the chance of acquiring an adenoma, a benign colon tumor that has the potential to become malignant, is 20 % (Sears and Garrett, 2014). Despite enormous progress in medical science, colorectal cancer remains a significant public health issue in affluent nations (Ahmadyousefi et al., 2019).

1.2.1 Incidence

In terms of the most common cancer diagnoses, worldwide, rectal cancer is ranked eighth, while colon cancer is ranked fourth, according to GLOBOCAN 2018 data. Colorectal malignancies (CRCs) are the third most prevalent type of cancer found worldwide, accounting for 11% of all cancer diagnoses (Figure *3*) (Bray et al., 2018, Ferlay J et al.). According to Herzig (2018), there were an estimated 1.8 million new instances of colorectal cancer (CRC) in 2018. Of these, around 1,096,000 new cases were of colon cancer, and 704,000 new cases were of rectal cancer. With 10.2% of the total cases reported worldwide, colorectal cancer (CRC) is the most frequent cancer among men in 191 countries. However, no country asserts that the most prevalent cancer among female patients is colon cancer (Bray et al., 2018).

1.2.2 Mortality

Colorectal cancer (CRC) was estimated to cause 881,000 deaths globally in 2018 and thus ranked as the second most lethal cancer worldwide. By sub-analysis, colon cancer ranked fifth in terms of lethality, contributing to 551,000 (5.8%) of all cancer deaths, and rectal cancer ranked tenth in terms of fatalities, accounting for 310,000 (3.2%) of all cancer deaths. The cumulative risk of dying from colon cancer is 0.66% for men and 0.44% for women in between the ages of 0 and 74. According to Shen et al. (2013), the risks of rectal cancer show a similar ratio for men and women, with 0.46% and 0.26%, respectively (Shen et al., 2013). According to Bray et al. (2018), the age-standardized death rate from CRC per 100,000 individuals is 8.9 worldwide.

Figure 4) (Bray et al., 2018).

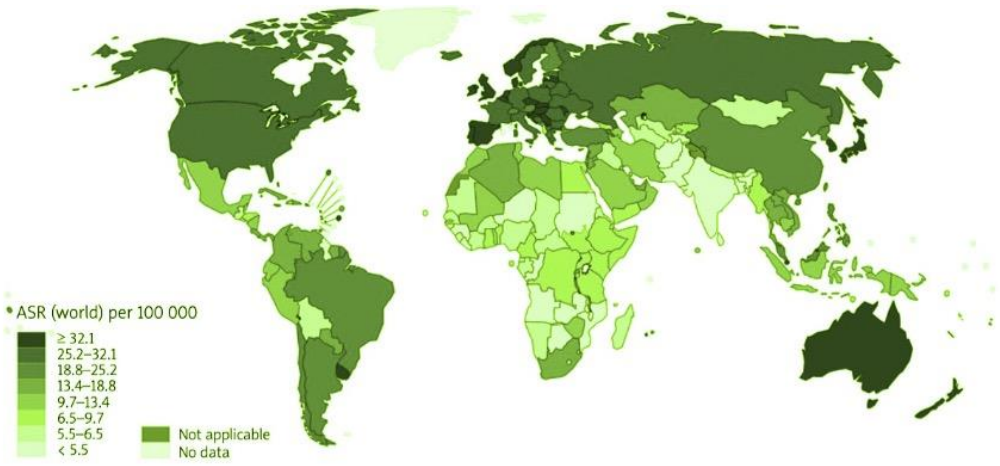

Figure 3: The color-coded representation illustrates the estimated age-standardized incidence rates for colorectal cancer globally in 2018. The data encompasses both sexes and all age groups. (Reproduced from http://globocan.iarc.fr/ (Ferlay J et al.)).

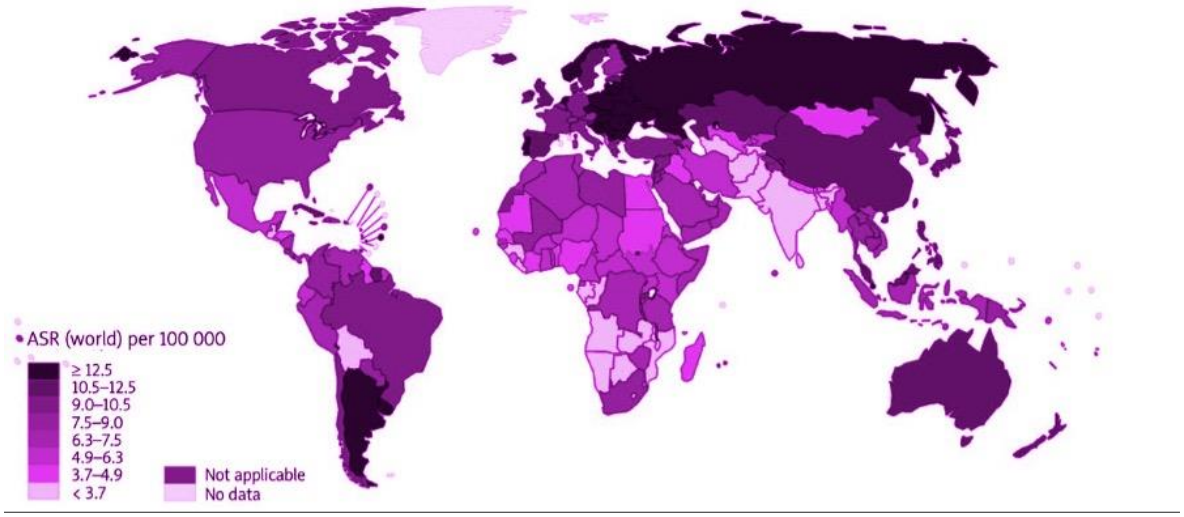

Figure 4: Map depicting the estimated age-standardized mortality rates for colorectal cancer worldwide in 2018 and considering both sexes and all age groups. (Reproduced from http://globocan.iarc.fr/ (Ferlay J et al.)

1.3 Risk factors

Worldwide, the probability of being diagnosed with colorectal cancer ranges from 4% to 5%. According to Johns and Houlston, about 70 % of colorectal cancer cases are random and linked to factors like diet, exercise, smoking, and drinking (Johns and Houlston, 2001). Genetic predisposition accounts for about 25% of colorectal cancer incidences, and 5% of individuals have inherited traits linked to the disease's progression (Jasperson et al., 2010, Migliore et al., 2011). As Figure *5* illustrates, several risk factors are linked to colorectal cancer.

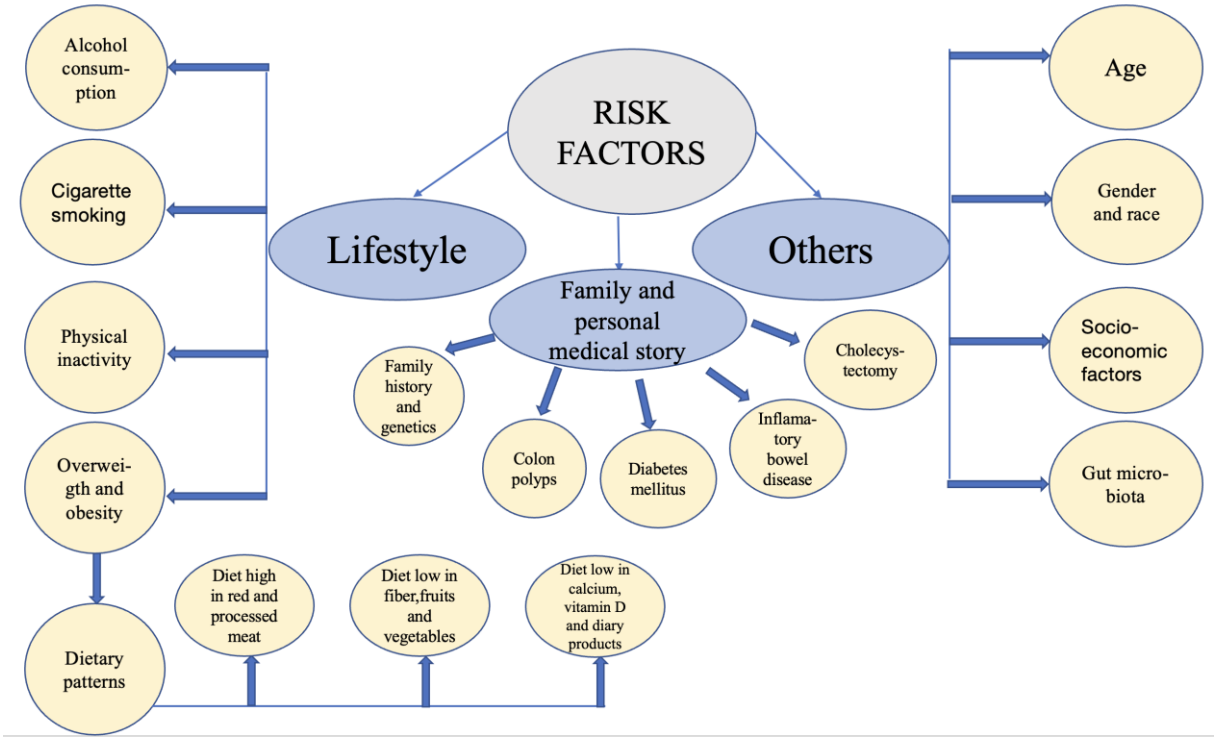

Figure 5: Colorectal cancer is primarily influenced by certain key risk factors (Reproduced from (Sawicki et al., 2021) pg. 4).

1.3.1 Lifestyle

Alcohol drinking

One of the main risk factors for colorectal cancer is alcohol consumption. Consuming two to three drinks daily raises the risk by approximately 20 % and consuming more than three drinks raises the risk by approximately 40 % (American Cancer Society. Colorectal Cancer Facts & Figures 2017–2019; American Cancer Society: Atlanta, Rawla et al., 2019). Individuals who consume four or more drinks per day regularly run a 52% higher risk of developing colorectal cancer (Marley and Nan, 2016).

Smoking

Colorectal cancer is a well-known example of cancers linked to smoking. According to research, smokers have a 2-3 times higher risk of developing colorectal cancer (CRC) than non-smokers, and this risk rises with the amount of cigarettes and length of time that a person smokes (Giovannucci, 2001).

Exercise

According to statistics from epidemiological research, a lack of physical activity may be causal to the increased incidence of colorectal cancer in both industrialized and developing countries. According to estimates, persons who lead sedentary lifestyles may be up to 50 % more likely to acquire colorectal cancer than people who have the physically most active lives (American Cancer Society. Colorectal Cancer Facts & Figures 2017–2019; American Cancer Society: Atlanta).

Excessive weight and obesity

Obesity or being overweight increases the risk of colorectal cancer significantly. Compared to those of normal weight, men and women who are overweight or obese have roughly a 50 % and 20 % increased chance of developing colon cancer, respectively. In addition, the overall risk of colorectal cancer is thought

to increase by 3% for every five kg of weight added (Rawla et al., 2019, American Cancer Society. Colorectal Cancer Facts & Figures 2017–2019; American Cancer Society: Atlanta).

Dietary factors

Colon cancer rates are often greater in areas with high-fat consumption than in those with lower fat intake (Rose et al., 1986). Nevertheless, there isn't always a statistically significant correlation between consuming meat and fat and colon cancer (Bingham, 1990).

1.3.2 Family history of colorectal cancer and personal medical story

Family background and genetics

Various studies indicate that the risk of colon cancer is 2–3 times higher in the close relatives, including parents and siblings, of individuals with colorectal cancer (Fernandez et al., 2004, Johns and Houlston, 2001).

Diabetes mellitus

Research indicates that diabetes raises the risk of colorectal cancer and other gastrointestinal malignancies on its own (Ma et al., 2018, Pang et al., 2018). Compared to people without diabetes, those with type 2 diabetes have a two to three times higher risk of developing colorectal cancer (Yao et al., 2014, Peeters et al., 2015).

Colon polyps

Histologically, colorectal polyps can be classified as either neoplastic or non-neoplastic, which includes inflammatory, hyperplastic, and hamartomatous polyps. Adenomatous polyps are the primary cause of 95% of colorectal cancer cases. Though adenomas are the source of most malignancies, only around 5% of polyps go on to develop into colorectal cancer (Shussman and Wexner, 2014).

Age

Growing older is thought to be one of the most important variables affecting the chance of acquiring colorectal cancer since people over 50 account for 90 % of new instances of the disease (Amersi et al., 2005, Rawla et al., 2019).

Gender and race

Men are around 30 % more likely than women to develop colorectal cancer. This information comes from the American Cancer Society (ACS). In addition, men who are diagnosed with colorectal cancer typically have a worse prognosis than women, with a mortality rate that is almost 40 % higher (American Cancer Society. Colorectal Cancer Facts & Figures 2017–2019; American Cancer Society: Atlanta).

Gut microbiota

Recent research indicates that the gut microbiota is involved in many health processes, including cancer development. According to recent studies, alterations in the makeup and activity of the gut microbiota may contribute to the development, propagation, and advancement of colorectal cancer. Thus, an imbalance in the microbiota of the gut can foster conditions that lead to the development of colorectal cancer (Cheng et al., 2020, Tabuchi and Japan; Kondo).

Socioeconomics factors

Individuals with lower socioeconomic classes are more likely to develop cancer. This may be because they smoke, have bad diets, lead sedentary lives, and have less access to healthcare. However, there is conflicting evidence linking socioeconomic position and colorectal cancer. While higher socioeconomic class groups may exhibit a greater risk in Europe, individuals with lower socioeconomic status are more prevalent in North America. To fully understand how socioeconomic position affects colorectal cancer matters, more research is required(Kondo, 2020)

1.4 Classification of colorectal cancer

The epithelial cells that border the colon mucosa are the site of the initiation of more than 90 % of colorectal malignancies (Hamilton SR, 2010). Neuroendocrine, squamous cell, adeno-squamous, spindle cell, and undifferentiated carcinomas are other rare forms of colorectal cancers. The most common type of adenocarcinoma, termed conventional adenocarcinoma, is distinguished by glandular development, the foundation for histologic tumor grading. Over 95 % of well-differentiated adenocarcinomas show gland formation, 50–95 % of moderately differentiated adenocarcinomas show gland formation, and less than 50 % of poorly differentiated adenocarcinomas are primarily solid. In real terms, well-differentiated carcinomas account for 10 % of cases and poorly differentiated carcinomas for 20 %, with 70 % of colorectal adenocarcinomas being diagnosed as such (Fleming et al., 2012).

1.4.1 Stages of colorectal cancer

Cancer stages indicate the stage at which a cancer has progressed and how far it has spread. To choose the best colon cancer treatment plans, staging is essential. Furthermore, the possibility of a cure is highly correlated with the stage of cancer (Moridikia et al., 2018). Stage 0 is the earliest stage of colon cancer, and stage 4 is the most advanced. Here is a description of the stages:

- **Stage 0:** Only the inner lining of the colon or rectum has aberrant cells in this stage, also referred to as carcinoma in situ.
- **Stage 1:** The cancer may have penetrated the mucosa, or lining, of the colon or rectum and may have spread into the muscle layer. Neither the surrounding lymph nodes nor the body's other organs have been affected.
- **Stage 2:** There is no impact on the lymph nodes. This stage denotes the spread of cancer to the colon or rectum's lining or through the lining of nearby tissues.
- **Stage IIa:** Cancer has spread to the colon's or rectum's outermost layers but has not penetrated them (T3). The organs nearby have not been affected. It has not progressed to distant sites (M0) or neighboring lymph nodes (N0).
- **Stage IIb:** The cancer has penetrated the colon's or rectum's wall but has not spread to neighboring tissues or organs (T4a). It hasn't reached distant locations (M0) or neighboring lymph nodes (N0).
- **Stage IIc:** The cancer has spread into adjacent tissues or organs and has penetrated the wall of the colon or rectum (T4b). It hasn't reached distant locations (M0) or neighboring lymph nodes (N0).
- **Stage 3:** At this point, the lymph nodes are the only locations where the cancer has spread.
- **Stage 4:** The liver or lungs are among the other organs where the cancer has progressed (Brar et al., 2021).

1.5 Signaling pathways involved in colorectal cancer

Genomic instability is a key component of the underlying structure of colorectal cancer. The pathogenic mechanisms that cause this syndrome can also travel via

the CpG island methylator phenotype (CIMP), microsatellite instability (MSI), and chromosome instability (CIN) (Mármol et al., 2017).

1.5.1 Chromosome instability (CIN)

The conventional pathway, or CIN route, is typified by chromosomal number abnormalities that lead to tumor aneuploidy and loss of heterozygosity (LOH). It accounts for up to 80 %–85 % of all CRC cases (Grady and Carethers, 2008).

1.5.2 Microsatellite instability (MSI)

The lack of DNA repair systems results in a hypermutable phenotype, which is the source of the microsatellite instability pathway. Microsatellite instability is characterized by an increased rate of mutations in tumors that have a diminished ability to repair short DNA chains or tandem repeats (two to five base-pair repetitions) (John and Schwartz, 2016). Changes to the reading frames of tumor suppressor or oncogene genes encoded by microsatellites cause these genes to overexpress themselves, which causes cancer. These changes can impact non-coding areas as well as microsatellites (Mármol et al., 2017, Boland and Goel, 2010). Another feature of CRC that is often noted is the CpG island methylator phenotype, which is caused by epigenetic instability. The primary characteristic that sets CIMP tumors apart is the hypermethylation of oncogene promoters, which results in decreased protein production and gene silence (Mármol et al., 2017, Lao and Grady, 2011).

1.5.3 The role of genomic abnormalities in determining the outcome of colorectal cancer

Many chromosomal abnormalities linked to colorectal cancer have been found recently, thanks to genomic approaches. Although most genomic changes in colorectal cancer (CRC) are mutations, chromosomal translocations and modifications are common. These abnormalities affect important cellular processes, including TP53 and cell-cycle regulation, as well as critical pathways like WNT, MAPK/PI3K, and TGF-β (Figure 6) (2012). The WNT pathway significantly impacts stem-cell differentiation and cellular proliferation (Moridikia et al., 2018). Thus, alterations in this system may be the cause of tumor formation. Weakened tight junctions have been connected to alterations in the WNT pathway in colorectal cancer. As a result, migration and metastasis are encouraged by a decrease in cellular adhesion (Brocardo and Henderson, 2008).

APC mutations are the main genomic aberration in CRC associated with the WNT pathway, while numerous other alterations may also affect this pathway (Mármol et al., 2017, Brocardo and Henderson, 2008). A poor prognosis is also associated with β-Catenin, which is overexpressed in CRC tumors and is a component of the WNT pathway (Herzig and Tsikitis, 2015).

Accordingly, it is believed that over-expression of c-MYC, which results from WNT pathway activation, is a favourable prognostic biomarker in colorectal carcinoma (CRC). (Rennoll and Yochum, 2015, Toon et al., 2014).

The MAPK and PI3K pathways control both cell division and survival. Thus, modifications to these pathways can confer a proliferative advantage to tumor cells. KRAS, BRAF, and PIK3CA (PI3K) mutations are the three most common mutations in colorectal cancer (CRC) (Chen et al., 2014, Sawicki et al., 2021).

These pathways, including those for growth, differentiation, and cell death are important cellular processes, which are influenced by the TGF-β pathway. However, due to their low frequency, spontaneous mutations in TGF-β and its pathway are not significant as prognostic indicators in colorectal cancer. However, the CIN pathway and TGF-β associated chromosomal changes in CRC are strongly linked (Herzig and Tsikitis, 2015).

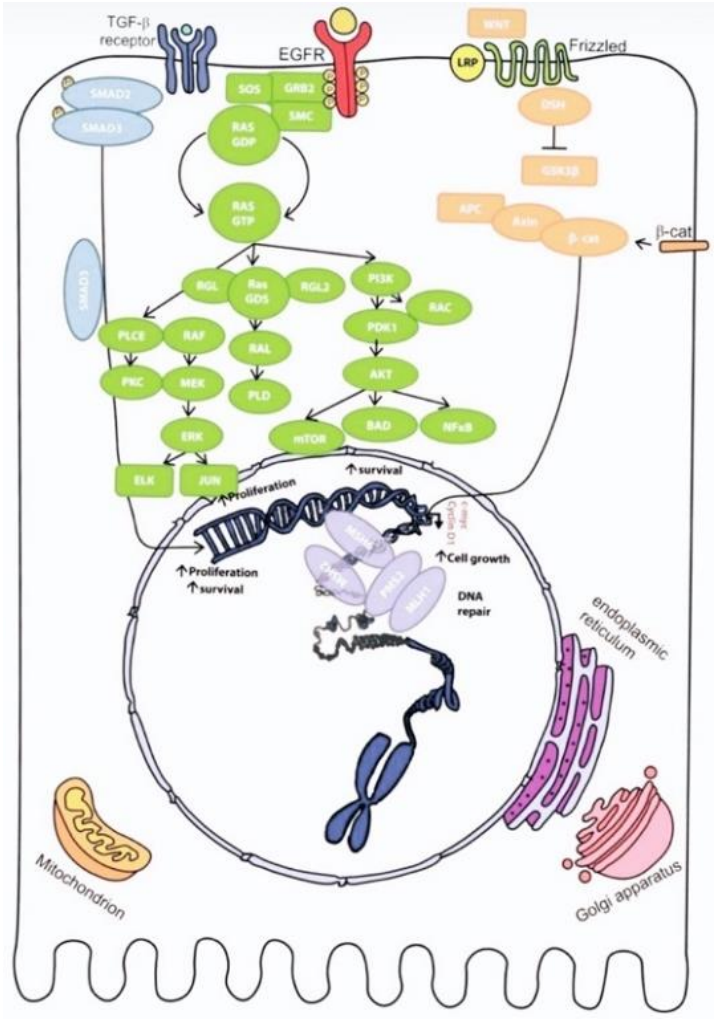

Figure 6: Cancer of the colon and the molecular processes involved. Cell proliferation and survival can be boosted by mutations in proteins implicated in the WNT (orange), MAPK/PI3K (green), SMAD/TGF- β (blue), or DNA repair (purple) pathways, leading to tumorigen expansion and carcinogenesis. Protein activation is represented by lines with arrowheads, whereas protein inhibition is shown by lines with bars. (Reproduced from (Mármol et al., 2017) pg. 6).

1.6 Liver Metastasis

Metastases are defined as cancerous cells that have spread to another organ, such as the liver. The major malignancy that frequently spreads to the liver is colorectal cancer. There is interaction between the surrounding tumor environment and cancer cells. This contact is essential for the cancer cells to adhere, endure, and increase to create metastases (Hess et al., 2006). It is noteworthy that approximately 50 % of people with various cancer types may eventually develop liver metastases, either initially or later (Jasperson et al., 2010). This viewpoint aligns with the seed and soil hypothesis, positing that the development of metastases in the liver is facilitated by a confluence of intricate biological systems. (Figure *7*). (Paget, 1889)

Identification of liver metastases is frequently accomplished by diagnostic imaging modalities such as ultrasound, CT, MRI, and PET scans. Untreated liver metastases have a very poor prognosis for patients, with an almost zero 5-year survival rate (Wagner et al., 1984).

A multidisciplinary strategy combining experts from several domains, including surgeons, radiologists, medical and radiation oncologists, pathologists, and trained nurses, is necessary to effectively manage patients with liver metastases. The implementation of tailored treatment plans, such as resection, ablation, locoregional therapies, systemic chemotherapy, or targeted therapies, depends on the early diagnosis of liver metastases. The degree of liver illness, the biology of the metastases, and the underlying tumor's origin all influence the chosen method (Tsilimigras et al., 2021).

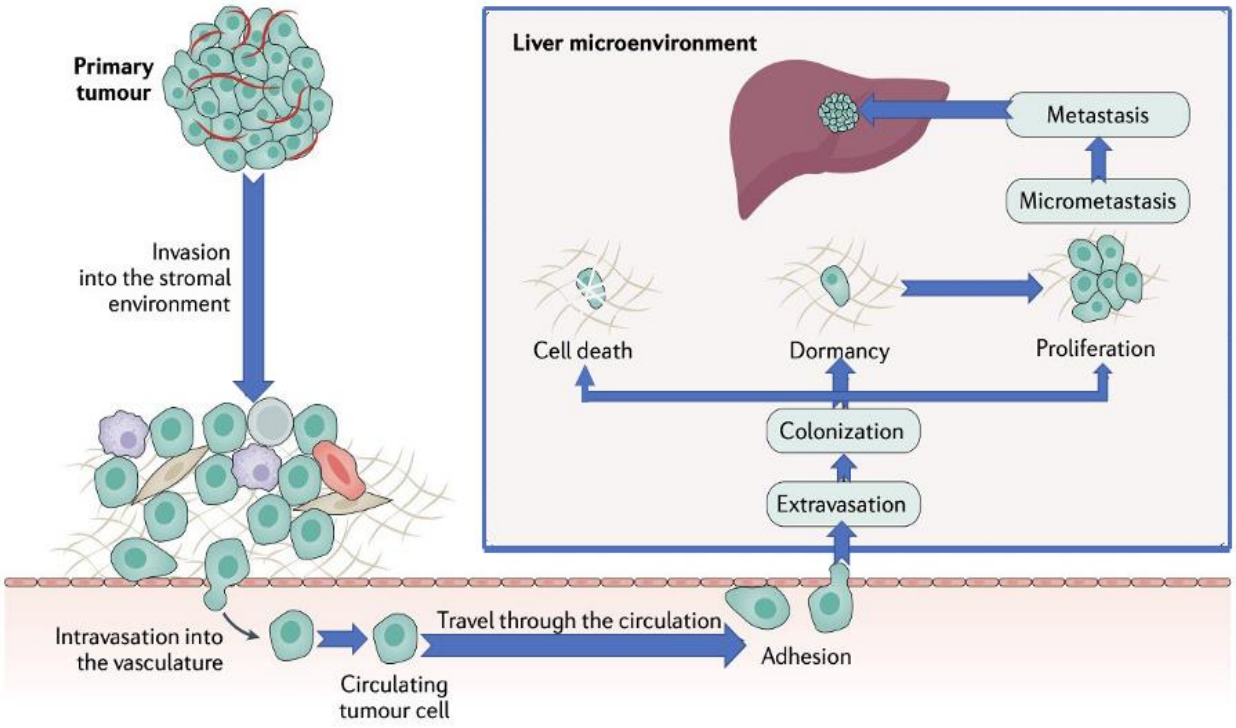

Figure 7: In the process of metastasis from primary tumors to the liver. (Reproduced from (Achrol et al., 2019) pg. 3).

1.7 Extracellular matrix (ECM) in tumor progression

The extracellular matrix (ECM) supports tissues and organs (Bonnans et al., 2014). Comprising of glycoproteins, proteoglycans, and extracellular proteins, it is a web of sheets and fibrils. The biochemical composition of the extracellular matrix, which contains covalent intermolecular cross-linkages, and its biophysical characteristics, such as topography, molecular density, stiffness/rigidity, and tension, distinguish it from other materials (Lu et al., 2012).

The ECM is very malleable due to its metabolic and biophysical characteristics and constant remodeling. The tumor stroma's extracellular matrix (ECM) is made up by cancer cells and the local fibroblasts that develop into cancer-associated fibroblasts (CAFs). When cancer cells spread from the primary tumor mass (Walker et al., 2018). the extracellular matrix (ECM) either acts as a barrier that needs to be broken down by invasive tumor cells by proteolysis, or it can help the cancer cells migrate (Chang et al., 2017, Eble and Niland, 2019).

Extracellular matrix (ECM) composition and cross-linkage changes, driven by cancer cells or mostly carried out by cancer-associated fibroblasts (CAFs), affect biochemical characteristics, growth factor storage, and biophysical aspects (Luo et al., 2016). This involves modifications to the tumor stroma's tension and rigidity (Stroka and Konstantopoulos, 2014, Paszek et al., 2005) (Malik et al., 2015).

Although the extracellular matrix (ECM) constantly changes, the tumor microenvironment's ability to adapt is limited by how long these changes last. This persistent characteristic may be interpreted as the tissue's "memory" or a unique "ECM signature" associated with malignancy (Giussani et al., 2015, Te Boekhorst and Friedl, 2016). In addition to providing a favorable environment for cancer cells to survive and proliferate, the extracellular matrix's (ECM) biochemical and biophysical characteristics also initiate and promote oncogenic transformation. Furthermore, it can affect the rates of somatic mutation (Holle et al., 2018, Stroka and Konstantopoulos, 2014, Bhowmick et al., 2004).

1.8 Screening, Diagnostics and Treatment

1.8.1 Screening

In industrialized nations, screening for colorectal cancer (CRC) is currently a common procedure for both average-risk and high-risk individuals. Several techniques are employed, such as CT colonography, colonic capsule endoscopy, fecal occult blood testing, and fecal DNA testing (Chu et al., 2019). However, endoscopy, more specifically, flexible sigmoidoscopy and colonoscopy, remains the most common method of screening in many nations, most notably the United States (Lin et al., 2014).

1.8.2 Diagnostics

Biomarkers are circulating biochemical substances that can be used in cancer detection. These substances include proteins, tumor DNA, tumor-derived cells, and miRNA in the blood. These elements are frequently used to diagnose colorectal cancer (CRC), identified by immunohistochemistry or blood-based protein quantification testing (How Kit et al., 2012, Gan et al., 2020).

1.8.3 Treatment

Treatment options for colorectal cancer involves a wide range of approaches including surgery, immunotherapy, targeted therapy, chemotherapy and radiation therapy. (Brar et al., 2021). Surgical resection is particularly important when the disease has not disseminated to distant sites (Chu, 2012).

1.8.4 Gene therapy

Gene therapy has been explored as an alternative for established colorectal cancer therapies. There are two methods for gene therapy: somatic gene therapy and germ line gene therapy. In somatic gene therapy, the introduced genetic material is not passed to the next generation as in gene therapy (Wirth e t al., 2013). However, in colorectal cancer, this approach is challenging because it is not feasible to replace all

mutated genes; rather, it is primarily utilized as an adjunct to enhance the effectiveness of existing therapies. Recent reviews have explored various gene therapy strategies, including the application of suicide genes such as cytokine deaminase and tumor necrosis factor, immune modulation via antigen-presenting cells (APCs) to boost the body's immune response to cancer cells, targeting oncogenes or tumor suppressor genes to limit tumor growth, and employing viral replication to destroy tumor cells (Naldini, 2015). APCs play a key role in initiating and regulating the immune response by processing and presenting tumor-associated antigens to T-cells, thereby enhancing the immune system's ability to recognize and attack cancer cells. Nevertheless, these approaches are associated with numerous challenges, as reviewed in (Hasbullah, 2021) and (Urnov et al., 2010).

1.9 Small interfering RNA (siRNA) Technique

Modifying the expression of genes, particularly by introducing small interfering RNAs (siRNAs), has emerged as a promising and rapidly expanding therapeutic approach. siRNA is a duplex RNA comprising 21–28 nucleotides that selectively ruin mRNA transcripts to prevent them from being translated into particular proteins (Ryther et al., 2005). Pre-mRNA is produced in eukaryotes through RNA polymerase II transcription of protein-coding genes. This pre-mRNA grows into the final mRNA form after further processing (Nikolova and Draga, 2008)

When mature mRNAs are translated into proteins by ribosomes, they go from the nucleus to the cytoplasm. The introduction of exogenous siRNA into cells results in the assembly of additional proteins, including Dicer and Argonaute, as part of the RNA-induced silencing complex (RISC), (Figure *8*). The siRNA is cleaved into a single-stranded form by activating argonaute proteins (Luo et al., 2016). The single-stranded siRNA carried by the RISC attaches itself in a sequence-specific way to the targeted mRNA in the cytoplasm. The mRNA is complementary to the antisense strand within the freshly created double-stranded RISC-mRNA complex and is then cleaved by slicer or argonaute proteins. The cell recognizes the cleaved mRNA strands as abnormal and eliminates them, thereby silencing the targeted gene's expression (Bernstein et al., 2001, Shen et al., 2013).

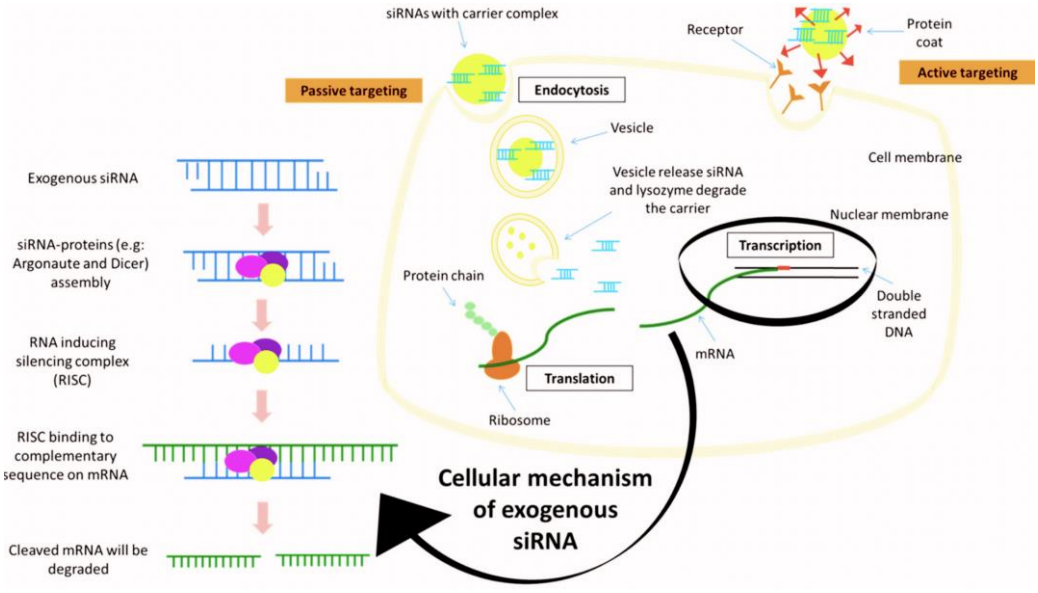

Figure 8: Small interfering RNA (siRNA) works to silence genes by targeting mRNA on the left side. On the right side, it shows how exogenous siRNA is delivered into the cytoplasmic compartment using passive and active targeted delivery (Reproduced from (Kamaruzman et al., 2019) pg. 8).

AIM OF THE STUDY, RESEARCH STATEMENT

Ranked third as the most common cancer globally, colorectal cancer has 5-year relative survival rate of 91% for localized disease. This 5-year relative survival rate, however, decreases to 14% for metastatic disease. The liver is the common site of metastasis with about 30 % of the patients developing liver disease. Since the current approaches to therapy (conventional surgery, radiotherapy and chemotherapy) do not cure this disease, there is need to identify genes associated with liver metastatic disease, which will serve as drug targets and aid in developing new therapies for colorectal cancer. This work was designed in the context of previously established animal models for liver colonization in order to identify genes of interest across cancer types and species differences. The human LS174T colorectal cancer cell line was chosen as model for this study based on its ability to grow in the liver of nude rats. This study was expected to yield new information regarding the modulation pattern (and pathways) for genes of interest, based on the available literature. With this in mind, the current study was designed to achieve the following objectives:

I). Inoculate luciferase transfected LS174T^{luc} cells into the rat colon and into the rat liver for assessing the respective growth.

II). Re-isolate these cells after defined periods for gene expression profiling by chip array.

III). With appropriate analytical tools, identify genes of interest for further validation.

IV. Compare genes of interest with those from previously established models of liver colonization

2. MATERIALS AND METHODS

All materials, instruments and software used in this study are listed in the following tables 1-11.

2.1 Materials

2.1.1 Culturing conditions and cell line

The cell line LS174T

used in this study was established in 1974 from the moderately well-differentiated primary colonic adenocarcinoma (Duke´s type B) of a 58-year-old woman (Tom et al., 1976).

Table 1: Details about the cell line used in the study.

Name	*LS174T*
Species of origin	*Homo sapiens, human*
Tissue	*Large intestine; Colon*
Disease	*Adenocarcinoma; Colorectal; Dukes' type B*
Morphology	*Epithelial*
Culture properties	*3D cell culture*
Provider	*DSMZ no.:759*

Table 2: Materials used for cell culture.

Materials	***Manufacturer***
Fetal Bovine Serum (FBS)	*Anprotec, South America*
L-Glutamine 200mM (100×)	*Gibco, Life Technologies*
Penicillin (100 IU/ml) streptomycin (100 µg/ml)	*Gibco, Life Technologies*
RPMI-1640 medium	*Gibco, Life Technologies*
Trypsin 2.5 %	*Gibco, Life Technologies*

2.1.2 Materials used in animal experiments

All the materials used for animal experiments in this study are listed in Table *3*.

Table 3: Mediums and buffers employed in liver perfusion and cell Isolation.

Materials	***Manufacturer***
0.9% NaCl solution	*B. Braun, Germany*
1 M Hepes	*Invitrogen, USA*
90° bent micro-forceps	*Aesculap, Germany*
Absorbable 3-0 VICRYL thread	*Ethicon, Germany*
Anatomical forceps	*Aesculap, Germany*
CaCl2	*Merck, Darmstadt, Germany*
Cannula 30 G 1/2 (0.3 × 13 mm)	*Ethicon, Germany*
Catgut surgical suture	*Ethicon, Germany*
Collagenase Type IV	*Serva, Heidelberg*
Cotton swabs	*Rossmann, Germany*
DMSO 100 %	*Roth, Karlsruhe*
EGTA	*Gerbu, Gaiberg*
Fine scissors	*Aesculap, Germany*
Geltrex	*Gibco, Germany*
Gentamicin 10 mg/ml	*Gibco/Invitrogen, Karlsruhe*
Glucose	*Merck, Darmstadt*
Glutamine	*Invitrogen, Karlsruhe*
Hair trimmer	*Wella, Germany*
Heparin 5000 U/ml	*Biochrom AG, Berlin*
Hydrocortisone	*Sigma, Steinheim,Germany*
Insulin	*Lilly GMBH, Giessen*
Isofluran	*Baxter, Germany*
KCl	*Sigma, Steinheim,Germany*
KolliphorR EL	*Sigma-Aldrich, Germany*
Luciferin	*BioMol, Germany*
$Na_2HPO_4.2H_2O$	*Merck, Darmstadt*
Needle holder	*Aesculap, Germany*
Needles 30 G and 25 G	*Becton Dickinson, Germany*
Pean clamps	*Aesculap, Germany*
Pronase E	*Sigma, Steinheim, Germany*
PVC catheter	*NeoLab, Germany*
retractor	*DKFZ, Germany*
Scissors	*Aesculap, Germany*
Spitacid solution	*Henkel, Germany*
Surgical clips	*Aesculap, Germany*
Surgical forceps	*Aesculap, Germany*
Surgical scissors	*Aesculap, Germany*
Surgical suture (6/0 silk)	*Ethicon, Germany*
Vessels clips	*Aesculap, Germany*
Vicryl 3/0 suture	*Ethicon, Germany*
Vicryl 6/0 suture	*Ethicon, Germany*
Williams Medium E	*Biochrom AG, Berlin*
Materials	***Manufacturer***

0.9% NaCl solution	*B. Braun, Germany*
1 M Hepes	*Invitrogen, USA*
90° bent micro-forceps	*Aesculap, Germany*
Absorbable 3-0 VICRYL thread	*Ethicon, Germany*
Anatomical forceps	*Aesculap, Germany*
CaCl2	*Merck, Darmstadt, Germany*
Cannula 30 G 1/2 (0.3 × 13 mm)	*Ethicon, Germany*
Catgut surgical suture	*Ethicon, Germany*
Collagenase Type IV	*Serva, Heidelberg*
Cotton swabs	*Rossmann, Germany*
DMSO 100 %	*Roth, Karlsruhe*
EGTA	*Gerbu, Gaiberg*
Fine scissors	*Aesculap, Germany*
Geltrex	*Gibco, Germany*
Gentamicin 10 mg/ml	*Gibco/Invitrogen, Karlsruhe*
Glucose	*Merck, Darmstadt*
Glutamine	*Invitrogen, Karlsruhe*
Hair trimmer	*Wella, Germany*
Heparin 5000 U/ml	*Biochrom AG, Berlin*
Hydrocortisone	*Sigma, Steinheim,Germany*
Insulin	*Lilly GMBH, Giessen*
Isofluran	*Baxter, Germany*
KCl	*Sigma, Steinheim,Germany*
KolliphorR EL	*Sigma-Aldrich, Germany*
Luciferin	*BioMol, Germany*
$Na_2HPO_4.2H_2O$	*Merck, Darmstadt*
Needle holder	*Aesculap, Germany*
Needles 30 G and 25 G	*Becton Dickinson, Germany*
Pean clamps	*Aesculap, Germany*
Pronase E	*Sigma, Steinheim, Germany*
PVC catheter	*NeoLab, Germany*
retractor	*DKFZ, Germany*
Scissors	*Aesculap, Germany*
Spitacid solution	*Henkel, Germany*
Surgical clips	*Aesculap, Germany*
Surgical forceps	*Aesculap, Germany*
Surgical scissors	*Aesculap, Germany*
Surgical suture (6/0 silk)	*Ethicon, Germany*
Vessels clips	*Aesculap, Germany*
Vicryl 3/0 suture	*Ethicon, Germany*
Vicryl 6/0 suture	*Ethicon, Germany*
Williams Medium E	*Biochrom AG, Berlin*

2.1.2.1 Hanks buffer (1 L)

- 400 mg KCl (Sigma, Steinheim, Germany)
- 60 mg $Na_2HPO_4.2H_2O$ (Merck, Darmstadt, Germany)
- 4 g NaCl (J.T. Baker-Holland)
- 3.55 g 1 M Hepes (Invitrogen, USA)
- 60 mg KH_2PO_4 (Sigma Chemical Co. USA)

Balanced with HCl to achieve a pH of 7.4, the solution was then brought to a final volume of 1 liter with distilled water. Hanks buffer underwent autoclaving and was subsequently added directly before utilization.

2.1.2.2 Pre-perfusion-medium (39-41 °C)

- 500 ml HBSS (Hanks balanced saline solution)
- 2.5 ml 100 mM EGTA* (Gerbu, Gaiberg)

*(3.8 g EGTA dissolved in 100 ml distilled water and sterile filtered)

- 1 ml Heparin 5000 U/ml (Biochrom, AG, Berlin)

2.1.2.3 Perfusion-medium (39-41 °C)

- 200 mg Collagenase Type IV* (Serva, Heidelberg)
  (200 mg of collagenase was measured and placed in a Falcon tube. It was then dissolved in 25 ml of freshly prepared Williams Medium E during the pre-perfusion stage. The resulting solution was sterile-filtered through a 0.22 µm filter.)
- Williams Medium E (Biochrom AG, Berlin) ad 250 ml

0.9 ml 1 M CaCl2** (Merck, Darmstadt, Germany)
** (14.7 g CaCl2 dissolved in 100 ml distilled water and sterile-filtered)

2.1.2.4 Wash-medium (4 °C)

- 500 ml Williams Medium E

-Maintenance-medium (for hepatocytes cultivation)

- 500 ml Williams Medium E (4 °C)
- 8.7 ml DMSO 100 % (RT) (Roth, Karlsruhe)
- 5 ml Gentamicin 10 mg/ml (RT) (Invitrogen, Karlsruhe)
- 0.5 ml Hydrocortisone (-20 °C) (Sigma, Steinheim)
- 1.4 ml 0.15 ml Insulin (Lilly GMBH, Giessen) buffered with 1.4 ml EBSS
- 28.7 ml PDH-Mix* (-20 °C)

* [602.7 ml PDH-Mix for 21 falcons (each 28.7 ml) prepared as follows and kept at -20 °C]

- 117.5 ml 200 mM Glutamine (Invitrogen, Karlsruhe)
- 126 ml Glucose** 5% (Merck, Darmstadt)
  ** (5 g glucose dissolved in 100 ml distilled water and filtered sterile)
- 241.5 ml 1 M HEPES
- 117.6 ml Pen/Strep 10.000 U/ml (Invitrogen, Karlsruhe)

2.1.2.5 Pronase E (protease type XIV)

- 125 mg Pronase E (Sigma, Steinheim, Germany)
- 3.125 ml DEPC-H_2O
  312.5 µl aliquots were kept at -20 °C and one portion/100 ml perfusion medium was used.

2.1.3 Primers

Table *4* contains a list of all the primers used in this study. These primers were purified using HPLC from Sigma-Aldrich. The primer bank was utilized in the primer design process.

Table 4: Human Primers designed in this study.

Gene Name	***Forward Primer (5'- 3'sequence)***	***Reverse Primer (3'- 5'sequence)***
PTEN	*TGGATTCGACTTAGACTTGACCT*	*GGTGGGTTATGGTCTTCAAAAGG*
DPT	*TGGGTGAATTTGAACCGGCAA*	*CGTAGTTCCATTGTCTGTCAGAA*
NTF3	*CCGTGGCATCCAAGGTAACAA*	*GCAGTTCGGTGTCCATTGC*
CRLF3	*GAAAGTGCATCACAGACAAGGG*	*TCTGGCAGTCATCTAGTGGTTT*
COL4A2	*CCCTGTGGGCATGAAAGGT*	*TCCTTTAAATCCAGGGCTTCCT*
TAF1D	*CTCAGTGTATCCCTTACTCACCT*	*CACTTGATGAATCACTTGCGTG*
COX1	*TCCTTATTCGAGCCGAGCTG*	*GGGCTGTGACGATAACGTTG*
COX2	*ATCATTCACCAGGCAAATTGC*	*GGCTTCAGCATAAAGCGTTTG*
MGST1	*ATTGGCCTCCTGTATTCCTTGA*	*GTGCTCCGACAAATAGTCTGAAG*
CA3	*AAACCAGTCGCCCGTTGAG*	*CCACCATCATAAGACACAGACCA*
SMOC2	*TTAAGGAACCATTTGGAGGACAG*	*CCACAAGCATCACAACATCAC*
FTL	*CAGCCTGGTCAATTTGTACCT*	*GCCAATTCGCGGAAGAAGTG*
RAB15	*ATGGCGAAGCAGTACGATGTG*	*GTGGAACTCGTTGTCGGTGAA*
HMGB2	*GCTCGCTATGACAGGGAGATG*	*GCGATGTTCAGAGCAAAACAGG*
Primers for Housekeeping genes		
Gene Name	***Forward Primer (5'- 3'sequence)***	***Reverse Primer (3'- 5'sequence)***
SDHA	*TGGCATTTCTACGACACCGTG*	*GCCTGCTCCGTCATGTAGTG*
GUSB	*GTCTGCGGCATTTTGTCGG*	*CACACGATGGCATAGGAATGG*
RRN18S	*AGAAACGGCTACCACATCCA*	*CACCAGACTTGCCCTCCA*
YWHAZ	*ACTTTTGGTACATTGTGGCTTCAA*	*CCGCCAGGACAAACCAGTAT*
RPLP0	*AGCCCAGAACACTGGTCTC*	*ACTCAGGATTTCAATGGTGCC*
ARBP	*TAGAGGGTGTCCGCAATGTG*	*CAGTGGGAAGGTGTAGTCAGTC*
HSPCB	*TCTGGGTATCGGAAAGCAAGCC*	*GTGCACTTCCTCAGGCATCTTG*
B4GALT6	*AGGAGGTCCCTATGGCACTAAC*	*TCTCTACAGACAGGCCCATTAGTC*
RRN18S	*ACGGACCAGAGCGAAAGCAT*	*TGTCAATCCTGTCCGTGTCC*

2.1.4 siRNAs

Table *5* contains information on all siRNAs used in this study.

Table 5: siRNAs used in this study.

siRNA	***Composition***	***Manufacturer***
SMARTpool non-targeting control	*4 individual siRNAs*	*Dharmacon*
SMARTpool, FTL	*4 individual siRNAs*	*Dharmacon*
SMARTpool, RAB15	*4 individual siRNAs*	*Dharmacon*
SMARTpool, MGST1	*4 individual siRNAs*	*Dharmacon*

2.1.5 General instrumentation

Table *6*Table *6* contains documentation for all instruments used in this investigation.

Table 6: Devices used in this study.

Machine	***Manufacturer***
ABI 7300 Real-time PCR System	*Applied Biosystems, Foster City, USA*
Accu-jet pro Pipette Controller	*VWR International, Radnor, USA*
Biofuge Fresco Centrifuge	*Heraeus, Hanau, Germany*
BioGard safety hood	*The Baker Company, USA*
Biological Safety Cabinet	*Eppendorf, Hamburg, Germany*
Bioluminescence Imaging (BLI) system	*Xenogen Corp, USA*
BioPhotometer	*Eppendorf, Hamburg, Germany*
BioRad Mini-gel apparatus	*Bio-Rad, Richmond, USA*
CASY Cell counter	*Schaerfe System, Reutlingen, Germany*
CASY cell counter and analyzer	*OLS-OMNI Life Science, ACCELA, BioTech-Europe*
CB 150 Incubator	*Binder, Tuttlingen, Germany*
Centrifuge 5415 D	*Eppendorf, Hamburg, Germany*
Centrifuge 5424	*Eppendorf, Hamburg, Germany*
Centrifuge 5424 R	*Eppendorf, Hamburg, Germany*
Centrifuge 5810 R	*Eppendorf, Hamburg, Germany*
ClarioStar Plus	*BMG LABTECH, Ortenberg, Germany*
Eppendorf 5415C Centrifuge	*Eppendorf, Germany*
FACS Canto II Flow Cytometer	*Becton Dickinson, Franklin Lakes, USA*
Fluoroskan Ascent Microplate Fluorometer	*Thermo Scientific, Dreieich, Germany*
Gel Documentation System	*Bio-Rad Laboratories, Hercules, USA*
Gel iX Imager System	*Intas Science Imaging Instruments, Göttingen, Germany*
HERAcell 150i CO2 Incubator	*ThermoFisher Scientific, Germany*
IVIS Spectrum imaging system	*Perkin Elmer, Germany*
Leica DM1L Microscope	*Leica, Wetzlar, Germany*
LSR II Flow Cytometer	*Becton Dickinson, Franklin Lakes, USA*
Magnetic stirrer	*Heidolph, Germany*
Megafuge 2.0R	*Heraeus, Hanau, Germany*

Micro-centrifuge 2 CMG-060	*neoLab Migge, Heidelberg, Germany*
Micro-centrifuge 5417R	*Eppendorf, Hamburg, Germany*
Micro-Dismembrator S	*Sartorius,Goettingen,Germany*
Mini Laboratory Centrifuge	*neoLab Migge, Heidelberg, Germany*
MP220 pH Meter	*Mettler Toledo, Columbus, USA*
MR 3002 S Magnetic stirring hot plate	*Heidolph Instruments, Schwabach, Germany*
Multifuge x3 FR centrifuge	*Heraeus, Hanau, Germany*
Multipipette E3x	*Eppendorf, Hamburg, Germany*
NanoDrop spectrophotometer	*NanoDrop Technologies, Germany*
Peltier Thermal Cycler PTC-200	*MJ Research, USA*
Pipetboy	*Brand, Wertheim, Germany*
Pipette (P2, P10, P100, P200, P1000)	*Gilson, Bad Camberg, Germany*
Plate Shaker, Polymax 1040	*Heidolph, Germany*
Power PAC 300 power supplier	*Bio-Rad, Richmond, Germany*
QuantStudio 3 Real-Time-PCR-Systeme	*Thermo Fisher Scientific, Waltham, USA*
Qubit fluorometer	*Thermo Fisher Scientific, Waltham, USA*
Refrigerator	*Liebherr, Ochsenhausen, Germany*
Refrigerator (-20 °C)	*Liebherr, Leimen, Germany*
Refrigerator (-4 °C)	*Liebherr, Leimen, Germany*
Refrigerator (-80 °C)	*Thermo Life Science, Germany*
Rotanta 460R centrifuge	*Hettich, Sigma-Aldrich, Germany*
Sorvall RT7 Centrifuge	*Sorvall, Newton, USA*
Synergy2 fluorescence plate reader	*BioTek Instruments*
The anesthetic machine "Sulla" model	*Dräger AG, Lübeck, Germany*
Thermomixer	*Eppendorf, Hamburg, Germany*
Trans-Blot Turbo Transfer System	*Bio-Rad Laboratories, Hercules, USA*
Verti 96-Well Thermal Cycler	*Applied Biosystems, Froster City, USA*
Vortex-Genie 2	*Scientific Industries, New York, USA*
Water bath	*Köttermann, Germany*
Water bath	*GFL, Burgwedel, Germany*
Western blot chamber	*Invitrogen and Serva, Germany*

2.1.6 General consumables

The list of general consumables used in this investigation is in Table 7.

Table 7: General consumables used in this study.

Material	***Manufacturer***
14 mL round bottom high clarity PP test tube	*Corning, New York, USA*
5 mL Polystyrene round bottom tube	*Corning, New York, USA*
Cap for PCR microcentrifuge tubes	*Nerbe plus, Winsen, Germany*
CASY cups	*OMNI Life Science, Bremen, Germany*
CASY ton	*OMNI Life Science, Bremen, Germany*
Cell culture flask 50 mL	*Greiner Bio-One, Kremsmünster, Austria*
Centrifuge tube pp with screw cap PE (15, 50 mL)	*Nerbe plus, Winsen, Germany*
Combitips advanced (0.1, 1, 2.5, 5, 25 ml)	*Eppendorf, Hamburg, Germany*
Corning® 96 well solid polystyrene microplate	*Sigma-Aldrich, St. Louis, USA*
Cryotubes	*Greiner, Frickenhausen, Germany*
Disposable serological pipette (5, 10, 25, 50 mL)	*Corning, New York, USA*
Eppendorf micro test tube 3810X 1.5 mL	*Eppendorf, Hamburg, Germany*
Eppendorf safe-lock microtubes, PCR clean 2.0 mL	*Eppendorf, Hamburg, Germany*
Eppendorf tube 3810X 1.5 mL	*Eppendorf, Hamburg, Germany*
Eppendorf tubes 5.0 mL	*Eppendorf, Hamburg, Germany*
Falcon tubes 15ml, 50ml	*Greiner, Frickenhausen, Germany*
Gloves small 6 - 6.5, Gentle skin classic	*Meditrade*
LumaPlate 96	*PerkinElmer, Waltham, USA*
MicroAmp optical 96-well pate	*Applied Biosytems, Foster City, USA*
MicroAmp optical adhesive film	*Applied Biosytems, Foster City, USA*
Mini-PROTEAN® Combs, 15-well, 1.5 mm, 40 µl	*Bio-Rad Laboratories, Hercules, USA*
Mini-PROTEAN® Short Plates 1.5 mm	*Bio-Rad Laboratories, Hercules, USA*
Mini-PROTEAN® tetra handcast systems, 1.5 mm, 40 µl	*Bio-Rad Laboratories, Hercules, USA*
Nitrocellulose membrane	*Whatmann, Dassel, Germany*
Parafilm M	*Pechiney Plastic Packaging, Chicago, USA*
PCR microcentrifuge tube PP, 0-2 mL, without cap	*Nerbe plus, Winsen, Germany*
Pipette filter tips (10, 20, 100, 200, 1000 µl)	*Starlab, Milton Keynes, United Kingdom*
Pipette tips (10, 20, 100, 200, 1000 µl)	*Greiner, Frickenhausen, Germany*
Plastic serium pipette	*Greiner Bio-One, Kremsmünster, Austria*
Premium Aluminium Foil	*VWR International, Radnor, USA*
Qubit Assay Tubes	*Thermo Fisher Scientific, Waltham, USA*
Reagent Reservoir	*Corning, New York, USA*
Round and Flat bottom 96-well plates	*TPP, Trasadingen, Switzerland*
Safe-Lock tubes (0.5, 1.5, 2 ml)	*Eppendorf, Hamburg, Germany*
Sealing Tape	*Thermo Fisher Scientific, Waltham, USA*
Sterile serological pipettes (5, 10, 25, 50 ml)	*Greiner, Frickenhausen, Germany*
strainer cap	*Becton Dickinson, Heidelberg, Germany*
Syringe	*Terumo, Germany*
Tissue culture flasks (25, 75, 150 cm2)	*TPP, Trasadingen, Switzerland*
Tissue culture plates (6, 12, 24, 96 wells)	*TPP, Trasadingen, Switzerland*

2.1.7 General chemicals and reagents

Table *8* provides an inventory of the chemicals and reagents employed in this study.

Table 8: General chemicals and reagents.

Chemical and reagent	***Manufacturer***
0.25 % Trypsin/EDTA	*Gibco, Carlsbad, USA*
1 × binding buffer	*Biolegend, Germany*
10 % SDS	*Lonza Group, Basel, Switzerland*
2 × LightCycler 480 probes Master	*Roche, Germany*
2-Isopropanol	*Sigma-Aldrich, Germany*
30 % Acrylamide/bis solution, 37.5:1	*Bio-Rad Laboratories, Hercules, USA*
6x Orange loading dye	*Fermantas, St. Leon-Rot, Germany*
Agar-Agar	*Carl Roth, Karlsruhe, Germany*
Agarose	*Sigma-Aldrich, St. Louis, USA*
Amersham ECL prime Western blotting	*GE Healthcare Life Sciences, Chalfont St*
Ammonium persulfate (APS)	*Sigma-Aldrich, St. Louis, USA*
Ampicillin sodium salt	*Sigma-Aldrich, St. Louis, USA*
BD Matrigel basement membrane matrix	*BD Biosciences, Bedford, USA*
Bio-Rad protein assay reagent	*Bio-Rad, Richmond, USA*
Bovine serum albumin (BSA)	*Sigma-Aldrich„ Saint Louis, USA*
Bromphenol blue	*Sigma-Aldrich, St. Louis, USA*
Cell dissociation reagent	*Trevigen, Gaithersburg, USA*
Cell lysis buffer	*Cell Signaling Technology, Beverly, USA*
CellTiter Glo reagent	*Promega, Mannheim, Germany*
Cycloheximide	*New England Biolabs, Frankfurt, Germany*
Detection Reagent	*Giles, USA*
Dimethyl sulfoxide (DMSO)	*AppliChem, Darmstadt, Germany*
DMEM	*Gibco, Carlsbad, USA*
dNTPs (each 10mM)	*Qiagen, Germany*
DPBS, no calcium, no magnesium	*Thermo Fisher Scientific, Waltham, USA*
Ethanol	*Sigma-Aldrich„ St. Louis, USA*
FCS superior	*Biochrom, Berlin, Germany*
Fetal calf serum (FCS)	*PAA Laboratories, Pasching, Austria*
Gene Ruler 100bp DNA ladder	*Fermantas, St. Leon-Rot, Germany*
Gluocose	*Carl Roth GmbH, Karlsruhe, Germany*
Glycine	*GERBU Biotechnik, Gaiberg, Germany*
HCl (1M)	*VWR Chemicals*
HEPES	*Carl Roth GmbH, Karlsruhe, Germany*
Hoechst 33342	*Thermo Scientific, Germany*
Lipofectamine RNAiMAX transfection reagent	*Thermo Fisher Scientific, Waltham, USA*
Magnesium chloride	*Sigma-Aldrich„ St. Louis, USA*
McCoy's 5A	*Gibco, Carlsbad, USA*
Methanol	*Sigma-Aldrich„ St. Louis, USA*
Non-fat milk powder	*Carl Roth GmbH, Karlsruhe, Germany*

O'Gene Ruler 1kb DNA Ladder	*Fermantas, St. Leon-Rot, Germany*
Oligo-dt-primer (each 10mM)	*Fermentas, Germany*
Phenylmethanesulfonyl fluoride	*Sigma-Aldrich, St. Louis, USA*
Phosphate buffered saline (PBS)	*Gibco, Carlsbad, USA*
Ponceau stain	*Thermo Scientific, Germany*
Potassium chloride	*Sigma-Aldrich, St. Louis, USA*
Precision Plus Protein Standard	*Bio-Rad, Richmond,USA*
Propidium Iodide	*Sigma-Aldrich, Germany*
Protein Marker IV (Prestained)	*VWR International, Radnor, USA*
Qubit RNA BR Assay Kit 500 reactons	*Thermo Fisher Scientific, Waltham, USA*
Reaction buffer for RT (5 ×)	*ThermoFisher Scientific, Germany*
Restriction enzymes	*Fermantas, St. Leon-Rot, Germany*
Reverse transcriptase (200 U/ µl)	*ThermoFisher Scientific, Germany*
rh Annexin V - APC (0.5 ml)	*ThermoFisher Scientific, Germany*
RiboLockTM RNAse inhibitor (40 U/ µl)	*ThermoFisher Scientific, Germany*
RNase/DNase free H_2O	*Roche, Germany*
RPMI 1640	*Gibco, Carlsbad, USA*
Sodium chloride (NaCl)	*Sigma-Aldrich, St. Louis, USA*
Sodium dodecyl sulfate (SDS)	*Sigma-Aldrich, St. Louis, USA*
Tetramethylethylendiamine (TMED)	*Sigma-Aldrich, St. Louis, USA*
Tris base	*Sigma-Aldrich, St. Louis, USA*
Trizol reagent	*ThermoFisher Scientific, Germany*
Tryptone	*Sigma-Aldrich, St. Louis, USA*
Tween20	*GERBU Biotechnik, Gaiberg, Germany*
β-Mercaptoethanol	*Sigma-Aldrich, St. Louis, USA*

2.1.7.1 RT-PCR buffers

- TBE buffer (**T**ris- **b**orate, **E**DTA buffer) (5× stock solution)

445 mM	Tris-base	
445 mM	Boric acid	in distilled water
10 mM	EDTA	

- TAE buffer (**T**ris-**a**cetate, **E**DTA buffer) (50× stock solution)

2 M	Tris-base	
2 M	Acetic acid	in distilled water
50 mM	EDTA	

- PAG (**P**oly**a**crylamide **g**el) (5%)

32 ml	distilled H_2O
4 ml	TBE buffer (5×)
5 ml	Acrylamide/Bisacrylamide (40 % solution)
48 µl	TEMED (Tetramethylethylenediamine; Carl Roth, Gaiberg)
128 µl	APS (Ammoniumpersulfate; Serva, Heidelberg)

2.1.7.2 Western blot solutions and buffers

First and secondary antibodies were diluted in PBS pH 7.5 (Sigma, Steinheim) + 0.1% dry milk (Roth, Karlsruhe) + 0.1% Triton X-100 (Gerbu, Gaiberg)

- Washing solution
  - PBS + 0.1% Tween20 (Steinheim, Germany)

  Stripping solution (100 ml)

  6.25 ml 1M Tris-HCl pH6.8

  20 ml 10 % SDS (Serva, Heidelberg)

  Millipore-H2O ad 100 ml

  700 µl β-Mercaptoethanol (Serva, Heidelberg) added directly before stripping

- **Suspension buffer**

  1 mM EDTA pH 8.0 (Gerbu, Gaiberg)

  10 mM Tris-HCl pH 7.6 (Biomol, Hamburg)

  100 mM NaCl (J.T. Baker, Holland)

- **Blocking solution**

  PBS + 5% dry milk (Roth, Karlsruhe)

- **Lysis buffer**

  100 mM Tris-HCl pH 6.8

  4% SDS (Serva, Heidelberg)

  20 % glycerol

- **Semi-dry transfer buffer (1 L)**

  3 g Tris-Base (Roth, Karlsruhe)

14.4 g glycin (Gerbu, Gaiberg)

200 ml methanol (Fluka, Sigma, Seelze)

In addition, Whatman papers were from Whatman Int. Ltd Maldstone, England.

2.1.8 Kits

Table *9* lists the kits that were used in this study.

Table 9: Kits used in this study.

Name	***Manufacterur***
12% Mini-PROTEAN TGX Stain-Free Protein	*Bio-Rad, Richmond, USA*
CellTiter Glo Luminescencent Cell Viability Assay	*Promega, Mannheim, Germany*
CellTrace™ Cell Proliferation Kits	*Thermo Scientific, Boston, USA*
Colorimetric Cell Viability Kit III (XTT)	*PromoKine, Heidelberg, Germany*
ECL Plus Western blotting Detection System	*GE Healthcare, Buckinghamshire, UK*
LightSwitchTM Luciferase Assay Kit	*Active Motif, La Hulpe, Belgium*
LIVE/DEAD® Fixable Yellow Dead Cell Stain Kit	*Life Technologies, Carlsbad, USA*
Malachite Green PO4 Detect Kit	*R& D Systems, Minneapolis, USA*
miRNeasy Mini Kit (250)	*Qiagen, Hilden,Germany*
Pierce BCA Protein Assay Kit	*Thermo Scientific, Boston, USA*
Pierce Renilla Luciferase Glow Assay Kit	*Thermo Scientific, Boston, USA*
QIAGEN Plasmid Maxi Kit	*Qiagen, Hilden, Germany*
RNAeasy Mini Kit	*Qiagen, Hilden, Germany*
SYBR green Master Mix	*Thermo Fisher Scientific, Waltham, USA*
TaqManTM Gene Expression Assays	*Applied Biosystems, Foster City, USA*
TaqManTM Gene Expression Assays	*Applied Biosystems, Foster City, USA*
TaqManTM MicroRNA Reverse Transcription Kit	*Applied Biosystems, Foster City, USA*
TaqManTM miRNA Assays	*Applied Biosystems, Foster City, CA, USA*
TaqManTM Universal PCR Master Mixture	*Applied Biosystems, Foster City, USA*
TGX Stain-FreeTM FastCastTM Acrylamide Kit, 12%	*Bio-Rad, Richmond, USA*
Trans-Blot Turbo Transfer Pack, nitrocelluose	*Bio-Rad, Richmond, USA*
Trans-Blot Turbo Transfer Pack, pvdf	*Bio-Rad, Richmond, USA*
Transcriptor First Strand cDNA Synthesis	*Roche, Applied Science, Mannheim, Germany*

2.1.9 Softwares

Table *10* records the software applications used in this study for data analysis and figure generation.

Table 10: Software used in this study.

Name	***Source***
Ascent Software	*Thermo Scientific, Dreieich, Germany*
Excel version 14.0	*Microsoft Cooperation, Redmond, USA*
FlowJo version 10	*Becton Dickinson, Heidelberg, Germany*
GraphPad Prism 7	*GraphPad Software, San Diego, USA*
Image Lab Software	*Bio-Rad, Richmond, USA*
Ingenuity Pathway Analysis (IPA)	*https://digitalinsights.qiagen.com/IPA*
Inkscape	*https://inkscape.org/*
R 3.0.1	*http://www.r-project.org/*
Transcriptome Analysis Console (TAC)	*Thermo Fisher Scientific, Waltham, USA*

2.1.10 Antibodies

Table *11* contains the antibodies used in this study.

Table 11: Antibodies used in this study.

Antibody	***isotype***	***Catalogue***	***Application***	***Manufacterur***
Anti-COX1	*Rabbit mAB*	*SAB4502490*	*WB*	*Sigma-Aldrich,Germany*
Anti-Rab15 antibody	*Rabbit pAB*	*ab272636*	*WB*	*Abcam, Cambridge, United Kingdom*
Anti-TAF1D Polyclonal AB	*Rabbit IgG*	*PA5-79670*	*WB*	*Invitrogen, Carlsbad, USA*
CD326 (EpCAM) anti-human	*mouse IgG1κ*	*130-113-268*	*FACS*	*Miltenyi Biotec B.V. & Co. KG, Germany*
Ferritin (FTL)	*Rabbit mAB IgG*	*MA5-32244*	*WB*	*Invitrogen, Carlsbad, USA*
Goat anti-Mouse	*IgG-HRP*	*A16072*	*WB*	*Invitrogen, Carlsbad, USA*
Goat anti-Rabbit	*IgG-HRP*	*A16110*	*WB*	*Invitrogen, Carlsbad, USA*
Human SMOC-2 Antibody	*mAB Mouse IgG2B*	*MAB5140*	*WB*	*R&D Systems, USA*
MGST1 Polyclonal Antibody	*Rabbit / IgG*	*PA5-79670*	*WB*	*Invitrogen, Carlsbad, USA*

2.2 Methods

2.2.1 Culturing

LS174T cells were cultured in RPMI 1640 media enriched with L-glutamine (2 mM), penicillin-streptomycin (Pen Strep: insert final concentrations), and 10 % heat-inactivated fetal bovine serum (FBS). Following that, these media were kept at 4°C until use. The LS174T cells were grown in these media in an incubator at 37°C and 5% CO2 in the air.

2.2.2 Introducing CD326 (EpCAM) antibody and a luciferase plasmid into LS174T cells through transfection Animals

Two days before transfection, 2 ml of RPMI medium supplemented with 10 % FCS was added to each well of a 6-well plate, and 4 × 10^4 LS174T cells were planted in each well. After that, the cells were kept at 37°C and 5% CO2 in air. The following day, the RPMI medium was replaced by the same volume of OptiMEM medium.

On the day of transfection, two solutions were prepared for each well:

1. Lipofectamine Solution: This was made up by mixing 5µl of lipofectamine with 245µl transfection medium (OptiMEM). The suspension was gently mixed and incubated at room temperature for 5 minutes.

2. Plasmid-DNA Solution (Figure *9*): This solution consisted of 10µl of plasmid-DNA mixed with 240µl of OptiMEM. The components were smoothly mixed and incubated at room temperature for 5 minutes.

500µl of transfection solution was produced for each well by carefully combining the Lipofectamine Solution and the Plasmid-DNA Solution. This resulted in the

Plasmid-DNA-lipofectamine solution. For twenty-five minutes, the mixture was incubated at room temperature. Then, 500µl of the transfection solution was added after 1.5 ml fresh OptiMEM medium had been added to each well to guarantee optimal transfection effectiveness. To evenly distribute the transfection solution in the well, the plates were gently shaken for one to two minutes. Following a 7–7-hour incubation period at 37°C and 5% CO2, the transfection medium was withdrawn and substituted by 2 ml RPMI medium containing 20 % FCS and 300 µg zeocin / ml. The cells were kept in this selective medium, which was replaced every three to four days for about two weeks or until the IVIS Spectrum imaging equipment could be used to discern the remaining cell foci.

In this instance, LS174T cells that had undergone successful transfection were separated using flow cytometry (FACS) and an EPCAM antibody as marker. The steps in the procedure were as follows:

1. Cell Preparation: Transfected LS174T cells were treated with trypsin, pelleted, and resuspended in 500µl of phosphate-buffered saline (PBS).

2. Filtration: The cell suspension was filtered into sterile FACS tubes to ensure a pure and consistent cell population.

3. FACS Sorting: By FACS technology, cells expressing EPCAM were sorted into individual wells of 96-well plates as single-cell deposits.

The technique made isolating and cultivating single LS1774T cells that completed transfection and displayed the EPCAM marker easier. The technique made it possible to examine and analyze these cells before transplanting them into animals and after they were re-isolated from the liver.

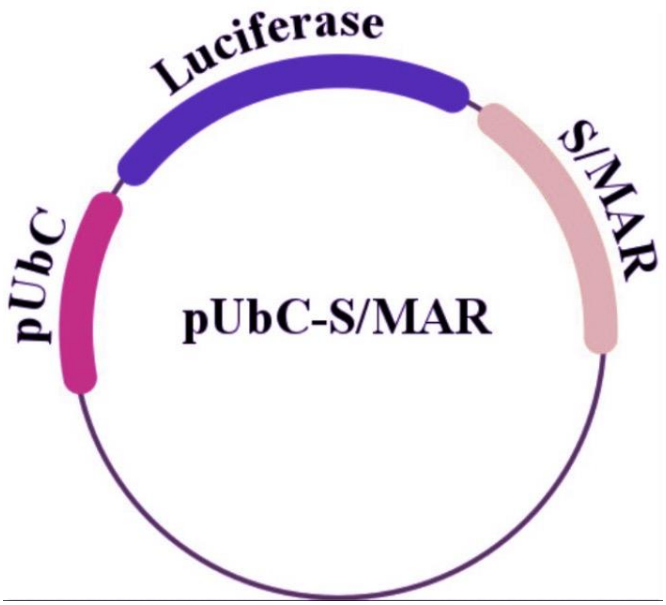

Figure 9: Diagram of the pUbC-S/MAR plasmid, featuring the human Ubiquitin C (UbC) promoter controlling the expression of the luciferase transgene.

2.2.3 Animals

Male nude RNU rats, weighing between 160 - 180 grams and approximately 6 to 8 weeks old, were purchased from Charles River (Sulzfeld, Germany). The controlled environment in which these rats were kept was intended to be specific pathogen-free (SPF). The animals were housed in macrolon III cages with individual ventilation systems installed (Ventirack, UN Roestvaststaal, Zevenaar, Netherlands). This allowed the cages to maintain positive air pressure and a constant 50-fold exchange of filtered air per hour (Bingham, 1990). The rats were fed a regular diet, had full access to autoclaved water and were kept in a controlled environment (temperature of 23°C ± 1°C, 50 % ± 10 % humidity, and a 12-hour dark-light cycle). The rats were allowed one week to acclimatize to their environment before any experimental procedures were started. The Regierungspräsidium Karlsruhe in Germany, which is the responsible institution for animal ethics, had approved all animal experiments for this study (G-235/17).

2.2.4 Anesthesia of Animals

The "Sulla" model anesthetic machine, made by Dräger AG in (Lübeck, Germany) was used to provide anesthesia and analgesia. A plastic tube connected the anesthetic machine to a perfusor, a breathing mask. The rats were anesthetized and placed in a sealed glass chamber with a gas mixture of 0.7 liters of oxygen (O_2), 1 liter of nitrous oxide (N_2O), and 4 volume percent isoflurane per minute. As an alternative, a different technique used compressor-supplied air and isoflurane. After a rat was rendered unconscious, it was placed safely on the operating table (Figure *10*). The air concentration of isoflurane was then adjusted to a range of 1.5–2 volume percent to maintain anesthesia throughout the subsequent procedures.

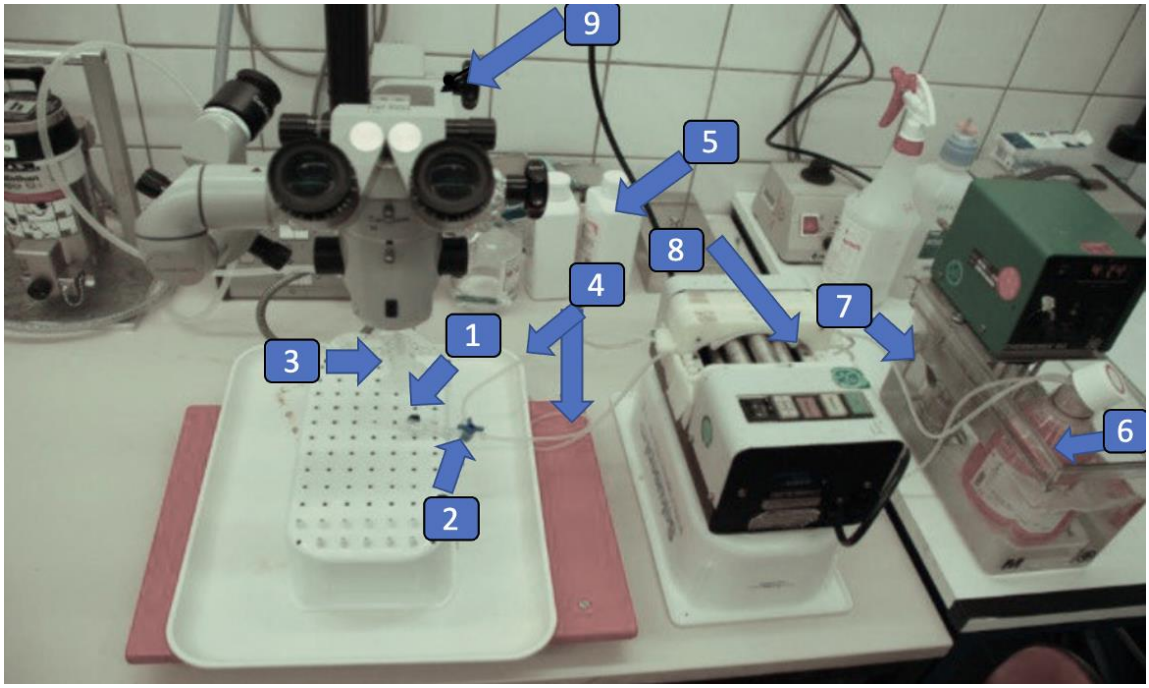

Figure 10: The workplace and equipment employed for liver perfusion.

1. 22 G (0.9 × 25 mm) cannula
2. 3-way-stopcock system
3. Anesthetic falcon (Isoflurane)
4. Connecting tubes
5. Disinfectant (Spitacid, Ecolab)
6. Warmed pre-perfusion/perfusion medium bottle

7. Water bath (warmed to 41 °C)
8. Pump
9. OP-microscope

2.2.5 Isolation of rat liver cells

The first step in the procedure was to prepare an anesthetized rat by shaving and disinfecting its abdomen with alcohol. The mesenteric vein was then carefully located by making an incision in the abdominal wall and gently removing the intestines from the abdominal cavity. The portal vein was punctured with a 22 G (0.9 × 25 mm) cannula, which was then firmly secured with a clip. The posterior (inferior) vena cava was cut to release pressure on the liver and shield the hepatocytes from harm after a one to two-minute pause. The rat was then euthanised by a diaphragm cut. Next, the cannula was attached to a three-way stopcock system, which was then connected without air bubbles to two tubes. These tubes were connected to a bottle holding Hanks' Balanced Salt Solution (HBSS) medium, which was submerged in a heated water bath (40–41 °C) to maintain a constant temperature of 37 °C. The liver was perfused with HBSS medium at a rate of 20 ml/min during the pre-perfusion stage that lasted ten to fifteen minutes. This stage persisted until the liver became light, signifying the blood had been successfully removed. Next, the pre-warmed perfusion medium (250 ml) containing 200 mg of collagenase Type IV (Serva, Heidelberg) and 1M $CaCl_2$ was added to the pre-perfusion media. This step was stopped after the liver had sufficiently softened, usually after about 10 minutes. The rat's liver was then gently removed and quickly put in a sterile Petri dish with cold wash medium.

The liver cells were separated after opening the Glisson capsule and gently suspending the cells in William's media (wash-medium) without using any

mechanical force to avoid damaging the cells. After that, the cell suspension was transferred into two 50 ml tubes and filtered through a sterile 70 µm Nylon cell strainer. Around 25 milliliters of the cell suspension were added to each tube, and wash medium was added up to a total volume of 50 milliliters. In the advanced stage, a micro-dismembrator S (Sartorius, Goettingen, Germany) was used to directly homogenize the tumor nodes. To improve the experiment's performance and produce high-quality data, all parts of the machine that came into touch with the tumor, the forceps, and the tumor itself were submerged in liquid nitrogen before use. Every part was shaken for a variable time, between 30 and 60 seconds, depending on the tumor size. The tubes containing the homogenized tumor powder were then submerged in liquid nitrogen, and the tubes, now containing the homogenized powder, were kept in storage for the next steps at -80°C. The final pellets from the two stages, enriched with hepatocytes, were taken up in Maintenance-Medium without FCS and plated on 6-well plates at a concentration of $7 \times 10^{\wedge 5}$–$10^{\wedge 6}$ per well for hepatocyte isolation.

2.2.6 Preparing LS174T tumor cells for injection

LS174T cells in the logarithmic growth phase were isolated by trypsinization, centrifugation (five minutes at 1500 rpm) and rinsing with PBS. Their number was counted by a Neubauer chamber. The tumor cells were then resuspended, depending on the experiment, at 4°C in a mixture of 350µl PBS and 150µl Biomatrix EHC (Serva, Heidelberg) to a final concentration of 4–8 × 10^6 cells/500µl. Until their implantation, these cell suspensions were kept on ice and shaken occasionally to avoid clumping.

2.2.7 Injection and isolation of LS174T cells Injection

To avoid dehydration, the cecum was carefully put on a sterile pad saturated with NaCl after the abdomen was opened. The mesenteric vein was then positioned using cotton swabs so that needle insertion was faciltated. Before the procedure, 400µl of the LS174T cell suspension was prepared and chilled on ice in a 1 ml syringe fitted with a 30 G needle (BD, Heidelberg, Germany). Cells were injected one to 1.5 centimeters away from the cecum to prevent possible hemorrhage and the dissection of the fat layer in that location. To guarantee ideal cell distribution across all liver lobes, the needle was carefully inserted into the vein, and the inoculation was carried out slowly over two to three minutes. Notably, tumor cells attached to the needle tip may cause tumor growth at the injection site if the circulation does not remove them. As a result, after injection, a 30- to 60-second pause was adhered to before the cannula was removed. To facilitate closure of the vein perforation site, the needle was removed and gently pressed with a cotton swab. After moving back, the cecum, non-absorbable 3-0 fibers were stitched to close the muscle. The skin was closed with staples, which were removed after a few days. Pending on the time, during which the cells were

allowed to grow in the liver, we distinguished between early, intermediate, and late periods, as shown in Figure *11*, before the rats were sacrificed and the LS174Tcells were re-isolated.

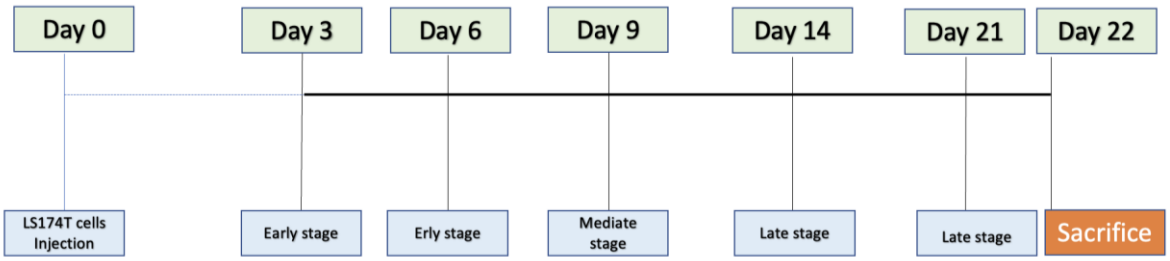

Figure 11: The schematic diagram of different stages and follow up in NUDE rats.

Isolation

This study aimed to investigate the temporal alterations in gene expression that transpire in LS174T tumor cells after homing to and colonization of liver tissue, the first and most important site of metastasis in colorectal cancer. Rat liver was used as model for early, medium, and late periods of metastasis. A large panel of human genes was subjected to microarray analysis to define the genes, which are essential for colorectal cancer cell metastasis on the basis of their altered transcription in response to the liver environment. To that purpose, 20 rats (four for each time point) were used in the re-isolation of LS174T cells after five distinct periods (3 and 6 days as examples of an early stage, 9 days as an example for a middle stage, and 14 and 21days as examples for a late stage of metastatic growth after tumor cell implantation), as shown in Figure *12*.

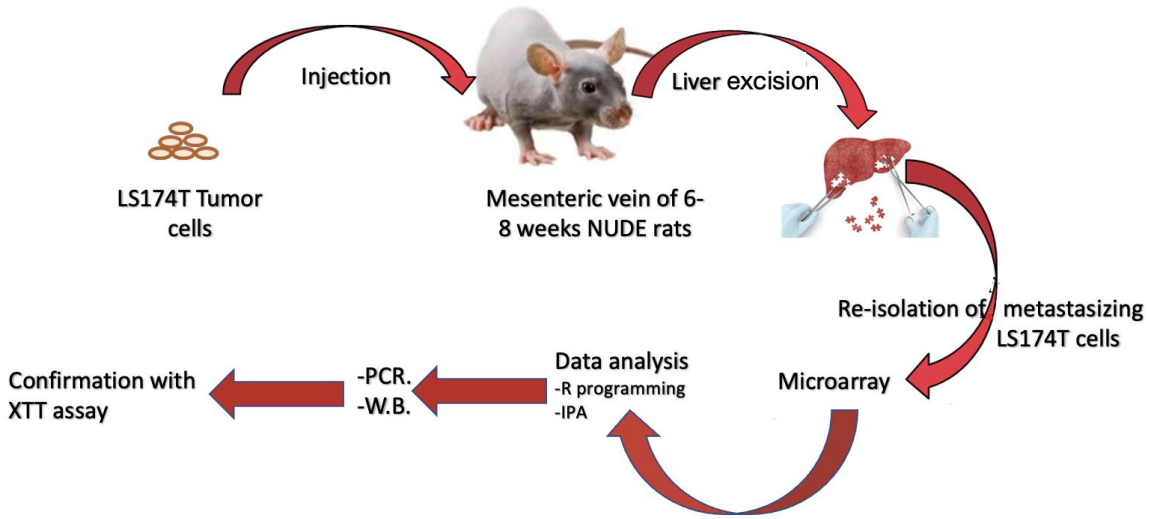

Figure 12:Diagram depicting the experimental process for transplanting, re-isolating, and processing LS174T cells.

Differential numbers of cells were injected according to the time point of tumor cell re-isolation: 8 × 10^6 for the third day of isolation, 6 × 10^6 for the sixth day, and 4 × 10^6 for the ninth, fourteen, and twenty-first days. This was done to guarantee a sufficient supply of re-isolated cells for the subsequent analysis. The protocol for re-isolation of tumor cells was the same as that used for isolating normal liver cells.

In short, the rat's abdominal cavity was opened, and the portal vein was punctured with a 22 G cannula. After that, the HBSS medium (20 ml/min, 37 °C for 10 min) was perfused into the liver. For the early stage, the cell suspension was filtered through a sterile 70μm Nylon filter (Cell strainer) and centrifuged at 300×g for 10 min. After that, the medium was changed to pre-warmed perfusion medium containing pronase to minimize the presence of parenchymal cells (125 ml HBSS with CaCl2 1M, 0.1% pronase, 100 mg collagenase Type IV) at 37 °C for the next 10 min. On a Ficoll gradient medium, the resultant cell suspension of

tumor and liver cells was carefully stacked. The tumor cells were extracted from the top of the interface and resuspended in RPMI media following a 15-minute centrifugation at 500 ×g.

In the early stage, no tumor nodes were visible on days 3 or 6. Tumor nodes were visible when we moved to the Intermediate stage (day 9). However, they weren't as numerous as in the Late stage (day 14 and day 21). Tumor nodes were quickly removed at the Late stage after liver perfusion, snap-frozen in liquid nitrogen, and used in the tests that followed. LS174T cells were further extracted utilizing the FACS technique using an EpCAM antibody as a marker to obtain high-purity of isolated tumor cells. Following a 5-minute centrifugation at 3000 rpm, the early and intermediate stages pure cells were snap-frozen at -80 °C. Reculturing LS174T cells in vitro was done using an aliquot of the cells extracted on day 21. These cells underwent propagation every 3 days, and two intervals (tumor cell explantation at days 14 and 22) were chosen for Western blot, PCR, and subsequent microarray analysis.

Comparative Analysis: Human Colorectal Cancer (LS174T) vs. Rat Colorectal Cancer (CC531) and Rat/Human Pancreatic Cell Lines (ASML & Suit2-007)

In addition to my project, three other projects within our group were selected for a comparative analysis of microarray data with human colorectal cancer data. All four cell lines were introduced via the mesenteric vein of Nude rats for both rat and human colorectal cancer (LS174T and CC531)(Georges, (2011)). For rat pancreatic cancer, ASML cells were injected into BDX rats (AL-Taee, (2016)), while for human pancreatic cancer (Huang, (2019)), Suit2-007 cells were injected into RNU rats. Re-isolation of cells was performed at nearly identical time points (3, 6, 9, 14, and 21) days after tumor cell implantation. The injected cell quantities were carefully standardized across all four studies, ensuring consistency, before proceeding to isolate total RNA for subsequent microarray analysis.(Georges et al., 2010, Al-Taee et al., 2016, Sagini et al., 2018, Huang et al., 2020)

2.2.8 Microarray analysis

Labeling of probes and hybridization on the Illumina Sentrix BeadChip Array

The RNeasy mini-kit (Qiagen, Hilden) was used per the manufacturer's instructions to extract RNA from LS174T cells. Using an Agilent 2100 Bioanalyzer (Agilent Technologies GmbH, Berlin, Germany) and the total RNA Nano chip assay, a gel analysis was used to evaluate the quality of the total RNA. Only samples with an RNA index value of more than 8.5 were selected for expression profiling, and the NanoDrop spectrophotometer (NanoDrop Technologies, Wilmington, DE) was used to measure RNA quantities. Then produced biotin-labeled cRNA samples were hybridized on Illumina human Sentrix-12 BeadChip

arrays (Illumina, San Diego, CA). The modified Eberwine protocol 216 followed Illumina's suggested sample labeling process. Briefly, 250 ng of total RNA was used for the production of complementary DNA (cDNA), and the MessageAmp II aRNA Amplification kit (Ambion, Austin, TX) was utilized for the amplification/labeling step (in vitro transcription) to produce biotin-labeled cRNA. The supplier of biotin-16-UTP was Roche Applied Science (Penzberg, Germany). After being purified on a column using the TotalPrep RNA Amplification Kit, the cRNA was eluted in 60µl water. Using an Agilent 2100 Bioanalyzer and the RNA Nano Chip Assay, the quality of the cRNA was evaluated and quantified spectrophotometrically (NanoDrop).

Unsealed hybridization was conducted in a wet chamber at 58 °C for 20 hours using 50 ng of cRNA/µl in GEX-HCB buffer (Illumina). Mismatch control and biotinylation control oligonucleotides were added, as well as spike-in controls for low, medium, and high abundance RNAs. Microarrays were twice washed in Illumina's E1BC buffer for five minutes at room temperature. A 10-min incubation in 2 ml solution Cy3-streptavidin (1µg/ml; Amersham Biosciences, Buckinghamshire, UK) and 1% blocking solution preceded developing the array signals after a final 5-minute blocking step in 4 ml of 1% (w/v) Blocker Casein in phosphate-buffered saline Hammarsten grade (Pierce Biotechnology, Inc., Rockford, IL, USA). The arrays underwent one last wash in E1BC, were dried, and then scanned.

Scanning and analysis of data

The microarray scanning procedure used a Beadstation array scanner with a scaling factor 1 and PMT settings 430. Every bead had unique data extracted, and outliers were removed if their median absolute deviation (MAD) exceeded 2.5. The standard deviation for each probe was calculated using the remaining data points, which also helped to calculate the mean average signal for a particular probe. The quantile normalization algorithm was used to normalize signals without background subtraction to analyze the data. Differentially regulated genes were found by calculating the standard deviation differences for every probe in one-to-one comparisons of samples or groups. When the bead standard error of treatment and control samples differed more than 12-fold, and the p values were 0.005 or below, the gene expression was significantly changed.

High quality RNA was isolated from transfected LS174T cells using RNeasy mini kit. Samples in triplicates were analyzed by the genomics and proteomics core facility at the DKFZ. Raw data of the microarray was analyzed by Chipster program. Gene expression profiles were then prepared from the analyzed data., where each sample was processed using an Affymetrix Clariom S human chip. The Core facility processed the raw data, and differential gene expression analysis was reliably carried out by comparing the samples to control samples. The Thermo Fisher website (Thermo Fisher Scientific, Waltham, USA) was used to create Venn diagrams.

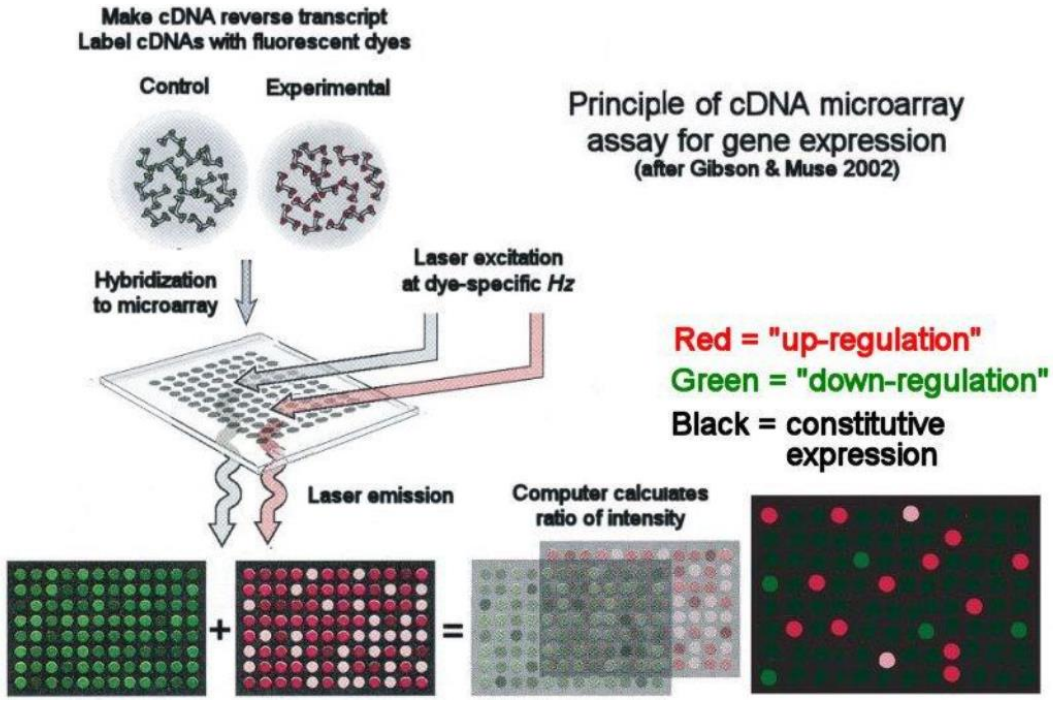

Figure 13: The diagram illustrates the concept of a cDNA microarray.

2.2.9 Isolation of RNA and subsequent Polymerase Chain Reaction (PCR)

Extraction of total RNA

LS174T cells were subjected to RNA isolation using the RNeasy mini-kit (Qiagen, Hilden, Germany). After gently flicking the tubes to ensure that the cell pellets were suspended sufficiently, the appropriate volumes of RLT buffer were added, with 10µl β-mercaptoethanol per 1 ml RLT buffer, to homogenize the samples using a vortex. By pipetting, 70 % of the ethanol was added in a volume equivalent to the homogenized lysate and thoroughly mixed. Next, the mixtures that were produced were put onto RNeasy columns. Following a 20-second centrifugation at 11,000 rpm, washing steps with RW1 and RPE buffers were carried out under the same centrifugation parameters. After binding to the RNeasy silica-gel membrane, the total RNA was eluted using 30–50µl of RNase-free water,

which was spun at 11,000 rpm for a minute. The 260/280 ratio was measured in a spectrophotometer to evaluate samples and quantify RNA amount and purity.

Generation of complementary DNA (cDNA)

A reaction mixture including 100 ng RNA, 1× buffer, 5μM dNTPs, 1μM oligo-dT primers, 10 units of RNAse inhibitor, and 4 units of reverse transcriptase enzyme was incubated at 37 °C for an hour in a total volume of 20 μl to synthesize cDNA from the isolated RNA.

Amplification of cDNA

As shown in Table *12*, two microliters of cDNA from the previous stage were mixed with 1.75 mM of MgCl2, 200μM of dNTPs, 1× buffer, 2.5 units of red taq DNA polymerase, and the appropriate primer pair (each at 0.5μM). The reaction mixture was incubated using the protocol described in Table *12* in a heat cycler (DNA engine, PTC200 Peltier). The PCR results were then examined using capillary electrophoresis or polyacrylamide gel electrophoresis and the samples stored in -80°c for further experiments.

Table 12: The employed PCR protocol.

Step	*Temperature (°C)*	*Time*
1.Initial heating	*95*	*3 min*
2.Denaturation	*95*	*40 sec*
3.Annealing	*60*	*1 min*
4.Elongation	*72*	*40 sec*
5.Final Elongation	*72*	*1o min*
6.Final hold	*4*	*For ever*

*Steps 2 to 4 were repeated for 30 cycles.

2.2.10 Western Blotting

Dissociation with a suitable volume of cell lysis solution enhanced with PMSF (phenylmethylsulfonyl fluoride) was required to isolate proteins from frozen cell pellets and tumor tissue. Following an ice-incubation period of 15 minutes, the samples were centrifuged for 30 minutes at 13,000 rpm and 4°C. Cell lysates were kept at -20°C, and protein quantities were measured using the PierceTM BCA Protein Assay Kit. Protein lysates were subjected to heat denaturation for five minutes at 95°C. Then, using the TransTurboBlot technology, 10–50 μg of protein was combined with 5 times loading dye and put onto a 10 % polyacrylamide gel for electrotransfer onto a nitrocellulose membrane.

The membrane was blocked at room temperature for an hour following transfer by blocking solution (5% nonfat milk). After that, the membrane was incubated over night at 4°C with the corresponding primary antibody in a 5% blocking solution in TBS-T. The membrane was thoroughly washed with TBS-T (1x 10 min, 4-5x 5 min) and then incubated at room temperature on a shaker with the corresponding secondary antibody. Protein signals were found following TBS-T washing using a BioRad ChemiDoc XRS machine and the enhanced chemiluminescence (ECL) system. Using ImageLab software, densitometric measurement of protein bands was carried out. Protein of interest

levels were normalized to Ponceau S levels, which functioned as the loading control.

2.2.11 Polyacrylamide Gel Electrophoresis (PAGE)

On a 5% polyacrylamide gel, the amplicons were separated for two hours at 180V in TBE buffer (10.8 g Tris-Base, 5.5 g Boric acid, 0.74 g EDTA, and H2O to 200 ml). After electrophoresis, the gel was exposed to UV light for two minutes, washed in water for another two minutes, and then submerged in a 0.1/ml ethidium bromide solution for ten minutes (Gel Doc XR, Bio-Rad, Munich, Germany). Quantity One (Bio-Rad Laboratories) was used to perform densitometric analysis.

2.2.12 qPCR

SYBR Green PowerUP PCR Mastermix and 2 µl of cDNA, diluted 1:5 with PCR-quality water, were used in a 20µl reaction for qPCR using cDNA generated from RNA. Table *13* lists all components needed for a single qPCR reaction in detail. Appropriate housekeeping (HK) genes that met the requirement of consistent expression at several time points were selected to normalize the samples. RPL0 or RPL19 were mainly employed as HK genes. When cDNA was produced from RNA, two microliters of the cDNA were added to a 20-microliter PCR reaction.

All qPCRs were performed using an Applied Biosystems 7300 Real-Time PCR equipment or a QuantStudio 3 Real-Time PCR system: Table *14* details the thermal conditions. Three technical replicates were performed on each sample, and the relative expression was ascertained by applying the $2^{\wedge(-\Delta\Delta Ct)}$ technique as follows:

$$\Delta Ct = Ct_{GOI} - Ct_{HK} \quad (2.2.12.1)$$

$$\Delta\Delta Ct = Ct_{siRNA\text{-}XYZ} - Ct_{control} \quad (2.2.12.2)$$

$$\text{Fold change: } FC = 2^{-\Delta\Delta Ct} \quad (2.2.12.3)$$

$$\log (FC) = \log_2(2^{-\Delta\Delta Ct}) \quad (2.2.12.4)$$

Table 13: Components of a single qPCR reaction.

2x Master mix	***fwd_Primer***	***rev_Primer***	***water***
one reaction			
10 ul	*0.4 ul*	*0.4 ul*	*7.2 ul*
20 reactions			
200 ul	*8 ul*	*8 ul*	*144 ul*

Table 14: Thermal conditions of qPCR.

Temperature (°c)	***Time***	***Cycle***
50	*2 min*	*1*
95	*2 min*	*1*
95	*15 sec*	*40*
60	*60 sec*	
72	*30 sec*	

2.2.13 Small Interfering RNA (siRNA) knockdown

Small interfering RNA duplexes were created, particularly targeted at human genes, such as MGST1, FTL, and RAB15. As a negative control, a nonspecific siRNA was also included. Commercially obtained siRNAs from Dharmacon were used for human-targeting siRNAs. The transfection process utilized for LS174T cells transfected with plasmids (described in Paragraph 2.2.1) was repeated for transfecting LS174T cells with siRNA, adhering to the manufacturer's instructions. The target gene determined the range of siRNA concentrations, which was 50–100nM. Cell treatment was carried out in three different plate formats: 96-well for the CFSE test, 24-well for wound healing, and 6-well for the XTT test. Cells were

harvested 24, 48, and 72 hours after administering specific or nonspecific siRNA for Western blot and PCR analysis.

2.2.14 XTT assay

The XTT Cell Viability Kit from Cell Signaling was used to perform XTT tests to evaluate cell proliferation and, more specifically, to determine the effect of particular siRNAs on proliferation. The essay depends on the ability of metabolically active cells to change the orange formazan dye (c) from the yellow tetrazolium salt (XTT). $1 \cdot 10^4$ cells per well of 96-well cell culture plates were used for seeding. The cells were treated, including transfection with siRNA, after 24 hours. After that, 48 hours after treatment, the proliferation was assessed by adding 25µl of the XTT detection solution to 100 µl of culture medium in each well. A ClarioStar microplate reader was used to measure the absorbance at 450 nm after a 60-minute incubation at 37 °C. The reference absorbance was measured at 630 nm. Following the measurement, 100µl of the new medium was added to each plate well and twice cleaned with PBS. This method made it possible to measure each time point using the same plate. For each condition, at least five replicates were carried out.

2.2.15 FLUORESCENCE-ACTIVATED CELL SORTING (FACS)

Idea: Using the flow cytometry technique, one may track and analyze the optical properties of individual cells or suspended particles. It stimulates individual cells with laser light to detect their distinct scattering properties, which are a reliable predictor of their size and shape. The fluorescence intensity of individual cells labeled with fluorescent reporter molecules such as GFP, EpCAM, or FITC can be

monitored simultaneously. This dual detection technique can differentiate particles less than 0.5 microns in diameter (Figure *14*, right).

The device quickly records thousands of cells' individual properties, capturing the data in less than a minute. The collected data can be processed, stored, and shown when the necessary software is installed on a linked computer. Every cell line's scatter and fluorescence properties are optimized by measuring a control probe with unmarked cells. The forward scatter (FSC) and side scatter (SSC) scales are initially set to linear (LIN). The settings of the FSC signal (E00, E01, E02, E03, or E-1) are modified based on the size of the studied cell line. Once the intended cell population is in the middle of the plot, the amplifier adjusts the settings. To remove tiny particles, such as cell debris, from the computation, a threshold is established in the FSC channel. To concentrate on the cells of interest, utilize the gating option in the histogram. A control unstained sample is used to help establish the voltage for the selected fluorescence channel (FL1, FL2, or FL3). Logarithmic representation is used to optimize the fluorescence settings. This ensures that most occurrences (cells) are shown in the first quadrant (left) of Figure *14*. CellQuestPro software is used for subsequent data analysis.

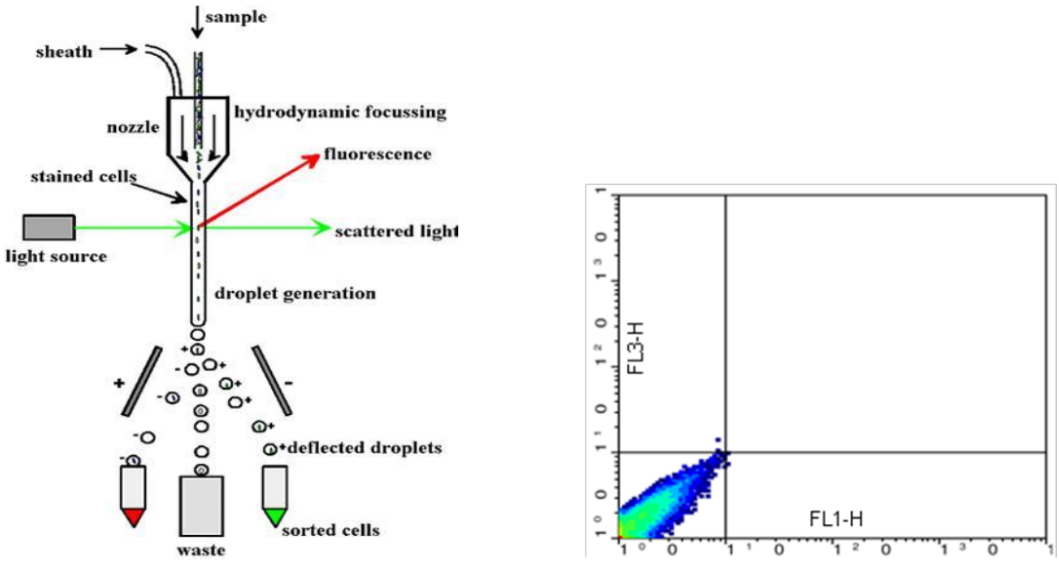

Figure 14: The right panel provides a straightforward depiction of sorting-stained cells through FACS. The left panel illustrates an instance of the fluorescence settings, ensuring that the control cells are positioned in the first quadrant.

2.2.16 Statistics

Re-isolated cells were sorted by FACS analysis with FlowJo (version 10) by gating the single and live cells. Microarray data were analyzed by Chipster, comparing cells re-isolated from liver with cells growing in vitro. A p value ($p < 0.5$) was considered statistically significant. This analysis resulted in expression fold changes for individual genes at each time point. For detailed analysis, filtered genes were evaluated by the R-program. Dynamic changes in gene expression (volcano plots) were generated by R, employing the Transcriptome Analysis Console (Thermo Fisher Scientific, Waltham, USA), limma, and calibrate packages. Category-related genes were visualized in heatmap and ggplots2 packages (https://cran.r-project.org/web/packages/). Statistical significance of dynamic gene changes between groups was determined using ANOVA with Tukey post hoc test, which generated significant p values ($P<0.001$). For comparing all data sets, filtered genes were evaluated with the Ingenuity Pathway Analysis. First, a core analysis was

performed for individual data sets for the common genes in all data sets ($p< 0.01$). For comparison, all data sets were viewed under a comparative feature, which generated a heatmap for respective signaling pathways and functional annotations.

Statistical analysis of the in vivo part:

By measuring signal counts, the dynamic tumor growth in the livers of NUDE rats was captured using an IVIS 100 image system. Student's t-test was used to assess statistical significance between various time points; p-values less than 0.05 were considered statistically significant.

3. RESULTS

3.1 Examining the gene expression profile of LS174T cells upon re-isolation

Using the protocols described in the Materials and Methods section, 21,448 human genes were examined for changes in their expression profiles using a whole mRNA microarray. This investigation aimed to determine the connection between LS174T cell gene expression and liver metastasis. To accomplish this, LS174T cells were intraportally injected into the mesenteric vein of NUDE rats. Figure *15* shows that re-isolation from rat livers was done at different times (3, 6, 9, 14, and 21) following tumor cell inoculation. The re-isolated cells were sorted by FACS.

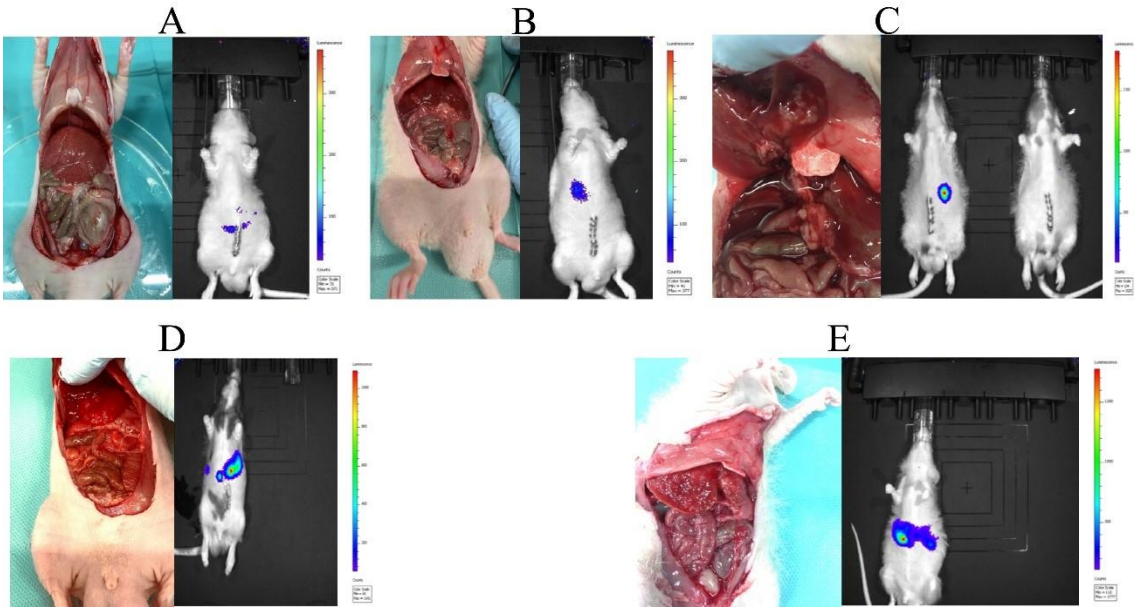

Figure 15: Overview of tumor cells in liver. A: Day 3 Early stage, B: Day 6 Early stage, C: Day 9 Intermediate stage, D: Day 14 Late stage, E: Day 21 Late stage.

The re-isolated cells from the early stages (days 3 and 6) were carefully sorted using FACS. Nodules were closely monitored during the intermediate stage (day 9), and the cells were re-isolated and then subjected to an additional FACS sorting procedure using an EpCAM antibody as shown in appendix Figure *16*. When the cells were re-isolated after 14 and 21 days, they had overgrown the liver, indicating a transition to the late stage. At this point, nodules and tumors were quickly snap-frozen in liquid nitrogen, and the resulting tumor powder was used to isolate mRNA. In addition, the cells were re-isolated and then grown in vitro for 14 and 22 days to perform additional tests.

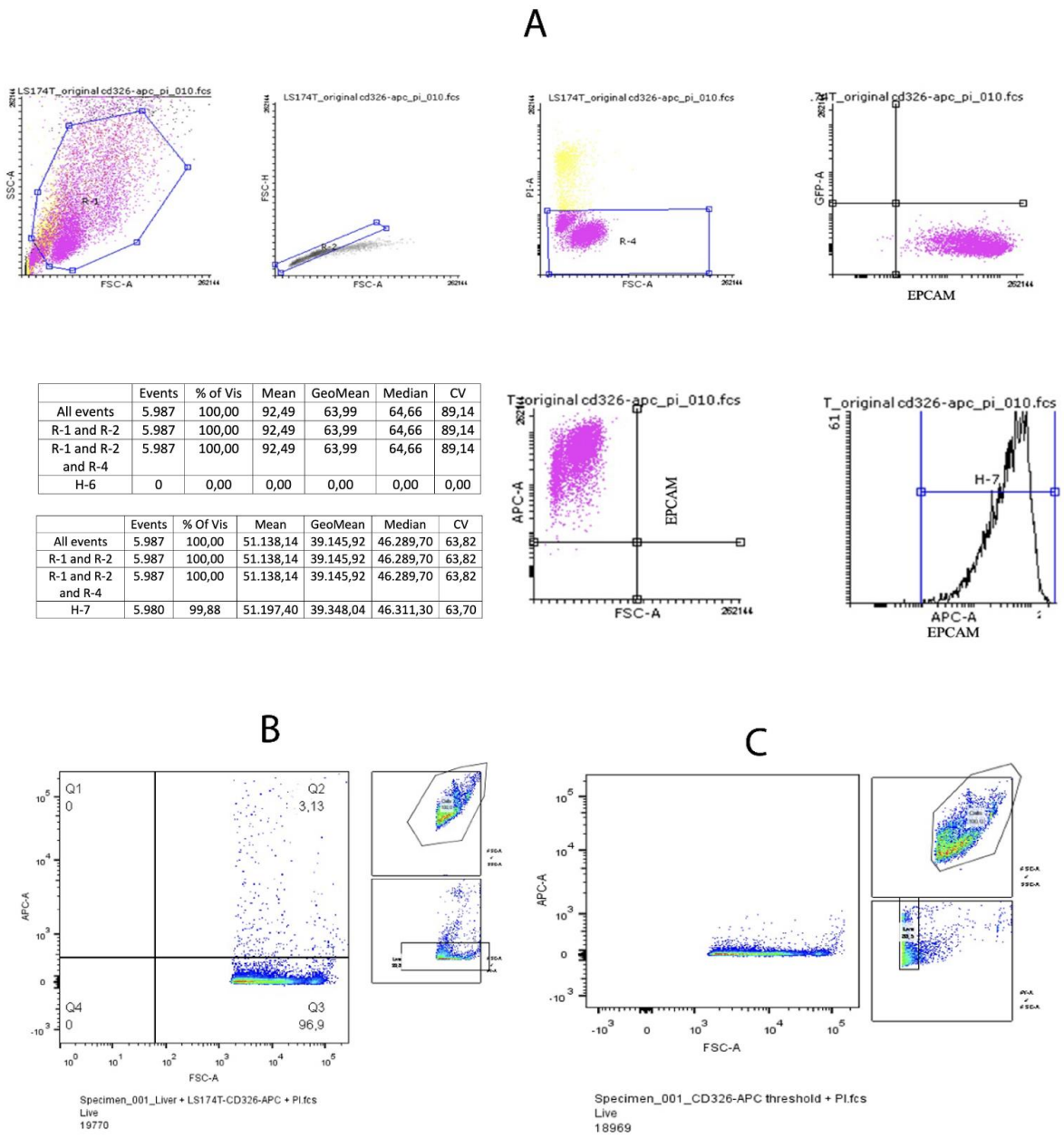

	Events	% of Vis	Mean	GeoMean	Median	CV
All events	5.987	100,00	92,49	63,99	64,66	89,14
R-1 and R-2	5.987	100,00	92,49	63,99	64,66	89,14
R-1 and R-2 and R-4	5.987	100,00	92,49	63,99	64,66	89,14
H-6	0	0,00	0,00	0,00	0,00	0,00

	Events	% Of Vis	Mean	GeoMean	Median	CV
All events	5.987	100,00	51.138,14	39.145,92	46.289,70	63,82
R-1 and R-2	5.987	100,00	51.138,14	39.145,92	46.289,70	63,82
R-1 and R-2 and R-4	5.987	100,00	51.138,14	39.145,92	46.289,70	63,82
H-7	5.980	99,88	51.197,40	39.348,04	46.311,30	63,70

Figure 16 :Overview of LS174T tumor cells in the Liver: First, cells were gated based on their FSC-A and SSC-A. Next, single cells ere gated based on FSC-A and FSC-H. Next, cells were gated on live cells based on staining with PI. Finally, cells were gated on EPCAM-positive population based on their APC signal. (A) A density plot visually represents the LS174T population, meticulously obtained through FACS sorting utilizing the EpCAM antibody (APC) as marker. (B) Illustration of LS174T cells spiked into a liver sample. (C) Visualization of a liver sample stained with EpCAM, highlighting the presence and distribution of LS174T cells.

The analysis revealed dynamic changes in gene expression of LS174T cells isolated at days 3 and 6. These periods were described as early colonization phases with no tumors visible to the unaided eye. 21,448 genes were examined at different stages of colonization. Figure *17* presents some genes and their expression profiles obtained from different time points. A comparative analysis was done to put these modifications into the context of colorectal cancer liver metastasis. When LS174T cells were re-isolated from rat livers at 3, 6, 9, 14, and 21 days after their injection into the mesenteric vein, they provided information on the gene profiles changes as they colonized the liver.

mRNA profile data during the first three and six days after injection showed that a considerable fraction of day three (n = 7231) and day six (n = 6705) genes showed a ≥2-fold increase in expression, while other genes showed a ≤-2-fold decrease in expression at days three (n = 5682) and six (n = 6705). As the cells advanced to the intermediate stage (day 9), they showed evidence of visible infiltration in the form of 1-2 mm-diameter white patches. At this stage, the expression profile was marked by 4343 genes showing a decline and 3332 genes showing a significant increase in expression.

By the time the late colonization stage was reached on day 14, 2346 genes had experienced at least twofold up-regulation, while 1012 genes had undergone at least twofold down-regulation. By day 21, LS174T cells had almost completely colonized the rat liver, signaling the end of the liver colonization process. In this case, 2040 genes were ≥ -2-fold downregulated, and 802 genes showed a ≥2-fold up-regulation.

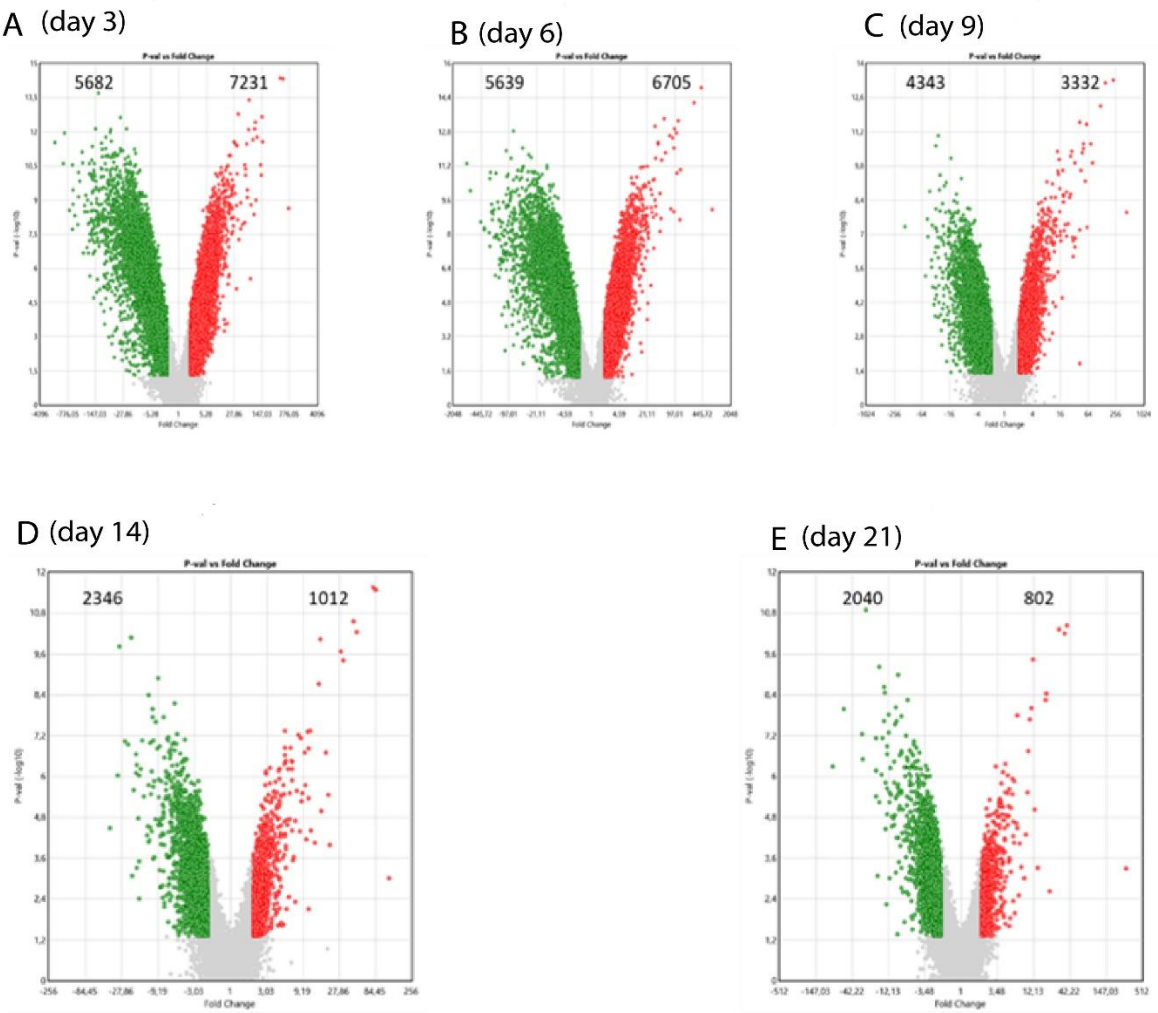

Figure 17: Show the volcano plots for genes modulated in the LS174T colorectal cancer liver metastasis rat model at day 3 (A), day 6 (B), day 9 (C) and day 21 (D). Green represents upregulated genes and red downregulated genes for the respective time points.

3.1.1 Analysis of chip array data

LS174T tumor cells, which had been re-isolated at 3, 6, 9, 14 and 21 days post *i.v.* injection, were analysed by the R-program for genes and genetic pathways showing a correlation with the metastatic process. For the three early time points, the tumor cells were highly pure, as they had been sorted by flow-cytometry from surrounding rat liver cells. For the two later time points (14 and 21 days), the tumor tissue in the liver was used without cell-sorting. Four biological replicates were performed per sample. According to the Principal Component Analysis (PCA)

depicted in Figure *18*, samples from various time points predominantly cluster into three distinct groups. Samples of days 3 and 6 cluster were similar and formed the early cluster. Samples of days 14 and 21 clustered also together (late cluster), whereas samples of day 9 fell in between the early and late clusters (intermediate cluster).

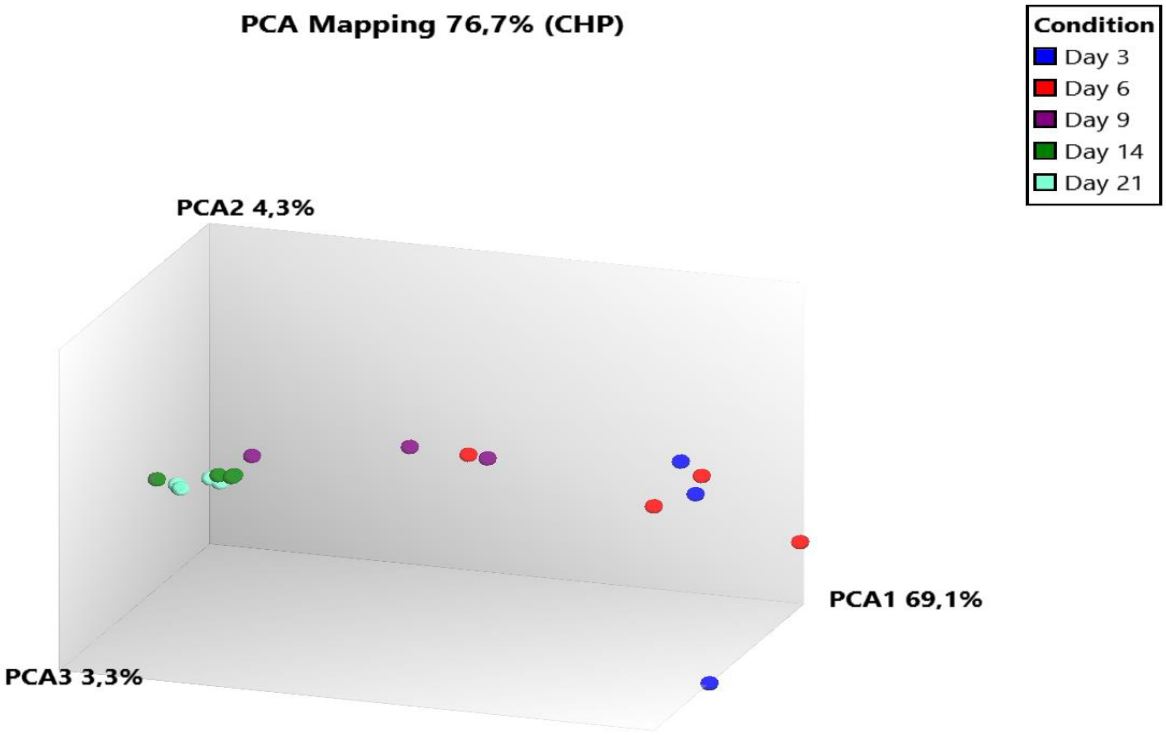

Figure 18: PCA-analysis of microarray data: The PCA mapping shows, that the different data points mainly cluster in three groups. Samples of Day 3 and Day 6 cluster together (early cluster). Samples of Day 14 and Day 21 cluster together (late cluster) and samples).

Using one-way ANOVA with Tukey's honest significance test, genes were selected that had a significant difference in their expression across all time points. Only genes with p-value < 0.005 were considered for subsequent analysis (in total 9352 genes). Mean expression of samples falling into a certain cluster (early, intermediate and late clusters) were calculated and fold changes between

temporally successive clusters were calculated to assess the dynamics of gene expression. Fold changes > 2 were considered as an up-regulation (up) and fold changes < 0.5 as a down regulation (down). Genes were then categorized into different categories:

I. gradually increasing
II. gradually decreasing
III. constant expression
IV. down up up/constant (early low)
V. up up/constant down (late low)
VI. up down down/constant (early high)
VII. down down/constant up (late high)
VIII. down up down or up down up (mixed expression)

Figure *19* shows an example gene for each of the catgories.

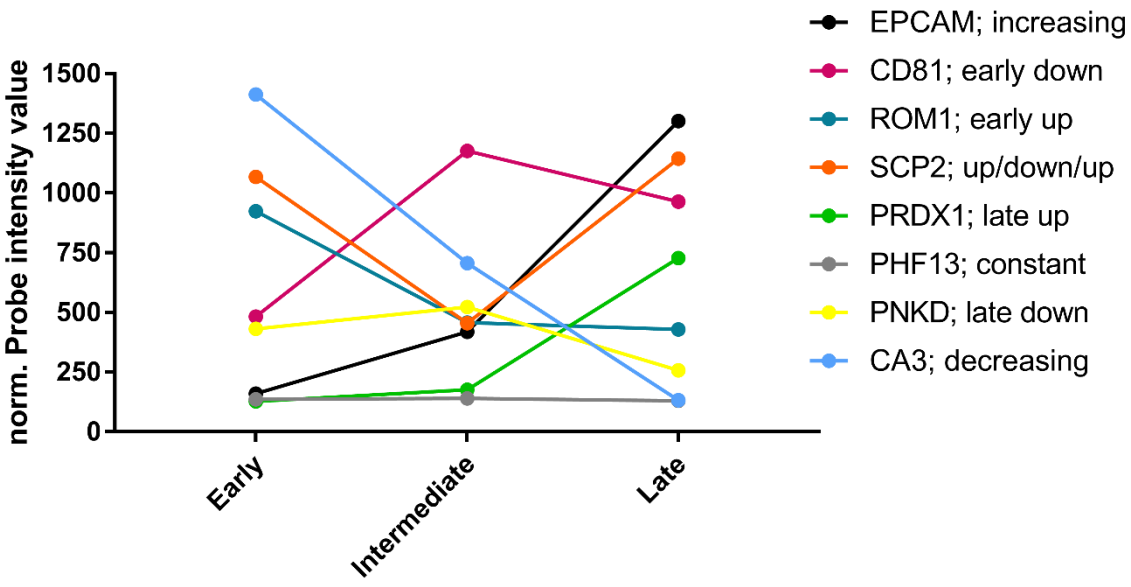

Figure 19: Represents the categorization of genes across different time points. Each gene with significant change across all samples was classified into different groups to examine their temporal expression behaviour. Fold changes > 2 (up) or < 0.5 (down) were considered as change in gene expression between adjacent clusters (early, intermediate, and late cluster). Fold changes between 0.5-2 were considered as constant expression. An example gene for each of the defined eight categories is shown.

Genes falling constantly into the same category were of least interest, since these genes are unlikely to be involved in metastatis formation. Overall, 3978 genes were considered to be constantly expressed across the time course of tumor cell inoculation. Three genes were classified as decreasing over time. 124 genes fell into the category late down and 65 genes into the category early up. Overall, 67 genes were classified as increasing over time. 103 genes fell into the category late up. The second largest category besides constantly expressed genes was early down, which comprised 881 genes.

From different categories (except for constantly expressed genes), several genes were selected for further validation as listed in Table *15*. First, qPCR analysis was performed to verifiy the microarray data. The results are shown in Figure *20*. For some genes their overall CT-values across all samples was very low (Ct > 30) as for CRLF3, COX2, CA3 and SMOC2. These genes were excluded from further evaluation. For most genes the qPCR could confirm the category they were assignerd to. For example, MGST1 and FTL are significantly increasing over time with highest expression at day 21. Noteworthy, the parental cells cultured *in vitro* also exhibit higher expression of these genes compared to cells from early timepoints from *ex vivo* sorted cells. RAB15 was confirmed to belong to the categoy of late up expressed genes and COX1 to the category of early down expressed genes.

Table 15: Selected Genes from different categories. (The full gene names and pathways are shown in Table 20)

Late Up	*Late Down*	*Early Up*	*Early Down*	*Decreasing over time*	*Increasing over time*
TAF1D	*PTEN*	*DPT*	*MT-CO1(COX1)*	*CA3*	*MGST1*
RAB15	*CRLF3*	*NTF3*	*MT-CO2(COX2)*		*SMOC2*
MT-ND4L		*COL4A2*			*FTL*
					HMGB2

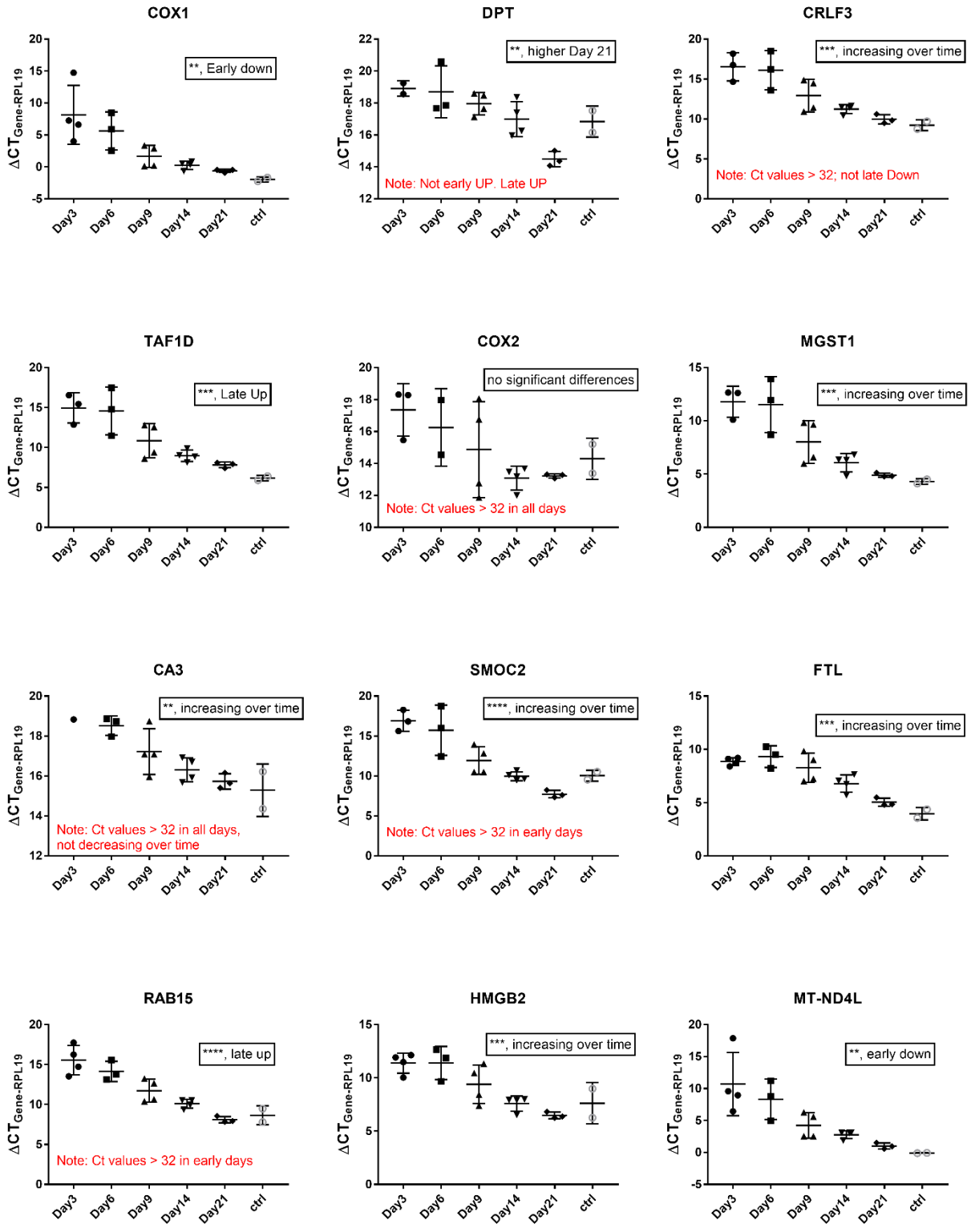

Figure 20: Verification of selected candidate genes by qPCR. The same sample RNA supplied for microarray analysis was used to quantify candidate mRNA levels by a second method (qPCR). RPL19 was used as housekeeping gene. Three technical replicates were performed per condition and 3-4 biological replicates were conducted per time point. Also control parental cells growing in vitro were included (ctrl).

Since RNA level might not reflect changes at corresponding protein level, the protein abundance of MGST1, RAB15, COX1 and FTL was checked in the different samples by Western Blot analysis Figure *32*-Figure *35*. Intensities were measured and quantified as shown in Figure *21*. For COX1 a trend for lower expression at the early time points (days 3 and 6) could be observed. But the deviation between the samples was quite high and no significant difference was seen. For MGST1 very high protein levels were measured for all conditions and no signficant difference was observed. For FTL protein level the increase over time could be confirmed, as there was a signifiant and constitutive increase in FTL protein level reaching its maximum at day 21.

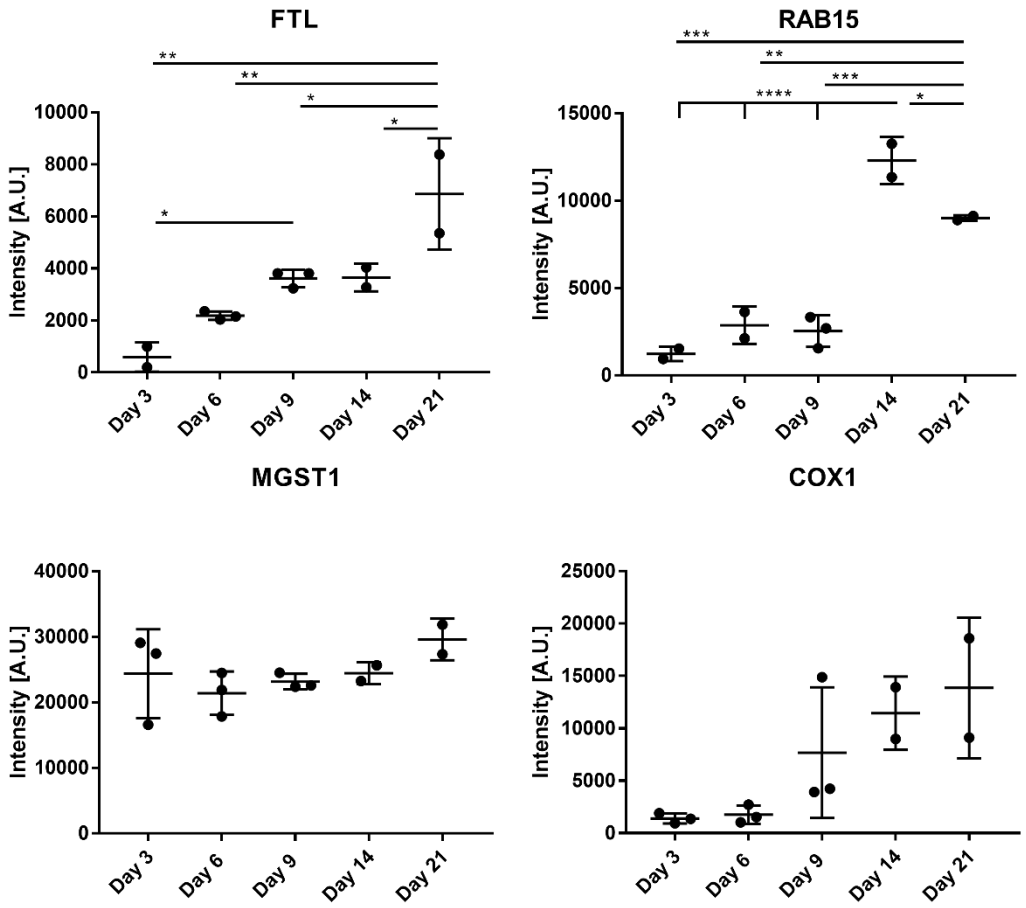

Figure 21: Represents a western blot for selected targets. Protein was isolated from the ex-vivo collected LS174T cells which were collected at different time points after tumour cell injection of LS174T cells into nude rats. For FTL a significant increase of protein expression could be measured across the different days (increasing over time). Also, for RAB15 a significant increase in protein expression was observed. For RAB15 the increase in protein level was not linear as for FTL, but rather a strong increase at Day 14 (late up). Mean values ± SD are depicted. Two to three biological replicates were performed per condition. Significance was assessed by one-way ANOVA with Turkey's multiple comparison test. *: $p < 0.05$; **: $p < 0.01$; ***: $p < 0.001$; ****: $p < 0.0001$.

For the genes FTL, MGST1 and RAB15 siRNAs were used to test functional effects of inhibiting these genes in the parental cell line. First, knock-down efficacy of siRNA pools (consisting of four sequences, targeting respective gene) were tested. As depicted in Figure *22*, all siRNA pools were capable of inhibiting mRNA levels of their respective target gene. FTL and RAB15 siRNA pools could decrease

target expression with a log2 fold change of around -1 (50 % knock-down). The MGST1 siRNA pool reduced target gene mRNA levels by a log2 fold change of around -2 (85 % knock-down). The knock-down was already achieved at 24 h post transfection and respective levels of inhibition were constant also at 48 after transfection.

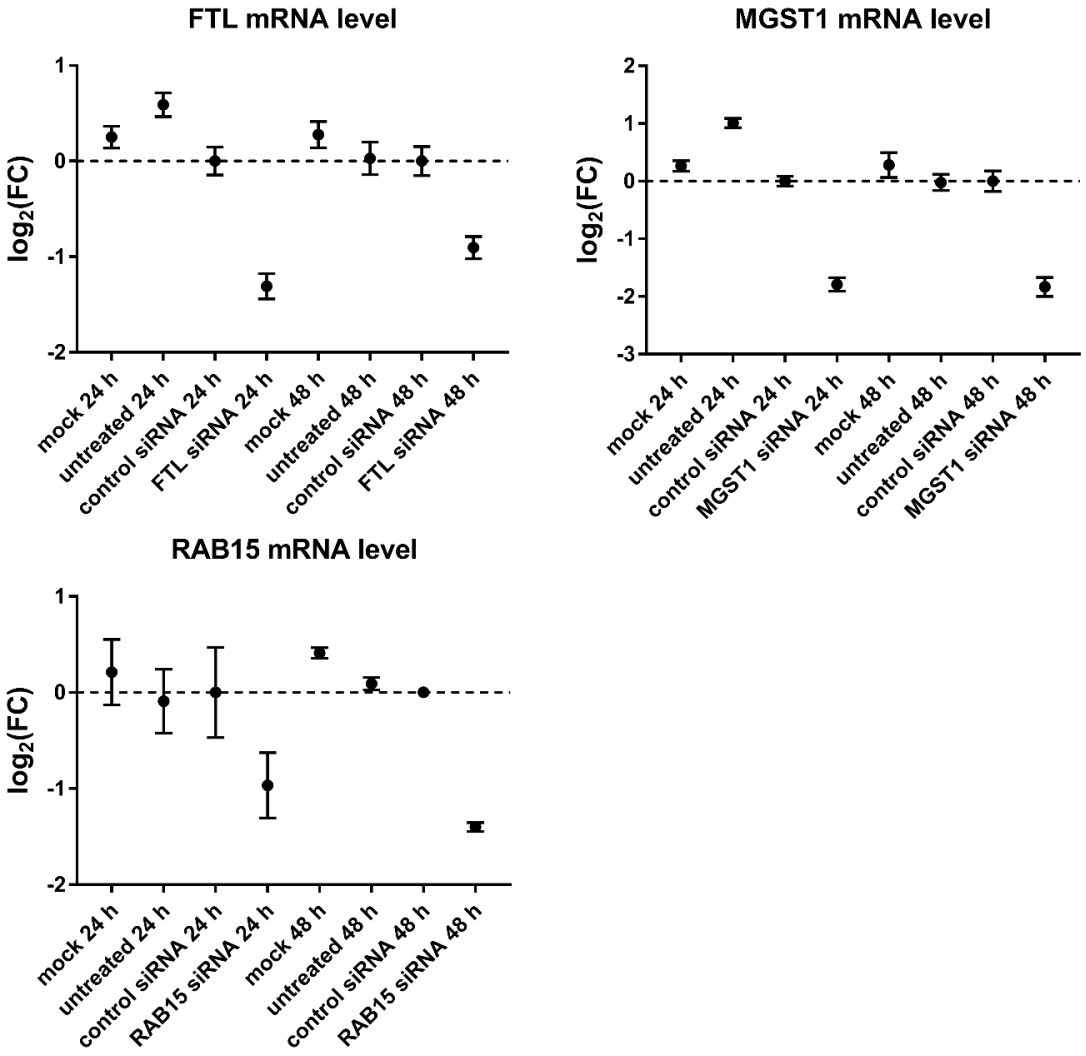

Figure 22: Verification of siRNA-mediated knock-down of FTL, MGST1 and RAB15, respectively. LS174T cells were transfected with 50nM siRNA. 24 h and 48 h post transfection cells were harvested, and RNA was isolated and used for qPCR. FTL, MGST1 and RAB15 mRNA levels were measured. RPLP0 was used as housekeeping gene. Samples were normalized to control siRNA transfection of the respective time point. FTL-, MGST1-, and RAB15-siRNA pools successfully reduced the mRNA level of their respective target. Three technical replicates were performed per condition.

Next, parental cells were transfected with different siRNA pools, and cell viability was assessed with XTT assay two days after transfection. The results are summarized in Figure *23*. The FTL siRNA pool had no significant effect on cell viability compared to control transfection. Both, MGST1- and RAB15 siRNA pools significantly enhanced cell viability. The strongest effect was observed with the RAB15 siRNA pool.

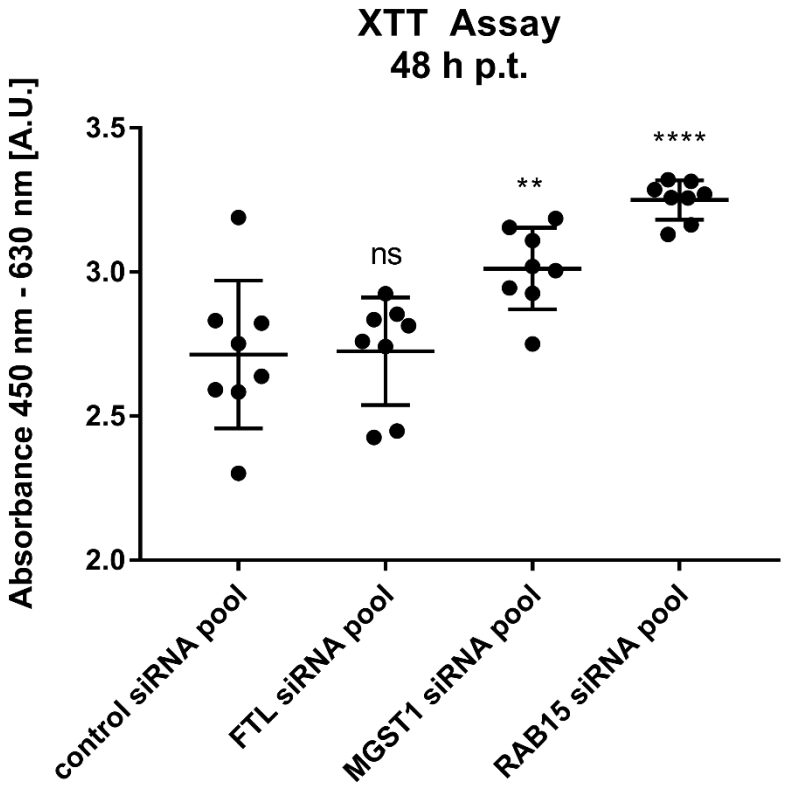

Figure 23: Effect of siRNA-mediated knock-down of FTL, MGST1 and RAB15 on cell viability, respectively. LS174T cells were transfected with 50-100 nM siRNA. 48 h post transfection, XTT assay was performed. Eight replicates were performed per condition. Samples were compared to control siRNA pool and significance was assessed by One-way ANOVA with Dunnett's multiple comparison test. *: $p < 0.05$; **: $p < 0.01$; ***: $p < 0.001$; ****: $p < 0.0001$.

3.2 miRNA expression profile in the LS174 liver metastasis model

Besides mRNA expression, also miRNA profiling was performed in LS174T cells at the different time points after they were injected i.v. into rats. Similar to mRNA data, the miRNAs were classified into different categories based on their expression level at the different time points. Most miRNAs showed a mixed expression pattern. Overall, 5578 miRNAs followed the pattern Down/Up/Down, with peak expression levels at day 9 and significantly lower expression at early days (3, 6) and late days (14, 21). These miRNAs were not considered for the following analysis. 27 miRNAs followed the expression pattern Late Down e.g., miR-1260a as shown in Figure *24*. Only the two miRNAs miR-200b-3p and miR-141-3p followed the expression pattern Increasing over time. 243 miRNAs were assigned to the category Early Down like miR-141-3p, miR-200c-3p or miR-17-5p, which are shown in Figure *25*.

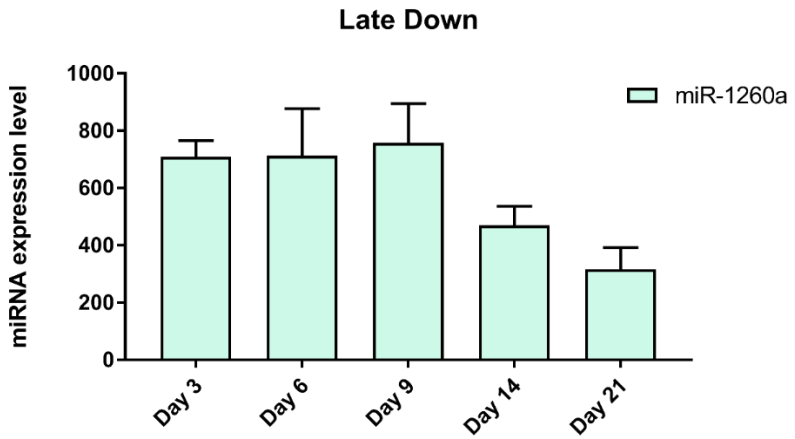

Figure 24: miR-1260a levels classified as expression pattern Late down. Overall, 27 miRNAs were grouped into this category. The expression level of miR-1260a across the different days are shown. Mean values ± SD are depicted. 4 biological replicates were performed per condition.

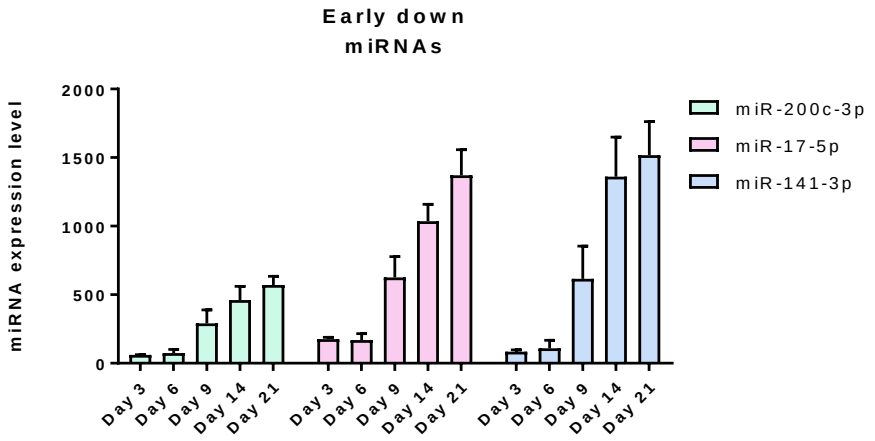

Figure 25: Example miRNAs following expression pattern Early down. Overall, 243 miRNAs were grouped into Early down miRNA category. The expression level of miR-200c-3p, miR-17-5p and miR-141-3p across the different days are shown. Mean values ± SD are depicted. 4 biological replicates were performed per condition.

Since miRNA microarrays were performed on the same samples as mRNA microarray (day 3, 6, 9, 14 and 21), it was specifically assessed, which miRNAs exhibit a negative correlation with certain genes. Of potential interest are for example potential oncogenes from the mRNA data (Increasing over time, Late Up or Early Down) and miRNAs with negative correlation showing a decreasing expression pattern over the measured time points. Also, miRNAs that showed increasing expression over the time points with a negative correlation to potential tumor suppressor genes (Decreasing over time, Early Up or Late Down) are interesting pairs. Thus, for all miRNAs (#4649) and all genes assigned to either of the categories decreasing over time, increasing over time, early up, late up, early down or late down (#1243) the pairwise Pearson correlation was calculated. Only miRNA-mRNA pairs with a Pearson Correlation Coefficient (PCC) < -0.8 were considered. Overall, 8523 miRNA-mRNA pairs were retrieved. For each of these pairs, the PCC, the category of the gene and potential miRNA 3'-UTR binding was documented. As shown in Figure *26*, the correlation of miR-1260a with selected genes (see Table *15*) is depicted. For two of the genes miR-1260a has predicted

binding sites within the targets 3'-UTR: BSG and SMOC2. For these genes, the down-regulation of miR-1260a is a potential explanation for the increased expression of these targets.

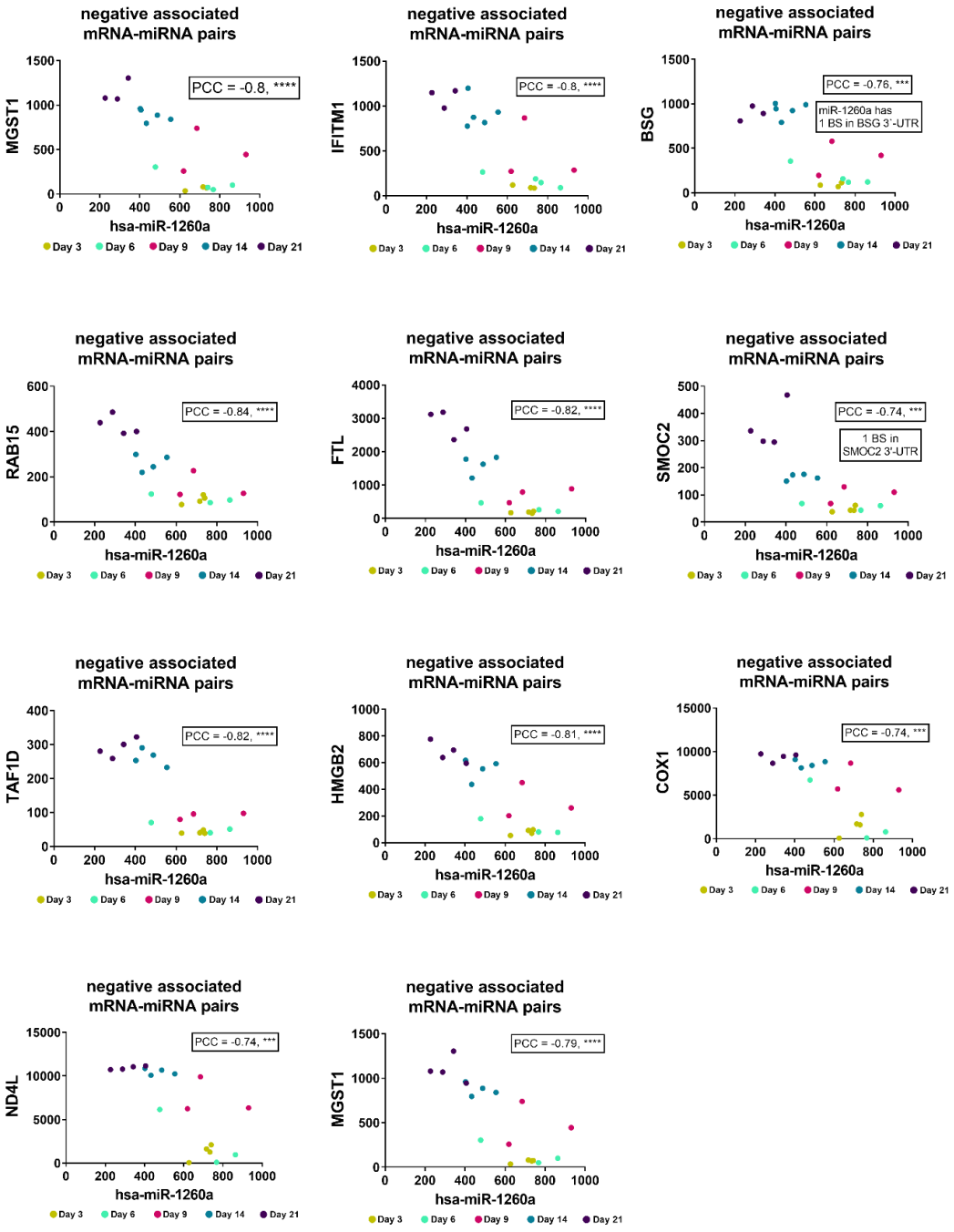

Figure 26: Correlation of miR-1260a levels with respective gene expression values. miR-1260a levels significantly correlate negatively with many genes' mRNA levels that show increasing expression pattern (Early Down, Late Up or Increasing over time). miR-1260a is a miRNA being down-regulated at the late days (14 & 21). Pearson Correlation Coefficients were calculated, and significance was assessed (two-tailed). *: $p < 0.05$; **: $p < 0.01$; ***: $p < 0.001$; ****: $p < 0.0001$.

In Figure *27* some more miRNA-mRNA pairs are shown. Especially PTEN, a known tumor suppressor, showed significant strong negative correlation with overall 31 miRNAs, amongst them miR-141-4p, miR-200b/c-3p and miR-17-5p. PTEN (Phosphatase And Tensin Homolog) levels are lowest at late time points (Late Down) whereas the miRNAs are high at late time points (Early Down). Direct targeting of miR-141-3p, miR-200b-3p or miR-200c-3p with PTEN 3'-UTR could be a possible mechanism for the observed downregulation of this gene. Also interesting might be the direct inhibition of chemokine CXCL12 (C-X-C Motif Chemokine Ligand 12) by miR-92a-3p. Furthermore, the downregulation of DPT (Dermatopontin) by miR-7-5p or miR-429 might be an interesting mechanism of metastasis formation and cancer cell survival at the new niche. DPT mediates adhesion by binding to surface integrins and activates TGFB1(Transforming Growth Factor Beta 1) activity (Okamoto et al., 1999). It is known to inhibit cell proliferation and its down-regulation at late time points might be beneficial for cancer cells to grow within the new microenvironment after successful extravasation and infiltration (Yang et al., 2021, Wang et al., 2019) (Kim et al., 2021).

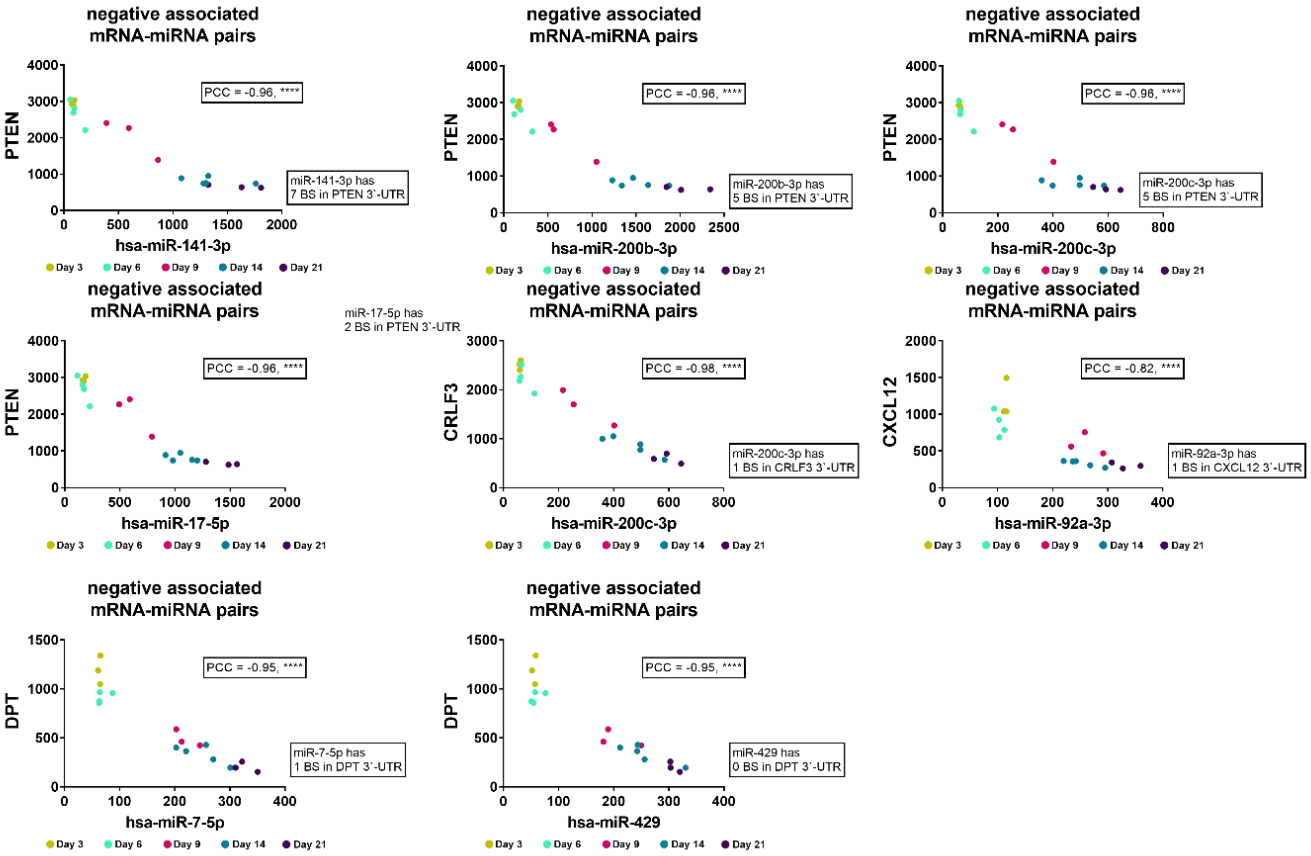

Figure 27: Correlation of selected miRNAs levels with respective gene expression values. miR-141-3p, miR-200b-3p, miR-200c-3p, miR-17-5p, miR-92a-3p, miR-7-5p and miR-429, levels significantly correlate negatively with target genes' mRNA levels that show an increasing expression pattern (Early Down, Late Up or Increasing over time). Pearson Correlation Coefficients were calculated, and significance was assessed (two-tailed). *: $p < 0.05$; **: $p < 0.01$; ***: $p < 0.001$; ****: $p < 0.0001$.

3.3 Analysis of chip array data by the Ingenuity Pathway Analysis

As described earlier, analysis of chip array data for the LS174T model with R-program, lead to the identification of genes associated with tumor progression. Based on these findings, it was necessary to investigate whether these findings are also observed in other cell lines growing in the rat liver. For this reason, the Ingenuity Pathway Analysis (IPA) platform was used for comparative analysis. The three data sets used for analysis include CC531 (rat colorectal cancer cell line), ASML and Suit2-007 (rat and human pancreatic cancer cell

lines). For CC531, the experimental design was similar to that of LS174T, as described in the methods section(Georges et al., 2010). For pancreatic cancer cells, tumor cells were injected intraportally into the rat liver, via the mesocolic vein. In the ASML model, a chip array was performed for cells re-isolated from the rat liver at different time points: day 3, 6, 15 and 21 (Al-Taee et al., 2016). However, in Suit2-007 model, cells growing in the liver were re-isolated at one time point only (day 21) (Sagini et al., 2018). For each of these data sets, cells re-isolated from the liver were compared to those growing in vitro. The comparison for these data was performed for the advanced (day 14 or 15) and terminal stages (day 21). This was necessary because the number of modulated genes in the principal data set (LS174T) were less compared to those in the early and intermediate stages (See Figure *17*). In addition, the data set for Suit2-007 animal model was obtained from the terminal stage. All four data sets were filtered and individually analyzed by IPA. A comparison of the most important signaling pathways and functional annotations were obtained as shown in Figure *28* A and B. A comparative evaluation of the four data sets by IPA resulted in identifying those signaling pathways that are important in the advanced and terminal stages in the LS174T rat model. A heat map for the most up-regulated and down-regulated pathways is given in Figure *28* B. In addition, the functional annotations for various genes are also presented. In total, 25 signaling pathways were identified from IPA. When comparing all data sets, the LS174T model had the most activated pathways. These pathways, were either inactivated or less activated in CC531, ASML or Suit2-007 rat models. This means, the genes associated with these signaling pathways were either downregulated or had insignificant expression fold changes in the

pathways of the respective animal models. The S100 family pathway, the tumor microenvironment pathway, colorectal cancer metastasis pathway, HIFα1 pathway and GP6 pathway were the most activated in the LS174T animal model. Comparatively, only the S100 family, IL-17 and calcium signaling pathways were slightly activated in Suit2-007 pancreatic cancer.

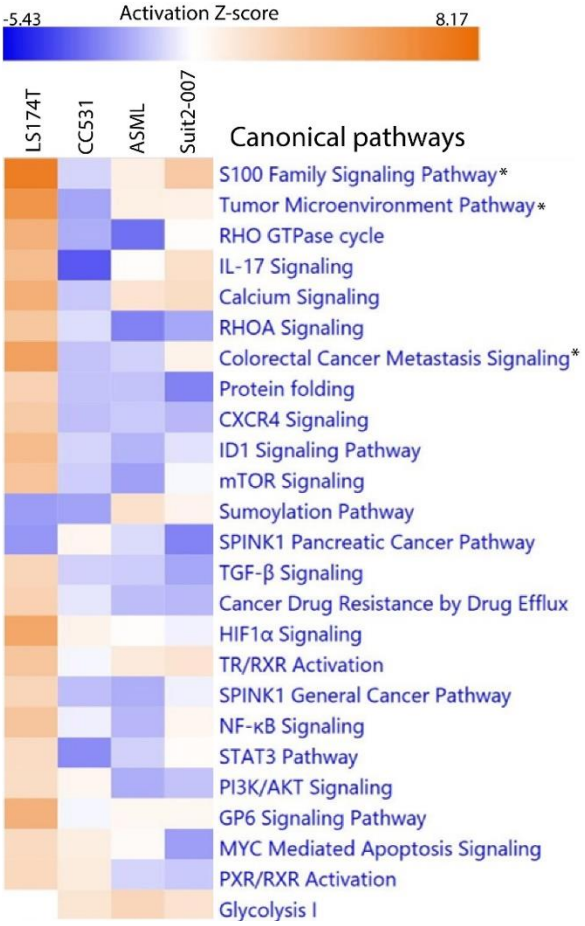

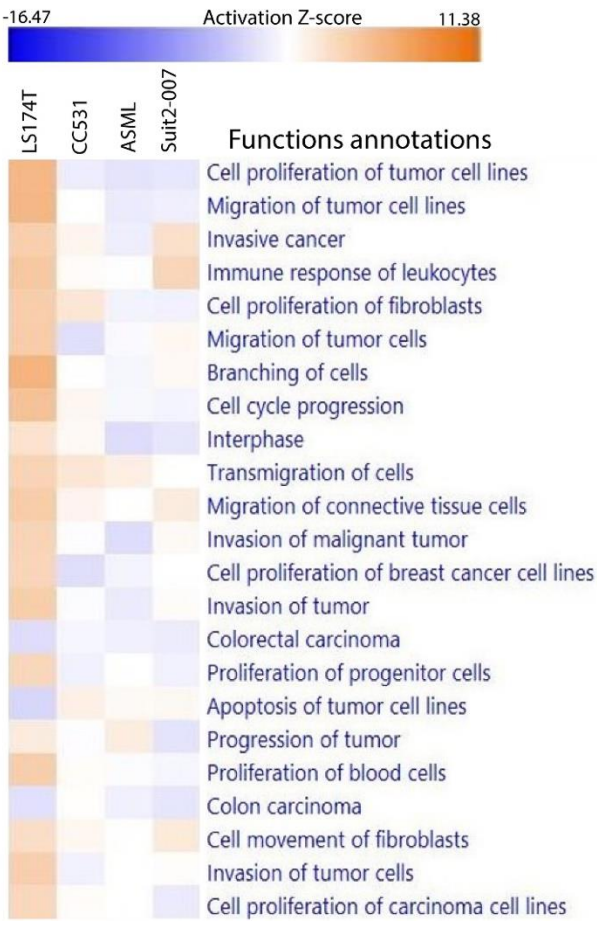

Figure 28 A

Figure 28 B

Figure 28: A: heatmap for important cell signaling pathways in four data sets from chip array experiments. Respective cell lines were implanted into animal models for tumor growth in the liver. The chip array was performed for tumor cell re-isolated from liver at various time points. 3.14B shows significant function annotations for the same data sets as evaluated by IPA. Red and blue represents activation and deactivation (of gene clusters), respectively. Faint red/blue to white represent insignificant to inactive or absence of the pathway.

Among the downregulated pathways, the IL-17 and RHO GTPase were the most activated in the CC531 and ASML rat models, respectively. However, in Suit2-007 model, the most deactivated (silenced) pathways include the protein folding and SPINK1 pancreatic cancer pathway. Interconnected with the signaling pathways are the functional annotations for individual genes or genes in a cluster. The biological function of the gene cluster is measured by the Z-score, which indicates the significance of individual gene expression changes in a cluster. A positive or negative score in the gene cluster indicates activation or deactivation of the whole pathway or biological function. In the LS174T model, functional annotations associated with metastasis (cell movement, cell migration, cell signaling, cell proliferation and cell survival) had a significant Z-score compared to data sets from other animal models. With a threshold of -2 or +2 Z-score, selected signaling pathways and functional annotations from the LS174T animal model are summarized in Table *16*. A significant Z-score (< -2 or > +2) indicates the importance of these pathways or functional annotations in colorectal cancer metastasis.

Table 16: Signaling pathways and functional annotations for LS174T animal model.

Canonical Pathways[a]	Z-score[b]	Function Annotations[c]	Z-score[d]
S100 family pathway	7.04	Cell viability/Survival	9.08
Tumor microenvironment pathway	5.83	Transport of molecules	8.43
Colorectal cancer metastasis	5.11	Microtubule dynamics	8.09
HIF1α signaling	4.81	Cell movement	7.31
Calcium signaling	4.36	Migration of cells	7.19
RHO GTPase cycle pathway	4.24	Fatty acid metabolism	7.18
GP6 signaling pathway	4.24	Cell-cell contact	6.63
Activin inhibin pathway	3.67	Invasion of tumor cell lines	6.27
ID1 signaling pathway	3.66	Phosphorylation of proteins	6.10
IL-17 signaling	3.64	Endocytosis	6.09
WNT/Ca+ pathway	3.16	Homing of cells	6.07
TR/RXR Activation	3.13	Branching of cells	5.69
RHOA signaling	3.05	Phagocytosis	5.65
CXCR4 signaling	2.84	Angiogenesis	5.60
Xenobiotic metabolism PXR pathway	2.67	Formation of actin filaments	5.54
Protein folding	2.45	Proliferation of connective tissue cells	5.35
MTOR signaling	2.24	Formation of cytoskeleton	5.17
MYC mediated apoptosis signaling	2.00	Metabolism of carbohydrate	4.97
Sumoylation pathway	-2.11	Cell cycle progression	4.64
SPINK1 pancreatic cancer pathway	-2.24	Transcription	4.45

a,b Signaling pathways and respective Z-scores for the LS174T model as evaluated by IPA.

c,d Functions annotations and respective Z-scores for the LS174T model as evaluated by IPA.

The most activated pathway include the s100 family signaling pathway, followed by the tumor microenvironment and the colorectal cancer signaling pathways.

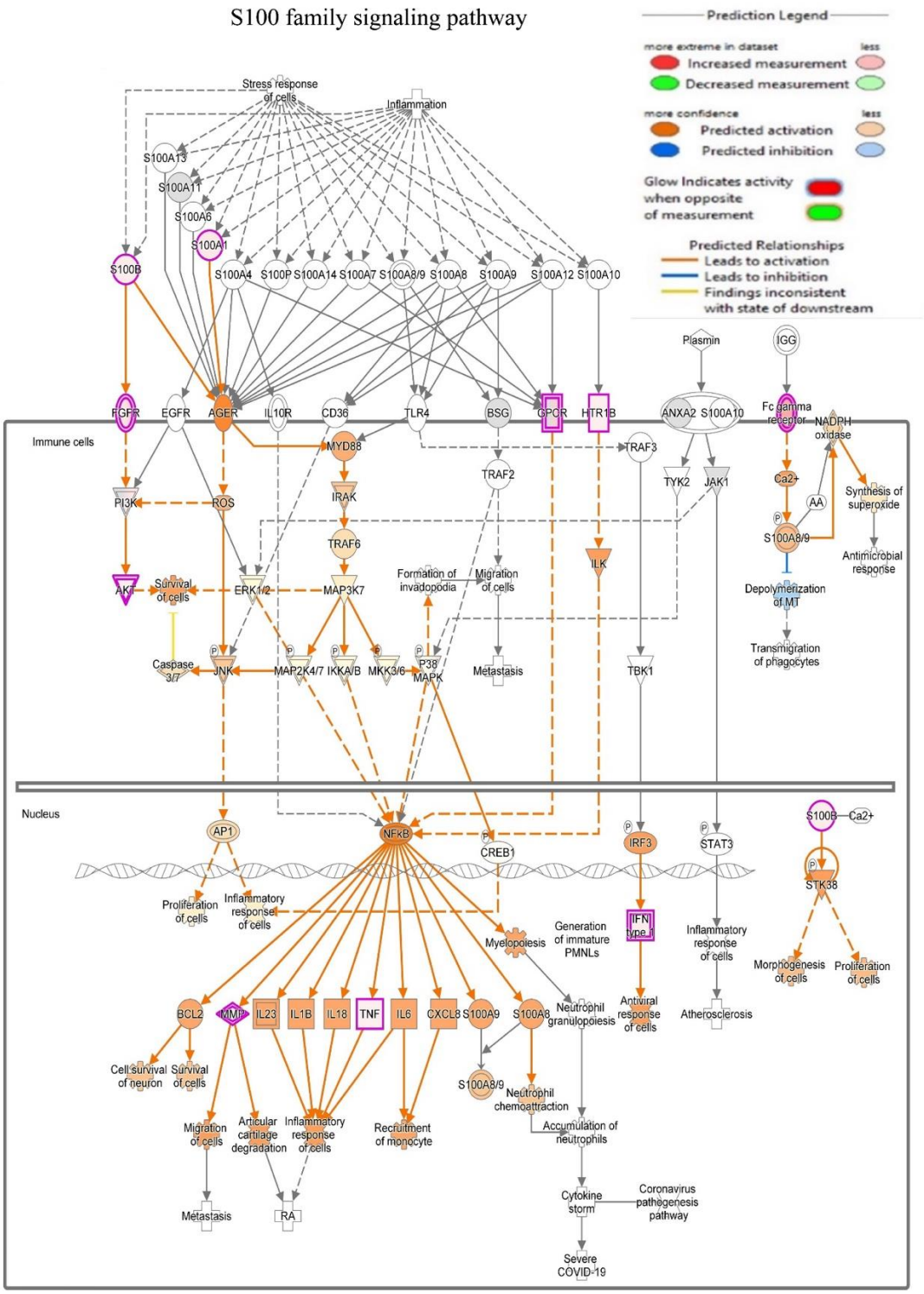

Figure 29: The S100 protein family signaling pathway. The pathway is activated by stress response and inflammation. The entire signaling pathways of S100 protein family is shown in the supplementary information. The S100 protein family had the greatest number of modulated genes (29). Of all the S100 family members, S100A1 and S100B were upregulated and can be activated by cellular stress and inflammatory signals. These proteins activate Fibroblast Growth Factor Receptor 1 (FGFR) and Advanced Glycosylation End-Product Specific Receptor (AGER), which induce cell proliferation and survival via cytoplasmic proteins including AKT and nucleus NK-kB.

Table 17: Genes modulated in the S100 family signaling pathway.

Gene symbol[a]	Description[a]	Expression FC[b]
NR3C1	Nuclear receptor subfamily 3 group C member 1	4.54
VCAM1	Vascular cell adhesion molecule 1	3.20
NOS2	Nitric oxide synthase 2	3.10
S100A1	S100 calcium binding protein A1	2.83
S100B	S100 calcium binding protein B	2.65
PLAT	Plasminogen activator, tissue type	2.59
CACYBP	Calcyclin binding protein	2.58
NCL	Nucleolin	2.47
HTR1B	5-hydroxytryptamine receptor 1B	2.47
TNF	Tumor necrosis factor	2.47
GSK3B	Glycogen synthase kinase 3 beta	0.41
SAPPalpha	Amyloid beta precursor protein	0.41
SMAD3	SMAD family member 3	0.41
TRPV6	Transient receptor potential cation channel subfamily V member 6	0.39
JAK1	Janus kinase 1	0.39
RHOA	Ras homolog family member A	0.38
MAP3K8	Mitogen-activated protein kinase kinase kinase 8	0.37
BSG	Basigin (Ok blood group)	0.36
IL1B	Interleukin 1 beta	0.34
CTSD	cathepsin D	0.32
SP1	Sp1 transcription factor	0.32
ANXA2	Annexin A2	0.30
RAC1	Rac family small GTPase 1	0.29
CDH1	Cadherin 1	0.28
IL18	Interleukin 18	0.23
S100A11	S100 calcium binding protein A11	0.22
CCL20	C-C motif chemokine ligand 20	0.16
CDKN1A	Cyclin dependent kinase inhibitor 1A	0.11
ANXA1	Annexin A1	0.03

[a] Genes modulated in the S100 signaling pathway as evaluated by IPA.
[b] Expression fold (FC) change for the modulated gene as evaluated by IPA.

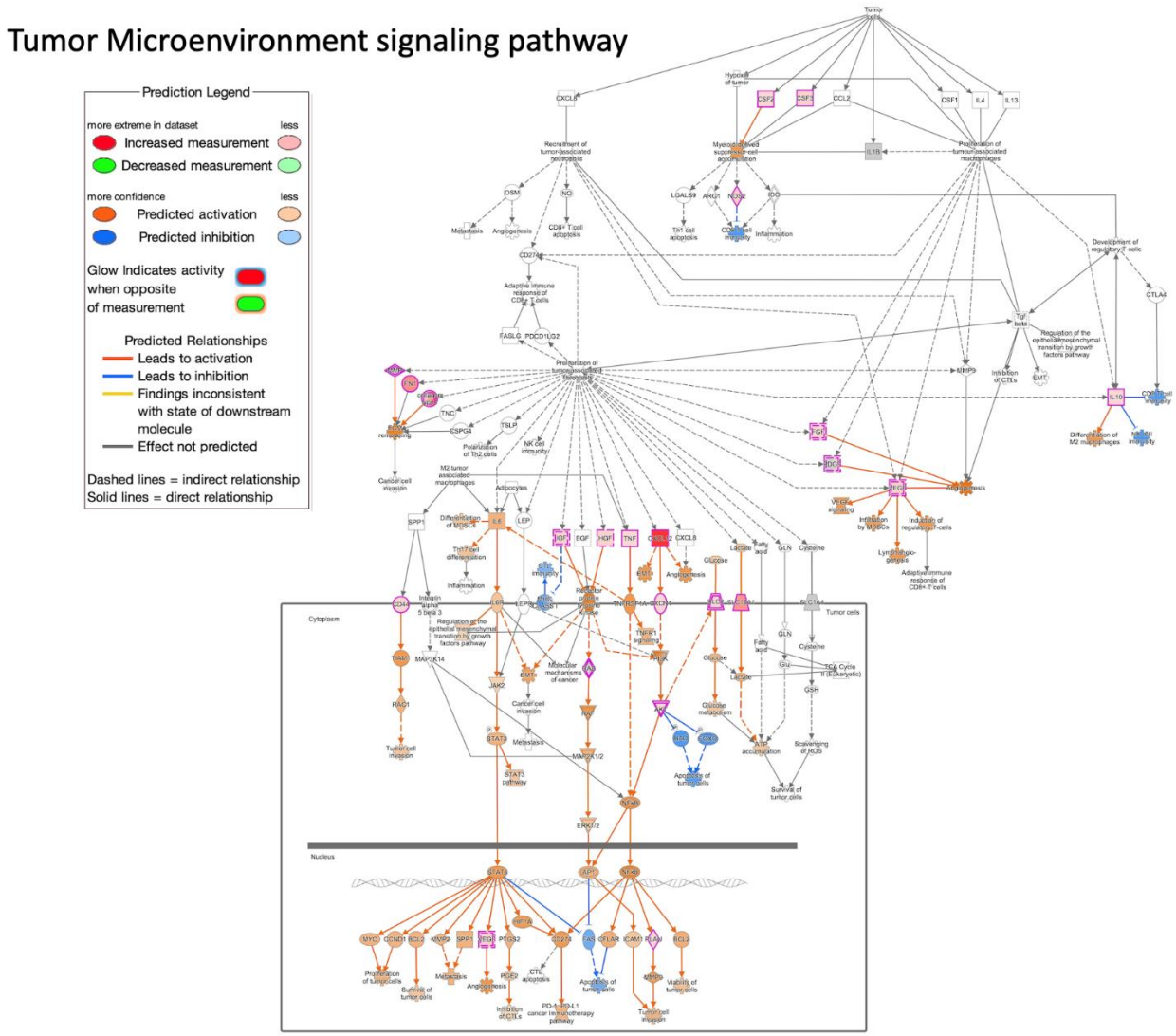

Figure 30: The tumor microenvironment signaling pathway. The pathway depicts the upregulated and dowregulated genes. The pathway operates via multiple signaling cascades. In total, 18 genes are modulated, the most active being C-X-C motif chemokine ligand 12 (CXCL12), which binds toCXCR4, impacting downstream genes in the cascade. Other upregulated genes in this pathway include colony stimulating factor 2/3, tumor necrosis factor (TNF), Hepatocyte growth factor (HGF), just to mention a few.

Table 18: Genes modulated in the tumor microenvironment signaling pathway.

Gene symbol[a]	Description	Expression FC[b]
CXCL12	C-X-C motif chemokine ligand 12	20.11
FN1	Fibronectin 1	7.00
SLC16A1	Solute carrier family 16-member 1	6.54
NOS2	Nitric oxide synthase 2	3.10
HGF	Hepatocyte growth factor	2.85
CSF3	Colony stimulating factor 3	2.75
CD44	CD44 molecule (Indian blood group)	2.65
CXCR4	C-X-C motif chemokine receptor 4	2.57
PLAU	Plasminogen activator, urokinase	2.55
IL10	Interleukin 10	2.50
CSF2	Colony stimulating factor 2	2.50
TNF	Tumor necrosis factor	2.47
HIF1A	Hypoxia inducible factor 1 subunit alpha	0.41
JAK2	Janus kinase 2	0.39
ICAM1	Intercellular adhesion molecule 1	0.39
IL1B	Interleukin 1 beta	0.34
RAC1	Rac family small GTPase 1	0.29
SLC1A4	Solute carrier family 1 member 4	0.28

[a] Genes modulated in the tumor microenvironment signaling pathway as evaluated by IPA.
[b] Expression fold (FC) change for the modulated gene as evaluated by IPA.

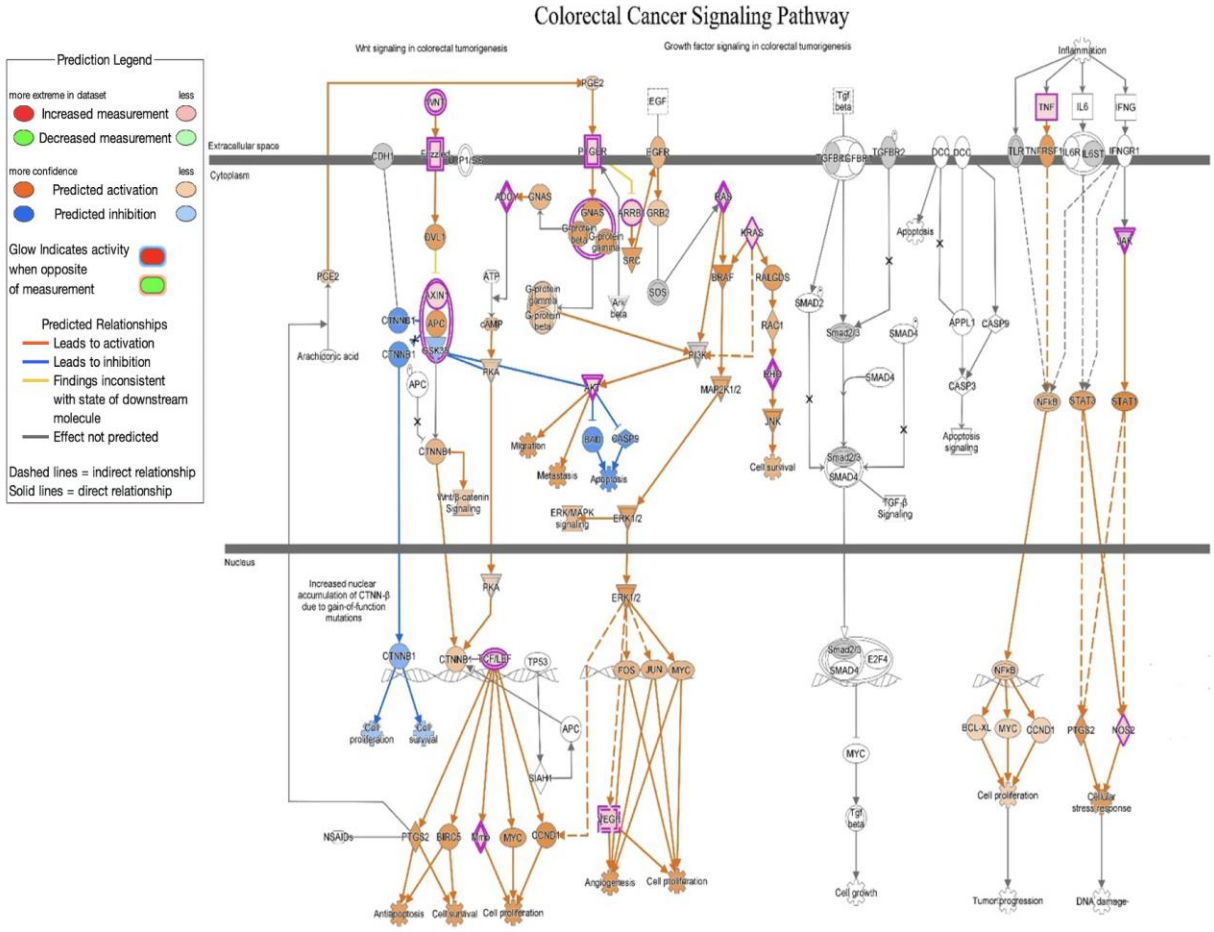

Figure 31: The colorectal cancer signaling pathway. The pathway contains 15 modulated genes. It is composed of the Wnt signaling pathway, prostaglandin E2 (PGE2), Epidermal Growth Factor (EGF), Transforming growth factor-β (TGF-β) and Tumor Necrosis Factor (TNF). The upstream stimulation of these genes sends signals to respective target genes in the cytoplasm via various signaling pathways. These genes eventually affect cellular processes associated with metastasis such as angiogenesis, cell growth and proliferation and cell survival (Figure 29-31 for details).

Table 19: Genes modulated in colorectal cancer signaling pathway.

Gene symbol[a]	Description	Expression FC[b]
NOS2	Nitric oxide synthase 2	3.10
ARRB1	Arrestin beta 1	2.88
AXIN1	Axin 1	2.73
KRAS	KRAS proto-oncogene, GTPase	2.58
TNF	Tumor necrosis factor	2.47
IL6ST	Interleukin 6 cytokine family signal transducer	0.41
GSK3B	Glycogen synthase kinase 3 beta	0.41
DVL1	Dishevelled segment polarity protein 1	0.39
STAT1	Signal transducer and activator of transcription 1	0.38
GNAS	GNAS complex locus	0.35
BCL-XL	BCL2 like 1	0.34
JUN	Jun proto-oncogene, AP-1 transcription factor subunit	0.32
RAC1	Rac family small GTPase 1	0.29
CDH1	Cadherin 1	0.28
TGFBR2	Transforming growth factor beta receptor 2	0.26

[a] Genes modulated in the Colorectal cancer signaling pathway as evaluated by IPA.
[b] Expression fold (FC) change for the modulated gene as evaluated by IPA.

4. DISCUSSION

Colorectal cancer is the second most common cause of cancer related mortality world wide, and causes a high death toll in men below 50 years (Siegel et al., 2023). Often, the liver is the prefered site of metastasis, followed by the lungs and the peritoneal cavity (He et al., 2023). Currently, surgery, chemotherapy and radiation therapy, offer a 5 year survival rate of < 20 % for a disease that has spread to distant organs (Biller and Schrag, 2021). Animal models mimicking a metastatic disease have proved essential in the discovery of new cancer therapies. The present study sought to identify genes driving the growth and progression of LS174T cells in the liver of nude rats, which then can be targeted for therapy. By using a similar approach to that rat bioassay, which had been established by Georges et al, as a colorectal cancer liver metastasis model, human LS174T colorectal cancer cells were injected into the mesenteric vein of nude rats for mimicking metastatic growth in the liver of these animals (Georges et al., 2010, Georges et al., 2011). For the purpose of reducing the number of animals used in the experiment, and more so to effectively detect and confirm the presence of tumor at various time points, LS174T cells were tranfected with luciferase as marker gene. This approach made it possible to detect tumor growth by imaging with the IVIS system, which is based on light emission following a reaction that metabolizes luciferin.

To determine the modulation pattern of genes of interest, tumor cells were re-isolated from the liver at defined time points after their implantation for expression

profiling. By comparing tumor cells growing in the rat model to original cells growing in vitro, a differential expression pattern for the genes of interest was obtained. This approach also made it possible to compare these genes with those obtained from similar experiments of related or different cell lines in previous experiments. For identifying genes of interest, two approaches were used for analysing chip array data. The first approach involved the R-program, in which a principal component analysis (PCA) was used to cluster genes at different time points. The second approach involved the IPA platform, in which filtered data sets were individually analyzed, and then compared with other related data sets for deciphering signaling pathways and functional annotations associated with the modulated genes.

Data analysis with R-program resulted in the clustering of genes expressed at days 3 and 6 of tumor growth, thus representing the early stage. Similarly, genes expressed at days 14 and 21 of tumor growth were clustered together, thus representing the late stage. The genes expressed at day 9 of tumor growth were solitary and represented the intermediate stage. This approach towards data analysis resulted in the identifaction of genes that were associated with tumor progression based on their differential pattern of expression over time. From this analysis, 124 genes ewere identified as those being downregulated in the late stage, and were therefore categorized in the ‘late down’ group. Another interesting group represented 65 genes, which were upregulated in the early stage and were grouped in the ‘early up’ category. From this correlation, it seems possible that these genes are be involved in liver colonization based on their significant expression at the early stage. The third category represented 67 genes, which showed a steadily increasing expression

pattern over the course of tumor development. For this reason, they were classified and placed in the ‘increasing over time category’. These could be the most important genes, which support tumor growth based on their increasing expression pattern. The fourth group consist of 103 genes that were crucial in mataining the advanced stage of the tumor and were classified in the ‘late up’ category (see Table *22*).

From these findings, experiments were designed to validate those genes showing increased expression over time such as Microsomal glutathione S-transferase 1 (MGST1), Ferritin light chain (FTL) or those upregulated in the late stage like the Ras-related protein Rab-15 (RAB15). MGST1 belongs to the glutathione transferase (GST) family of genes, which detoxify endogenous compounds and foreign materials, and alleviate oxidative stress (Kelner et al., 2000, Johansson et al., 2011) (Nebert and Vasiliou, 2004). Recent studies show that MGST1 was significantly expressed in lung adenocarcinoma, and its knockdown suppressed tumor growth in vivo. (Zeng et al., 2020) This report supports our findings, which implicates MGST1 in the progression of LS174T tumors in the animal model. However, more experiments will be required to validate these findings since other reports indicate that overexpression of MGST1in the tumor is associated with resistance against cytostatic drugs including cisplatin and doxorubicin (Johansson et al., 2010).

In addition to MGST1, Ferritin light chain (FTL) was another protein categorized among those that increased over time. FTL is one of the subunits (19 kDa) of ferritin, a key protein that stores iron. The other subunit is the ferritin heavy chain (FTH) with 21 kDa. Although more studies have investigated the role of iron in cancer, only a few have focused on individual subunit proteins (FTL and FTH).

Therefore, a brief discussion is given to support findings on FTL in the LS174T model. Overexpression of FTL and FTH has been shown to impact the activities of tumor associated macrophages and T-regulatory cells in many cancers.(Shi et al., 2023) Similarly, in acute myeloid leukemia, deruglation of ferritin may be associated with chemoresistance and could be targeted for therapy (Bertoli et al., 2019). These reports, though in different malignancies, substanciate the present findings that FTL may be associated with colorectal liver metastasis. Another protein selected for further investigation was the Ras-related protein Rab-15 (RAB15). Dissimilar to MGST1 and FTL, RAB15 was upregulated in the late stage and therefore grouped in the 'late up' category. RAB15 are small proteins belonging to the GTPase family, which swings between the active (GTP-bound) and inactive (GDP-bound) states. These switched-on' and 'switch-off' states are facilitated by the binding to Guanosine Exchange Factors and GTPase-activating proteins, which affect downstream genes in the signaling cascade. These proteins are involved in membrane trafficking, cell differentiation and tumor progression or suppression in many cancers (Gopal Krishnan et al., 2020).

4.1 Role of microRNA (miRNA) in LS174T progression in rat liver

As with gene expression profiling, analysis was also performed for microRNA (miRNA), which was extracted from the LS174T cells that were re-isolated at days 3, 6, 9, 14 and 21. MicroRNAs are small noncoding RNAs that bind to untranslated region of mRNAs (UTR), to modulate target genes (Zhang and Wang, 2017).

A number of miRNAs have been shown to target genes in various malignancies including colorectal cancer. In the present study, samples were analyzed to

identify miRNAs that targets genes associated with progression of the LS174T model in rat liver. Like the chip array data, different miRNA categories were identified, which followed the same expression pattern of the analyzed genes. The most interesting ones were those that increased over time such as miR-200b-3p and miR-141-3p. Other miRNAs that were assigned in the 'early down' category include miR-141-3p, miR-200c-3p or miR-17-5p. In addition, miRNA-1260a, which was down-regulated at the late stage (days 14 & 21) significantly correlated negatively with many genes showing increasing expression pattern (Early Down, Late Up or Increasing over time). Among those genes increasing overtime were MGST1, FTL and RAB15. Published reports show that miR-200-3p targets the Wnt signaling pathway by inhibing proliferation and inducing apoptosis (Chen et al., 2018). This report corroborates findings of the present work since miR200-3p was found to increase overtime and can target the Wnt/β-catenine signaling in colorectal cancer, which was activated as indicated in the results section. miR-17 has also been shown to play a role in the progression of colorectal cancer. For instance, colorectal cancer cells expressing miR-17 showed increased cell invasion and migration, an effect that was reversed by miR-17 inhibitor. In this study SIK1 was identified as a potential target of miR-17 (Huang et al., 2019). This report is in line with the findings of this study, which shows both miR-17 and SIK1 significantly expressed in the LS147T model.

Apart from miR-17, a role of miR-141-3p in colorectal cancer has been reported. As reviewed by Liang et al, although miR-141-3p is constituitivelylow in colorectal cancer cells, it inhibits invasion, migration and proliferation of these cells (Liang et al., 2019).

4.2 Signaling pathways and function annotations associated with LS174T progression

As mentioned earlier, the second approach in data analysis by IPA was intended to identify key signaling pathways and functional annotations in the LS174T model. With IPA, it was possible to compare the gene expression found for the LS174T model with that of related data sets. From this analysis, the LS174T model had the highest number of activated signaling pathways and functional annotations. The top three most activated signaling pathways include the 'S100 family', the 'tumor microenvironment' and the 'colorectal cancer' pathways. Ranked on the basis of a significant Z-score, the 'S100 family signaling pathway' contained the highest number (29 of ~60 genes) of modulated genes, 10 of which were upregulated and 19 downregulated. It was followed by the 'tumor microenviroment pathway', which contained 18 of ~90 genes genes, 12 of which were upregulated and 6 downregulated. The 'colorectal cancer pathway' came 3rd with 15 of ~95 genes genes, 5 of which were upregulated and 10 downregulated. These findings show that multiple signaling pathways were activated during tumor growth in the LS174T model and could play a role in tumor progression to the liver. Some of these genes identified in these pathways are documented with regard to metastasis formation. The S100 proteins for instance, are calcium binding proteins, which have been investigated for their role in cancer (Bresnick et al., 2015). From the S100 family pathway, S100A1 and S100 B are activated by inflamation and stress. Upon receiving inflamatory and stress signals, they activate NF-Kappa B in the nuclues via Advanced Glycosylation End-Product Specific Receptors (AGER). NF-Kappa B in turn, interacts with other elements in the pathway, thus influencing survival and migration of cancer cells. In support of these findings, reports from literature

indicate that S100A8 is involved in epithelial-mesenchymal transition and colorectal cancer metastasis through the TGF-β/USF2 pathway (Li et al., 2021). Other studies have also proved that S100 B is a possible drug target in melanoma because of its increased expression (Bresnick et al., 2015, Zimmer et al., 2013).

The tumor environment in which tumor cells interact with host cells is another central component influencing metastasis. Studies aimed at understanding the role of tumor microenvironment in colorectal cancer metastastasis and its possible exploitation for therapy have been reported (Wu et al., 2023). In line with these studies, the present study idenfied the 'tumor microenvironment signaling' pathway as one of the drivers of the LS174T model in the liver. The most interesting genes within this pathway include cytokines, colony stimulating factors, chemokines and extracellular matrix proteins. Interaction of these genes within the tumor microenvirnment is believed to modulate cellular processes associated tumor progression, which include formation of new blood vessels, cell movement, cell proliferation and cell survival. A brief discussion of a select number of these genes (CXCL12, CXCR4 and CD44) is given below.

CXCL12 (SDF-1) belongs to the CXC family of chemokines, which bind to CXCR4 (Billadeau et al., 2006). These genes are significantly expressed in tumor tissues of various malignancies, and play a crucial role in signaling pathways associated with metatastasis (Kukreja et al., 2005, Li et al., 2012). The CXCL12/CXCR4 pathway is well documented in various cell types and has been targeted by a small molecule antagonist (Biasci et al., 2020, Fearon and Janowitz, 2021). Based on analysis by IPA, both CXCL12 and CXCR4 were significantly upregulated in the 'tumor microenvironment pathway', pointing to their role in

progression of LS174T model in the liver. A recent article by Sagini et al. (2024) has shown, that a small peptide inhibitor of CXCR4, termed EPI-X4, is capable of inducing complete remissions of human Suit2-007 pancreatic cancer cells growing in the liver of nude rats (Sagini et al., 2023).The present study findings regarding increased expression levels of CXCL12 and CXCR4 in human colorectal cancer LST174T cells growing in the liver of nude rats indicate that this peptide could have a similar therapeutic potential in colorectal cancer liver metastasis.

CD44 is a transmembrane glycoprotein with different isoforms, some of which are overexpressed in cancer tissues and are associated with tumor progression (Dhir et al., 1997, Zhou et al., 2016). It interacts with hyaluronic acid (its main ligand) and other ligands including osteopontin (OPN), chondroitin, collagen, fibronectin and sulfated proteoglycan, as reviewed before (Chen et al., 2018). In colorectal cancer, metastatic spread is mediated by CD44 variant 6 (CD44v6), which is a prognostic marker and drug target for this malignancy (Todaro et al., 2014). This reports supports the present study, which shows that CD44 is one of the key molecules that is upregulated in the Tumor microenvironment pathway and is listed along with its ligand fibronectin 1 (FN1, see Table *18*), which was also significantly increased.

The 3rd most activated signaling pathway in the LS174T model was the ‘colorectal cancer pathway’. The pathway is regulated by 15 genes, which function via different pathways. One of the components of this pathway is the Wnt signaling pathway, which is divided into two branches: the canonical Wnt/β-catenine, and non canonical Wnt/β-catenine pathway. The canonical Wnt/β-catenine is frequently overstimulated due to a mutation of the adenomatous polyposis coli (APC) gene, as reviewed before (Zhong et al., 2021). As indicated in Figure *31*,

the binding of Wnt to Frizzled (FZD) inhibits the activity of the destruction complex (AXIN-APC-Catenin-GSKβ3) through Dishevelled1 (DvL1) leading to acculation of cytosolic β-catenine. Increased levels of β-catenine lead to its translocation into the nucleus and activates Wnt associated genes, trigering cell survival and proliferation. As shown in Table *19*, three genes (AXIN, DvL1 and GSKβ3) were modulated. ANXIN (up regulated), DVL1 (down regulated) and GSKβ3 (down regulated).

Besides Wnt/ β-catenine signaling pathway, others that feature prominently in the 'colorectal cancer pathway' include the 'prostaglandins E2 (PGE2) pathway', 'epidermal growth factor receptor (EGFR) pathway' and 'tumor necrosis factor (TNF) pathway'. The roles of these pathways have been documented, particulary with regard to colorectal cancer metastasis. For instance, PGE2 has been shown to promote colorectal cancer stemness in colorectal cancer liver metastasis and is considered a possible drug target (Wang et al., 2015). The EGFR is a transmembrane glycoprotein that activates various signaling pathways in various malignancies including colorectal cancer (Spano et al., 2005). This has lead to development of EGFR targeted therapies for this receptor (Piawah and Venook, 2019, Plattner and Hackl, 2019). Another signaling pathway in colorectal cancer metastasis is represented by tumor necrosis factor (TNF), a key mediator of inflammation in solid malignancies including colorectal cancer (Alotaibi et al., 2023). In the present study, TNF was upregulated and featured in the three most activated pathways, attesting the importance of this factor in colorectal cancer liver metastasis (see Table *19*).

Interlinked with the signaling pathways defined above are the functional annotations for individual genes or groups of genes. For cells to spread to distant organs, they

have to establish contact with each other or with those of the host in the tumor, which then helps to proliferate, migrate to distant sites, survive in a hostile environment and finally establish growth in the distant sites. The present study identified important function annotations attributed to the progression of LS174T model for colorectal liver metastasis. These functions include cell survival/viability, cell movement, cell migration, cell proliferation and angiogenesis. Some of these functions feature in the above discussed signaling pathways in relation to metastasis. With IPA, these functions were ranked based on their Z-score and are summarized in Table *16*.

5. SUMMARY

The study aimed to analyze the gene expression patterns of LS174T colorectal cancer cells as they proliferate within the liver of nude rats over defined time intervals. LS174T cells were initially introduced into the rat mesenteric vein, facilitating subsequent growth within the liver. To streamline the experimental process and ensure precise tumor detection at specific stages (days 3, 6, 9, 14, and 21), LS174T cells were transfected with a luciferase marker gene for bioluminescence imaging. For efficient re-isolation of tumor cells, rat liver perfusion was done, followed by fluorescent activated cell sorting (FACS) and subsequent reculturing for further analysis.

Total RNA extracted from re-isolated LS174T cells was subjected to chip array analysis, comparing re-isolated cells to those originally cultured before implantation into nude rats. Additionally, miRNA profiles were obtained from re-isolated cells at corresponding time points. Data analysis employed two approaches: analysis using the R programming language and Ingenuity Pathways Analysis (IPA). The R analysis focused on identifying gene categories associated with metastatic progression and important miRNAs related to tumor advancement. IPA was utilized to identify key signaling pathways and functional annotations associated with LS174T progression in the liver, comparing chip array data sets from a rat colorectal cancer cell line (CC531) and rat/human pancreatic cancer cells (ASML and Suit2-007).

Analysis using the R-program revealed expression patterns of 21,448 genes at different stages of LS174T growth in the liver. Gene categories associated with tumor progression were identified, including those decreasing over time, upregulated during

early stages (Early up), increasing over time, and exhibiting late-stage upregulation (Late up). Selected genes increasing over time were confirmed via qPCR and western blot, including MGST1, FTL, and RAB15. Furthermore, miRNA analysis identified different categories, with some exhibiting similar expression patterns to genes, such as miR-200b-3p and miR-141-3p. Furthermore, among the miRNAs categorized as 'early down,' notable members include miR-141-3p, miR-200c-3p, and miR-17-5p. Intriguingly, miRNA-1260a, exhibiting downregulation during the late stages (days 14 & 21), displayed a negative correlation with MGST1, FTL, and RAB15, all of which demonstrated an increase over time.

IPA analysis identified 20 signaling pathways and functional annotations based on significant Z-scores, including the S100 family pathway, tumor microenvironment pathway, and colorectal cancer pathway. Additionally, common functions relevant to metastasis, such as cell survival, migration, proliferation, and angiogenesis, were identified.

Overall, this study provides valuable insights for future research, particularly in identifying target genes for colorectal cancer therapy.

6. REFRENCES

Colorectal Cancer Stages. [Online]. Available: https://www.cancercenter.com [accessed on 16 March 2022] [Accessed].

2012. Comprehensive molecular characterization of human colon and rectal cancer. *Nature,* 487**,** 330-7.

AHMADYOUSEFI, Y., MALIH, S., MIRZAEE, Y. & SAIDIJAM, M. 2019. Nucleic acid aptamers in diagnosis of colorectal cancer. *Biochimie,* 156**,** 1-11.

AL-TAEE, K. M., BERGER, M. R. & ADWAN, H. 2016. Re-isolated metastatic pancreatic cancer cells show distinct modulation of gene expression during liver colonization. *Cancer Research,* 76**,** 1548-1548.

AL-TAEE, K. M. K. (2016). ***Identification of genes in ASML rat pancreatic cells, as assessed by the modulation of messenger- and microRNA expression, which contribute to liver colonization****.* Ruprecht-Karls-Universität.

ALOTAIBI, A. G., LI, J. V. & GOODERHAM, N. J. 2023. Tumour Necrosis Factor-Alpha (TNF-α)-Induced Metastatic Phenotype in Colorectal Cancer Epithelial Cells: Mechanistic Support for the Role of MicroRNA-21. *Cancers* [Online], 15.

AMERICAN CANCER SOCIETY. COLORECTAL CANCER FACTS & FIGURES 2017–2019; AMERICAN CANCER SOCIETY: ATLANTA, G., USA, 2017.

AMERSI, F., AGUSTIN, M. & KO, C. Y. 2005. Colorectal cancer: epidemiology, risk factors, and health services. *Clin Colon Rectal Surg,* 18**,** 133-40.

BERNSTEIN, E., DENLI, A. M. & HANNON, G. J. 2001. The rest is silence. *Rna,* 7**,** 1509-21.

BERTOLI, S., PAUBELLE, E., BERARD, E., SALAND, E., THOMAS, X., TAVITIAN, S., LARCHER, M. V., VERGEZ, F., DELABESSE, E., SARRY, A., HUGUET, F., LARRUE, C., BOSC, C., FARGE, T., SARRY, J. E., MICHALLET, M. & RECHER, C. 2019. Ferritin heavy/light chain (FTH1/FTL) expression, serum ferritin levels, and their functional as well as prognostic roles in acute myeloid leukemia. *Eur J Haematol,* 102**,** 131-142.

BHOWMICK, N. A., NEILSON, E. G. & MOSES, H. L. 2004. Stromal fibroblasts in cancer initiation and progression. *Nature,* 432**,** 332-7.

BIASCI, D., SMORAGIEWICZ, M., CONNELL, C. M., WANG, Z., GAO, Y., THAVENTHIRAN, J. E. D., BASU, B., MAGIERA, L., JOHNSON, T. I., BAX, L., GOPINATHAN, A., ISHERWOOD, C., GALLAGHER, F. A., PAWULA, M., HUDECOVA, I., GALE, D., ROSENFELD, N., BARMPOUNAKIS, P., POPA, E. C., BRAIS, R., GODFREY, E., MIR, F., RICHARDS, F. M., FEARON, D. T., JANOWITZ, T. & JODRELL, D. I. 2020. CXCR4 inhibition in human pancreatic and colorectal cancers induces an integrated immune response. *Proc Natl Acad Sci U S A,* 117**,** 28960-28970.

BILLADEAU, D. D., CHATTERJEE, S., BRAMATI, P., SREEKUMAR, R., SHAH, V., HEDIN, K. & URRUTIA, R. 2006. Characterization of the CXCR4 signaling in pancreatic cancer cells. *Int J Gastrointest Cancer,* 37**,** 110-9.

BILLER, L. H. & SCHRAG, D. 2021. Diagnosis and Treatment of Metastatic Colorectal Cancer: A Review. *JAMA,* 325**,** 669-685.

BINGHAM, S. A. 1990. Diet and large bowel cancer. *J R Soc Med,* 83**,** 420-2.

BOAKYE, D., JANSEN, L., SCHNEIDER, M., CHANG-CLAUDE, J., HOFFMEISTER, M. & BRENNER, H. 2019. Personalizing the Prediction of Colorectal Cancer Prognosis by Incorporating Comorbidities and Functional Status into Prognostic Nomograms. *Cancers (Basel),* 11.

BOLAND, C. R. & GOEL, A. 2010. Microsatellite instability in colorectal cancer. *Gastroenterology,* 138**,** 2073-2087.e3.

BONNANS, C., CHOU, J. & WERB, Z. 2014. Remodelling the extracellular matrix in development and disease. *Nat Rev Mol Cell Biol,* 15**,** 786-801.

BRAR, B., RANJAN, K., PALRIA, A., KUMAR, R., GHOSH, M., SIHAG, S. & MINAKSHI, P. 2021. Nanotechnology in Colorectal Cancer for Precision Diagnosis and Therapy. *Frontiers in Nanotechnology,* 3.

BRAY, F., FERLAY, J., SOERJOMATARAM, I., SIEGEL, R. L., TORRE, L. A. & JEMAL, A. 2018. Global cancer statistics 2018: GLOBOCAN estimates of incidence and mortality worldwide for 36 cancers in 185 countries. *CA Cancer J Clin,* 68**,** 394-424.

BRESNICK, A. R., WEBER, D. J. & ZIMMER, D. B. 2015. S100 proteins in cancer. *Nat Rev Cancer,* 15**,** 96-109.

BROCARDO, M. & HENDERSON, B. R. 2008. APC shuttling to the membrane, nucleus and beyond. *Trends Cell Biol,* 18**,** 587-96.

CHANG, T. T., THAKAR, D. & WEAVER, V. M. 2017. Force-dependent breaching of the basement membrane. *Matrix Biol,* 57-58**,** 178-189.

CHEN, C., ZHAO, S., KARNAD, A. & FREEMAN, J. W. 2018. The biology and role of CD44 in cancer progression: therapeutic implications. *Journal of Hematology & Oncology,* 11**,** 64.

CHEN, J., GUO, F., SHI, X., ZHANG, L., ZHANG, A., JIN, H. & HE, Y. 2014. BRAF V600E mutation and KRAS codon 13 mutations predict poor survival in Chinese colorectal cancer patients. *BMC Cancer,* 14**,** 802.

CHENG, Y., LING, Z. & LI, L. 2020. The Intestinal Microbiota and Colorectal Cancer. *Front Immunol,* 11**,** 615056.

CHU, C., MURDOCK, M. H., JING, D., WON, T. H., CHUNG, H., KRESSEL, A. M., TSAAVA, T., ADDORISIO, M. E., PUTZEL, G. G., ZHOU, L., BESSMAN, N. J., YANG, R., MORIYAMA, S., PARKHURST, C. N., LI, A., MEYER, H. C., TENG, F., CHAVAN, S. S., TRACEY, K. J., REGEV, A., SCHROEDER, F. C., LEE, F. S., LISTON, C. & ARTIS, D. 2019. The microbiota regulate neuronal function and fear extinction learning. *Nature,* 574**,** 543-548.

CHU, E. 2012. An update on the current and emerging targeted agents in metastatic colorectal cancer. *Clin Colorectal Cancer,* 11**,** 1-13.

DHIR, R., GAU, J.-T., KRILL, D., BASTACKY, S., BAHNSON, R. R., COOPER, D. L. & BECICH, M. J. 1997. CD44 expression in benign and neoplastic human prostates. *Molecular Diagnosis,* 2**,** 197-204.

EBLE, J. A. & NILAND, S. 2019. The extracellular matrix in tumor progression and metastasis. *Clin Exp Metastasis,* 36**,** 171-198.

FEARON, D. T. & JANOWITZ, T. 2021. AMD3100/Plerixafor overcomes immune inhibition by the CXCL12-KRT19 coating on pancreatic and colorectal cancer cells. *Br J Cancer,* 125**,** 149-151.

FERLAY, J., COLOMBET, M., SOERJOMATARAM, I., PARKIN, D. M., PIÑEROS, M., ZNAOR, A. & BRAY, F. 2021. Cancer statistics for the year 2020: An overview. *Int J Cancer*.

FERLAY J, E. M., LAM F, ET AL. GLOBAL CANCER OBSERVATORY: CANCER TODAY. LYON, FRANCE: INTERNATIONAL AGENCY FOR RESEARCH ON, CANCER. AVAILABLE FROM: HTTPS://GCO.IARC.FR/TODAY, A. & 2018., N.

FERNANDEZ, E., GALLUS, S., LA VECCHIA, C., TALAMINI, R., NEGRI, E. & FRANCESCHI, S. 2004. Family history and environmental risk factors for colon cancer. *Cancer Epidemiol Biomarkers Prev,* 13**,** 658-61.

FLEMING, M., RAVULA, S., TATISHCHEV, S. F. & WANG, H. L. 2012. Colorectal carcinoma: Pathologic aspects. *J Gastrointest Oncol,* 3**,** 153-73.

GAN, X., WANG, T., CHEN, Z. Y. & ZHANG, K. H. 2020. Blood-derived molecular signatures as biomarker panels for the early detection of colorectal cancer. *Mol Biol Rep,* 47**,** 8159-8168.

GEORGES, R. (2011). ***Investigation of genes that are related to colorectal cancer and liver metastasis.***, Ruprecht-Karls-Universität.

GEORGES, R., ADWAN, H., ZHIVKOVA, M., EYOL, E., BERGMANN, F. & BERGER, M. R. 2010. Regulation of osteopontin and related proteins in rat CC531 colorectal cancer cells. *Int J Oncol,* 37**,** 249-56.

GEORGES, R. B., ADWAN, H., HAMDI, H., HIELSCHER, T., LINNEMANN, U. & BERGER, M. R. 2011. The insulin-like growth factor binding proteins 3 and 7 are associated with colorectal cancer and liver metastasis. *Cancer Biol Ther,* 12**,** 69-79.

GIOVANNUCCI, E. 2001. An updated review of the epidemiological evidence that cigarette smoking increases risk of colorectal cancer. *Cancer Epidemiol Biomarkers Prev,* 10**,** 725-31.

GIUSSANI, M., MERLINO, G., CAPPELLETTI, V., TAGLIABUE, E. & DAIDONE, M. G. 2015. Tumor-extracellular matrix interactions: Identification of tools associated with breast cancer progression. *Semin Cancer Biol,* 35**,** 3-10.

GOPAL KRISHNAN, P. D., GOLDEN, E., WOODWARD, E. A., PAVLOS, N. J. & BLANCAFORT, P. 2020. Rab GTPases: Emerging Oncogenes and Tumor Suppressive Regulators for the Editing of Survival Pathways in Cancer. *Cancers (Basel),* 12.

GRADY, W. M. & CARETHERS, J. M. 2008. Genomic and epigenetic instability in colorectal cancer pathogenesis. *Gastroenterology,* 135**,** 1079-99.

HAMILTON SR, B. F., BOFFETTA P, ET AL. 2010. Carcinoma of the colon and rectum In: WHO Classification of Tumours of the Digestive System.

Hasbullah & Musa. (2021). Gene Therapy Targeting p53 and KRAS for Colorectal Cancer Treatment: A Myth or the Way Forward? International Journal of Molecular Sciences 22, no. 21: 11941. doi:https://doi.org/10.3390/ijms222111941

HE, K., WANG, Z., LUO, M., LI, B., DING, N., LI, L., HE, B., WANG, H., CAO, J., HUANG, C., YANG, J. & CHEN, H.-N. 2023. Metastasis organotropism in colorectal cancer: advancing toward innovative therapies. Journal of Translational Medicine, 21, 612.

HERZIG, D. O. & TSIKITIS, V. L. 2015. Molecular markers for colon diagnosis, prognosis and targeted therapy. *J Surg Oncol,* 111**,** 96-102.

HESS, K. R., VARADHACHARY, G. R., TAYLOR, S. H., WEI, W., RABER, M. N., LENZI, R. & ABBRUZZESE, J. L. 2006. Metastatic patterns in adenocarcinoma. *Cancer,* 106**,** 1624-33.

HOLLE, A. W., YOUNG, J. L., VAN VLIET, K. J., KAMM, R. D., DISCHER, D., JANMEY, P., SPATZ, J. P. & SAIF, T. 2018. Cell-Extracellular Matrix Mechanobiology: Forceful Tools and Emerging Needs for Basic and Translational Research. *Nano Lett,* 18**,** 1-8.

HOW KIT, A., NIELSEN, H. M. & TOST, J. 2012. DNA methylation based biomarkers: practical considerations and applications. *Biochimie,* 94**,** 2314-37.

HUANG, C., LIU, J., XU, L., HU, W., WANG, J., WANG, M. & YAO, X. 2019. MicroRNA-17 promotes cell proliferation and migration in human colorectal cancer by downregulating SIK1. *Cancer Manag Res,* 11**,** 3521-3534.

HUANG, H. (2019). ***The CCR5 chemokine receptor antagonist MARAVIROC exerts anti-neoplastic activity in pancreatic cancer cells, which may be a novel sterategy for treating pancreatic cancer metastatic.***, Ruprecht-Karls-Universität.

HUANG, H., ZEPP, M., GEORGES, R. B., JARAHIAN, M., KAZEMI, M., EYOL, E. & BERGER, M. R. 2020. The CCR5 antagonist maraviroc causes remission of pancreatic cancer liver metastasis in nude rats based on cell cycle inhibition and apoptosis induction. *Cancer Lett,* 474**,** 82-93.

JASPERSON, K. W., TUOHY, T. M., NEKLASON, D. W. & BURT, R. W. 2010. Hereditary and familial colon cancer. *Gastroenterology,* 138**,** 2044-58.

JOHANSSON, K., ITO, M., SCHOPHUIZEN, C. M., MATHEW THENGUMTHARAYIL, S., HEUSER, V. D., ZHANG, J., SHIMOJI, M., VAHTER, M., ANG, W. H., DYSON, P. J., SHIBATA, A., SHUTO, S., ITO, Y., ABE, H. & MORGENSTERN, R. 2011. Characterization of new potential anticancer drugs designed to overcome glutathione transferase mediated resistance. *Mol Pharm,* 8**,** 1698-708.

JOHANSSON, K., JÄRVLIDEN, J., GOGVADZE, V. & MORGENSTERN, R. 2010. Multiple roles of microsomal glutathione transferase 1 in cellular protection: A mechanistic study. *Free Radical Biology and Medicine,* 49**,** 1638-1645.

JOHN, A. M. & SCHWARTZ, R. A. 2016. Muir-Torre syndrome (MTS): An update and approach to diagnosis and management. *J Am Acad Dermatol,* 74**,** 558-66.

JOHNS, L. E. & HOULSTON, R. S. 2001. A systematic review and meta-analysis of familial colorectal cancer risk. *Am J Gastroenterol,* 96**,** 2992-3003.

KAMARUZMAN, N. I., AZIZ, N. A., POH, C. L. & CHOWDHURY, E. H. 2019. Oncogenic Signaling in Tumorigenesis and Applications of siRNA Nanotherapeutics in Breast Cancer. *Cancers (Basel),* 11.

KELNER, M. J., BAGNELL, R. D., MONTOYA, M. A., ESTES, L. A., FORSBERG, L. & MORGENSTERN, R. 2000. Structural Organization of the Microsomal Glutathione S-Transferase Gene (MGST1) on Chromosome 12p13.1–13.2: IDENTIFICATION OF THE CORRECT PROMOTER REGION AND DEMONSTRATION OF TRANSCRIPTIONAL REGULATION IN RESPONSE TO OXIDATIVE STRESS*. *Journal of Biological Chemistry,* 275**,** 13000-13006.

KIM, H. S., OH, H. N., KWAK, A. W., KIM, E., LEE, M. H., SEO, J. H., CHO, S. S., YOON, G., CHAE, J. I. & SHIM, J. H. 2021. Deoxypodophyllotoxin Inhibits Cell Growth and Induces Apoptosis by Blocking EGFR and MET in Gefitinib-Resistant Non-Small Cell Lung Cancer. *J Microbiol Biotechnol,* 31**,** 559-569.

KONDO, K. 2020. *Social determinants of health in non-communicable diseases: case studies from Japan*, Springer Nature.

KUKREJA, P., ABDEL-MAGEED, A. B., MONDAL, D., LIU, K. & AGRAWAL, K. C. 2005. Up-regulation of CXCR4 expression in PC-3 cells by stromal-derived factor-1alpha (CXCL12) increases endothelial adhesion and transendothelial migration: role of MEK/ERK signaling pathway-dependent NF-kappaB activation. *Cancer Res,* 65**,** 9891-8.

LAO, V. V. & GRADY, W. M. 2011. Epigenetics and colorectal cancer. *Nat Rev Gastroenterol Hepatol,* 8**,** 686-700.

LI, S., ZHANG, J., QIAN, S., WU, X., SUN, L., LING, T., JIN, Y., LI, W., SUN, L., LAI, M. & XU, F. 2021. S100A8 promotes epithelial-mesenchymal transition and metastasis under TGF-β/USF2 axis in colorectal cancer. *Cancer Commun (Lond),* 41**,** 154-170.

LI, X., MA, Q., XU, Q., LIU, H., LEI, J., DUAN, W., BHAT, K., WANG, F., WU, E. & WANG, Z. 2012. SDF-1/CXCR4 signaling induces pancreatic cancer cell invasion and epithelial-mesenchymal transition in vitro through non-canonical activation of Hedgehog pathway. *Cancer Lett,* 322**,** 169-76.

LIANG, Z., LI, X., LIU, S., LI, C., WANG, X. & XING, J. 2019. MiR-141-3p inhibits cell proliferation, migration and invasion by targeting TRAF5 in colorectal cancer. *Biochem Biophys Res Commun,* 514**,** 699-705.

LIN, O. S., KOZAREK, R. A. & CHA, J. M. 2014. Impact of sigmoidoscopy and colonoscopy on colorectal cancer incidence and mortality: an evidence-based review of published prospective and retrospective studies. *Intest Res,* 12**,** 268-74.

LU, P., WEAVER, V. M. & WERB, Z. 2012. The extracellular matrix: a dynamic niche in cancer progression. *J Cell Biol,* 196**,** 395-406.

LUO, Z., WANG, Q., LAU, W. B., LAU, B., XU, L., ZHAO, L., YANG, H., FENG, M., XUAN, Y., YANG, Y., LEI, L., WANG, C., YI, T., ZHAO, X., WEI, Y. & ZHOU, S. 2016. Tumor microenvironment: The culprit for ovarian cancer metastasis? *Cancer Lett,* 377**,** 174-82.

MA, Y., YANG, W., SONG, M., SMITH-WARNER, S. A., YANG, J., LI, Y., MA, W., HU, Y., OGINO, S., HU, F. B., WEN, D., CHAN, A. T., GIOVANNUCCI, E. L. & ZHANG, X. 2018. Type 2 diabetes and risk of colorectal cancer in two large U.S. prospective cohorts. *Br J Cancer,* 119**,** 1436-1442.

MALIK, R., LELKES, P. I. & CUKIERMAN, E. 2015. Biomechanical and biochemical remodeling of stromal extracellular matrix in cancer. *Trends Biotechnol,* 33**,** 230-6.

MARLEY, A. R. & NAN, H. 2016. Epidemiology of colorectal cancer. *Int J Mol Epidemiol Genet,* 7**,** 105-114.

MÁRMOL, I., SÁNCHEZ-DE-DIEGO, C., PRADILLA DIESTE, A., CERRADA, E. & RODRIGUEZ YOLDI, M. J. 2017. Colorectal Carcinoma: A General Overview and Future Perspectives in Colorectal Cancer. *Int J Mol Sci,* 18.

MIGLIORE, L., MIGHELI, F., SPISNI, R. & COPPEDÈ, F. 2011. Genetics, cytogenetics, and epigenetics of colorectal cancer. *J Biomed Biotechnol,* 2011**,** 792362.

MORIDIKIA, A., MIRZAEI, H., SAHEBKAR, A. & SALIMIAN, J. 2018. MicroRNAs: Potential candidates for diagnosis and treatment of colorectal cancer. *J Cell Physiol,* 233**,** 901-913.

Naldini, L. (2015). Gene therapy returns to centre stage. *Nature 526*, 351-360. doi:https://doi.org/10.1038/nature15818

NEBERT, D. W. & VASILIOU, V. 2004. Analysis of the glutathione S-transferase (GST) gene family. *Human Genomics,* 1**,** 460.

NIKOLOVA, D. & DRAGA, T. 2008. RNA Interference – Regulations and Application in Oncology. *Journal of Cancer Molecules,* 4.

OKAMOTO, O., FUJIWARA, S., ABE, M. & SATO, Y. 1999. Dermatopontin interacts with transforming growth factor beta and enhances its biological activity. *Biochem J,* 337 (Pt 3)**,** 537-41.

PAGET, G. 1889. Remarks on a Case of Alternate Partial Anaesthesia. *Br Med J,* 1**,** 1-3.

PANG, Y., KARTSONAKI, C., GUO, Y., CHEN, Y., YANG, L., BIAN, Z., BRAGG, F., MILLWOOD, I. Y., SHEN, L., ZHOU, S., LIU, J., CHEN, J., LI, L., HOLMES, M. V. & CHEN, Z. 2018. Diabetes,

plasma glucose and incidence of colorectal cancer in Chinese adults: a prospective study of 0.5 million people. *J Epidemiol Community Health,* 72**,** 919-925.

PASZEK, M. J., ZAHIR, N., JOHNSON, K. R., LAKINS, J. N., ROZENBERG, G. I., GEFEN, A., REINHART-KING, C. A., MARGULIES, S. S., DEMBO, M., BOETTIGER, D., HAMMER, D. A. & WEAVER, V. M. 2005. Tensional homeostasis and the malignant phenotype. *Cancer Cell,* 8**,** 241-54.

PEETERS, P. J., BAZELIER, M. T., LEUFKENS, H. G., DE VRIES, F. & DE BRUIN, M. L. 2015. The risk of colorectal cancer in patients with type 2 diabetes: associations with treatment stage and obesity. *Diabetes Care,* 38**,** 495-502.

PIAWAH, S. & VENOOK, A. P. 2019. Targeted therapy for colorectal cancer metastases: A review of current methods of molecularly targeted therapy and the use of tumor biomarkers in the treatment of metastatic colorectal cancer. *Cancer,* 125**,** 4139-4147.

PLATTNER, C. & HACKL, H. 2019. Modeling therapy resistance via the EGFR signaling pathway. *The FEBS Journal,* 286**,** 1284-1286.

RAWLA, P., SUNKARA, T. & BARSOUK, A. 2019. Epidemiology of colorectal cancer: incidence, mortality, survival, and risk factors. *Prz Gastroenterol,* 14**,** 89-103.

RENNOLL, S. & YOCHUM, G. 2015. Regulation of MYC gene expression by aberrant Wnt/β-catenin signaling in colorectal cancer. *World J Biol Chem,* 6**,** 290-300.

ROSE, D. P., BOYAR, A. P. & WYNDER, E. L. 1986. International comparisons of mortality rates for cancer of the breast, ovary, prostate, and colon, and per capita food consumption. *Cancer,* 58**,** 2363-71.

RYTHER, R. C., FLYNT, A. S., PHILLIPS, J. A., 3RD & PATTON, J. G. 2005. siRNA therapeutics: big potential from small RNAs. *Gene Ther,* 12**,** 5-11.

SAGINI, M. N., ZEPP, M., BERGMANN, F., BOZZA, M., HARBOTTLE, R. & BERGER, M. R. 2018. The expression of genes contributing to pancreatic adenocarcinoma progression is influenced by the respective environment. *Genes Cancer,* 9**,** 114-129.

SAGINI, M. N., ZEPP, M., EYOL, E., ALI, D. M., GROMOVA, S., DAHLMANN, M., BEHRENS, D., GROESCHEL, C., TISCHMEIER, L., HOFFMANN, J., BERGER, M. R. & FORSSMANN, W. G. 2023. EPI-X4, a CXCR4 antagonist inhibits tumor growth in pancreatic cancer and lymphoma models. *Peptides***,** 171111.

SAWICKI, T., RUSZKOWSKA, M., DANIELEWICZ, A., NIEDŹWIEDZKA, E., ARŁUKOWICZ, T. & PRZYBYŁOWICZ, K. E. 2021. A Review of Colorectal Cancer in Terms of Epidemiology, Risk Factors, Development, Symptoms and Diagnosis. *Cancers (Basel),* 13.

SEARS, C. L. & GARRETT, W. S. 2014. Microbes, microbiota, and colon cancer. *Cell Host Microbe,* 15**,** 317-28.

SHEN, H., MITTAL, V., FERRARI, M. & CHANG, J. 2013. Delivery of gene silencing agents for breast cancer therapy. *Breast Cancer Res,* 15**,** 205.

SHI, X., ZHANG, A., LU, J., WANG, X., YI, C. & YANG, F. 2023. An Overview of Heavy Chain Ferritin in Cancer. *Front Biosci (Landmark Ed),* 28**,** 182.

SHUSSMAN, N. & WEXNER, S. D. 2014. Colorectal polyps and polyposis syndromes. *Gastroenterol Rep (Oxf),* 2**,** 1-15.

SIEGEL, R. L., WAGLE, N. S., CERCEK, A., SMITH, R. A. & JEMAL, A. 2023. Colorectal cancer statistics, 2023. 73**,** 233-254.

SPANO, J. P., FAGARD, R., SORIA, J. C., RIXE, O., KHAYAT, D. & MILANO, G. 2005. Epidermal growth factor receptor signaling in colorectal cancer: preclinical data and therapeutic perspectives. *Annals of Oncology,* 16**,** 189-194.

STROKA, K. M. & KONSTANTOPOULOS, K. 2014. Physical biology in cancer. 4. Physical cues guide tumor cell adhesion and migration. *Am J Physiol Cell Physiol,* 306**,** C98-c109.

SUNG, H., FERLAY, J., SIEGEL, R. L., LAVERSANNE, M., SOERJOMATARAM, I., JEMAL, A. & BRAY, F. 2021. Global Cancer Statistics 2020: GLOBOCAN Estimates of Incidence and Mortality Worldwide for 36 Cancers in 185 Countries. *CA Cancer J Clin,* 71**,** 209-249.

TABUCHI, T. C. A. S. S. I. S. D. O. H. I. N.-C. D. C. S. F. & JAPAN; KONDO, K., ED.; SPRINGER: SINGAPORE, 2020; PP. 31–40.

TE BOEKHORST, V. & FRIEDL, P. 2016. Plasticity of Cancer Cell Invasion-Mechanisms and Implications for Therapy. *Adv Cancer Res,* 132**,** 209-64.

TODARO, M., GAGGIANESI, M., CATALANO, V., BENFANTE, A., IOVINO, F., BIFFONI, M., APUZZO, T., SPERDUTI, I., VOLPE, S., COCORULLO, G., GULOTTA, G., DIELI, F., DE MARIA, R. & STASSI, G. 2014. CD44v6 is a marker of constitutive and reprogrammed cancer stem cells driving colon cancer metastasis. *Cell Stem Cell,* 14**,** 342-56.

TOM, B. H., RUTZKY, L. P., JAKSTYS, M. M., OYASU, R., KAYE, C. I. & KAHAN, B. D. 1976. Human colonic adenocarcinoma cells. I. Establishment and description of a new line. *In Vitro,* 12**,** 180-91.

TOON, C. W., CHOU, A., CLARKSON, A., DESILVA, K., HOUANG, M., CHAN, J. C., SIOSON, L. L., JANKOVA, L. & GILL, A. J. 2014. Immunohistochemistry for myc predicts survival in colorectal cancer. *PLoS One,* 9**,** e87456.

TSILIMIGRAS, D. I., BRODT, P., CLAVIEN, P. A., MUSCHEL, R. J., D'ANGELICA, M. I., ENDO, I., PARKS, R. W., DOYLE, M., DE SANTIBAÑES, E. & PAWLIK, T. M. 2021. Liver metastases. *Nat Rev Dis Primers,* 7**,** 27.

URNOV, F. D., REBAR, E. J., HOLMES, M. C., ZHANG, H. S. & GREGORY, P. D. 2010. Genome editing with engineered zinc finger nucleases. *Nat Rev Genet,* 11**,** 636-46.

WAGNER, J. S., ADSON, M. A., VAN HEERDEN, J. A., ADSON, M. H. & ILSTRUP, D. M. 1984. The natural history of hepatic metastases from colorectal cancer. A comparison with resective treatment. *Ann Surg,* 199**,** 502-8.

WALKER, C., MOJARES, E. & DEL RÍO HERNÁNDEZ, A. 2018. Role of Extracellular Matrix in Development and Cancer Progression. *Int J Mol Sci,* 19.

WANG, D., FU, L., SUN, H., GUO, L. & DUBOIS, R. N. 2015. Prostaglandin E2 Promotes Colorectal Cancer Stem Cell Expansion and Metastasis in Mice. *Gastroenterology,* 149**,** 1884-1895.e4.

WANG, W., GAO, W., ZHANG, L., ZHANG, D., ZHAO, Z. & BAO, Y. 2019. Deoxypodophyllotoxin inhibits cell viability and invasion by blocking the PI3K/Akt signaling pathway in human glioblastoma cells. *Oncol Rep,* 41**,** 2453-2463.

WIRTH, T., PARKER, N. & YLA-HERTTUALA, S. 2013. History of gene therapy. *Gene,* 525**,** 162-9.

WU, X., YAN, H., QIU, M., QU, X., WANG, J., XU, S., ZHENG, Y., GE, M., YAN, L. & LIANG, L. 2023. Comprehensive characterization of tumor microenvironment in colorectal cancer via molecular analysis. *Elife,* 12.

YANG, Y., LIU, L., SUN, J., WANG, S., YANG, Z., LI, H., HUANG, N. & ZHAO, W. 2021. Deoxypodophyllotoxin Inhibits Non-Small Cell Lung Cancer Cell Growth by Reducing HIF-1alpha-Mediated Glycolysis. *Front Oncol,* 11**,** 629543.

YAO, C., NASH, G. F. & HICKISH, T. 2014. Management of colorectal cancer and diabetes. *J R Soc Med,* 107**,** 103-9.

ZENG, B., GE, C., LI, R., ZHANG, Z., FU, Q., LI, Z., LIN, Z., LIU, L., XUE, Y., XU, Y., HE, J., GUO, H., LI, C., HUANG, W., SONG, X. & HUANG, Y. 2020. Knockdown of microsomal glutathione

S-transferase 1 inhibits lung adenocarcinoma cell proliferation and induces apoptosis. *Biomedicine & Pharmacotherapy,* 121**,** 109562.

ZHANG, F. & WANG, D. 2017. The Pattern of microRNA Binding Site Distribution. *Genes (Basel),* 8.

ZHONG, Z. A., MICHALSKI, M. N., STEVENS, P. D., SALL, E. A. & WILLIAMS, B. O. 2021. Regulation of Wnt receptor activity: Implications for therapeutic development in colon cancer. *J Biol Chem,* 296**,** 100782.

ZHOU, Q., WEI, Y., WEI, X., WEI, Q. & FENG, R. 2016. CD44 over Expression Caused Drug Resistance in Activated B Cell-like Diffuse Large B-Cell Lymphoma. *Blood,* 128**,** 5316-5316.

ZIMMER, D. B., LAPIDUS, R. G. & WEBER, D. J. 2013. In vivo screening of S100B inhibitors for melanoma therapy. *Methods Mol Biol,* 963**,** 303-17.

SUPPLEMENTARY

Table 20: Full gene name in different category.

Category	Symbol	Full Gene Name	Pathways	Pathways	Pathways
Late Up	TAF1D	TATA-Box Binding Protein Associated Factor, RNA Polymerase I Subunit D	RNA processing	Involved in regulation of DNA-templated transcription	-
Late Up	RAB15	RAB15, Member RAS Oncogene Family	Involved in protein transport	Involved in Rab protein signal transduction	Involved in positive regulation of regulated secretory pathway
Late Up	MT-ND4L	Mitochondrially Encoded NADH:Ubiquinone Oxidoreductase Core Subunit 4L	Involved in mitochondrial electron transport, NADH to ubiquinone	Involved in aerobic respiration	ATP synthesis coupled electron transport
Late Down	PTEN	Phosphatase And Tensin Homolog	Involved in negative regulation of protein phosphorylation	Involved in protein dephosphorylation	lipid metabolic process
Late Down	CRLF3	Cytokine Receptor Like Factor 3	Involved in negative regulation of cell growth	Involved in positive regulation of DNA-templated transcription	Involved in positive regulation of transcription by RNA polymerase II
Early Up	DPT	Dermatopontin	Involved in cell adhesion	Involved in negative regulation of cell population proliferation	Involved in collagen fibril organization
Early Up	NTF3	Neurotrophin 3	Involved in positive regulation of receptor internalization	Involved in signal transduction	Involved in transmembrane receptor protein tyrosine kinase signaling pathway
Early Up	COL4A2	Collagen Type IV Alpha 2 Chain	Involved in angiogenesis	Involved in DNA-templated transcription	Involved in response to activity
Early Down	COX1	Mitochondrially Encoded Cytochrome C Oxidase I	Involved in response to hypoxia	oxidative phosphorylation	Involved in mitochondrial electron transport, cytochrome c to oxygen
Early Down	COX2	Mitochondrially Encoded Cytochrome C Oxidase II	Involved in response to hypoxia	Involved in mitochondrial electron transport, cytochrome c to oxygen	Involved in lactation
Decreasing over time	CA3	Carbonic Anhydrase 3	Involved in one-carbon metabolic process	Involved in response to bacterium	
Increasing over time	MGST1	Microsomal Glutathione S-Transferase 1	Involved in glutathione transport	Involved in cellular response to lipid hydroperoxide	Involved in cellular oxidant detoxification

Increasing over time	SMOC2	SPARC Related Modular Calcium Binding 2	Involved in positive regulation of endothelial cell migration	Involved in extracellular matrix organization	Involved in positive regulation of vascular wound healing
Increasing over time	FTL	Ferritin Light Chain	Involved in iron ion transport	Involved in intracellular iron ion homeostasis	Involved in intracellular sequestering of iron ion
Increasing over time	HMGB2	High Mobility Group Box 2	Involved in negative regulation of transcription by RNA polymerase II	Involved in positive regulation of endothelial cell proliferation	Immune system process

Table 21: Genes in late-up category.

No.	Gene	Fold_Day3/6_Day9	Fold_Day9_Day14/Day21
1	NPIPA7	0,593	0,402
2	TAF1D	0,511	0,33
3	CFAP97	0,644	0,424
4	TRIM59	0,545	0,48
5	ARL5B	0,602	0,493
6	BRD7	0,588	0,311
7	GAGE1	0,599	0,452
8	AKR1B10	0,769	0,248
9	AKR1C3	0,573	0,253
10	RHEB	0,672	0,458
11	KDM3A	0,672	0,499
12	MRPS9	0,932	0,495
13	NPIPA8	0,691	0,465
14	LRRCC1	0,718	0,455
15	SREK1	0,698	0,47
16	HELLS	0,553	0,439
17	AKR1C1	0,67	0,191
18	RPS14	0,649	0,487
19	MCUR1	0,548	0,435
20	CKAP2	0,62	0,418
21	NPIPA2	0,613	0,465
22	NPIPA3	0,678	0,44
23	USP34	0,961	0,455
24	BBS2	0,662	0,472

25	RAB15	0,632	0,459
26	LEO1	0,786	0,415
27	GPBP1L1	0,939	0,474
28	EIF2AK2	0,515	0,494
29	OCIAD2	0,769	0,433
30	VAMP7.1	0,683	0,423
31	NPIPB5	0,503	0,489
32	RSRC2	0,606	0,347
33	ROCK1	0,692	0,493
34	UGGT2	0,735	0,447
35	ANKRD36C	0,636	0,383
36	AKR1B15	0,746	0,296
37	USP9X	0,517	0,462
38	CPSF6	0,662	0,456
39	GCLC	0,651	0,477
40	DARS	0,586	0,487
41	AKR1C2	0,715	0,254
42	LRIG3	0,571	0,499
43	TPR	0,639	0,417
44	NPIPA5	0,757	0,465
45	TCERG1	0,559	0,457
46	PSMA2	0,506	0,451
47	SLC6A8	0,702	0,495
48	ARFGEF2	0,568	0,483
49	TENM3	1,141	0,483
50	UBE2E1	0,54	0,466
51	LMBRD1	0,545	0,493
52	LCMT1	0,586	0,496
53	FRA10AC1	0,739	0,474
54	CCAR1	0,536	0,439
55	PLK4	0,676	0,493
56	KIF20B	0,715	0,411
57	GCLM	0,957	0,499
58	ZC3H13	0,601	0,409
59	MKI67	0,534	0,422
60	ANKRD36B	0,669	0,414

61	RBBP8	0,505	0,392
62	CENPU	0,643	0,454
63	NPIPA1	0,55	0,408
64	FNBP4	0,906	0,479
65	NPIPB6	0,532	0,496
66	MANEA	0,506	0,495
67	UXT	0,661	0,44
68	COPG2	0,807	0,468
69	NDUFS1	0,623	0,371
70	DIS3	0,578	0,483
71	ETFA	0,714	0,469
72	HOOK1	0,927	0,489
73	HIST1H4A	0,755	0,436
74	RCN1	0,577	0,498
75	CHD1	0,587	0,421
76	NDUFA1	0,613	0,445
77	PTPN12	0,73	0,444
78	ZNF799	1,178	0,48
79	DNAJC3	0,728	0,494
80	GCC2	0,578	0,447
81	EZH2	0,971	0,435
82	CMAS	0,611	0,496
83	VAMP7	0,711	0,459
84	STC1	1,175	0,438
85	PRKAR1A	0,645	0,482
86	KIF15.4	0,712	0,5
87	TBX3	0,794	0,495
88	ZNF280D	0,744	0,487
89	HOXA7	0,844	0,492
90	C10orf99	0,82	0,38
91	CDKN1B	0,9	0,428
92	TJP1	0,676	0,471
93	PLOD2	0,754	0,476
94	UTRN	1,205	0,472
95	ANKRD36.1	0,661	0,458
96	TMEM165	0,701	0,492

97	RASA1	0,895	0,493
98	PAXIP1	0,612	0,482
99	HIST2H4B	0,597	0,444
100	NDUFB9	1,342	0,458
101	HIST2H4A	0,639	0,451
102	ND2	0,94	0,392
103	C1D	0,932	0,49

Table 22: Genes in Early-up category.

No.	Gene	Fold_Day3/6_Day9	Fold_Day9_Day14/Day21
1	DPT	2,144	1,725
2	HDAC6	2,052	1,233
3	HHAT	2,489	0,965
4	FFAR1	2,367	1,253
5	BBC3	2,529	1,3
6	LSP1	2,03	1,081
7	VCX	2,669	1,078
8	ORAI2	2,102	0,855
9	LZTS1	2,219	1,09
10	TKFC	2,046	1,593
11	SIX5	2,217	1,041
12	ARPIN	2,147	1,299
13	HRCT1	2,003	1,143
14	NAALADL2	2,219	1,549
15	LARP6	2,312	1,569
16	HMX2	2,331	1,058
17	VCX3A	2,792	1,306
18	KRTAP10-2	2,223	1,036
19	TYROBP	2,255	1,185
20	XRCC1	2,219	1,153
21	NTF3	2,072	1,211
22	HIST1H4D	2,003	1,317
23	LOC101928093	2,384	0,855
24	BHLHA9	2,728	1,015
25	RPS6KA1.5	2,055	0,864
26	LGALS7B	2,192	1,456
27	H2AFB1	2,092	0,866
28	SPANXA1	2,245	1,471
29	RAB2A.1	2,318	0,684
30	GTPBP3.1	2,28	0,894
31	GIMAP6	2,133	1,168
32	ZAN	2,028	0,905
33	CACFD1.3	2,006	1,272

34	OBP2B.4	2,037	1,214
35	PSME3	2,74	0,856
36	RASAL3	2,063	1,457
37	AQP8	2,116	1,074
38	COL4A2	2,331	1,367
39	GGT2	2,174	1,203
40	C7orf34	2,151	1,239
41	NR1D1	2,248	1,137
42	SCGB1D2	2,114	1,044
43	DPP9	2,059	1,401
44	TNFRSF8	2,083	1,085
45	WFDC5	2,006	0,882
46	COL7A1	2,095	1,664
47	HECA	2,04	1,078
48	AATK	2,167	1,071
49	PDE6C	2,422	0,936
50	DSCR10	2,186	0,999
51	FRAT1	2,209	0,952
52	RESP18	2,004	0,868
53	OVOL3	2,223	0,726
54	IL6R.1	2,113	1,3
55	PHLDB3	2,06	1,285
56	AMPD2	2,144	1,415
57	TGFBR3L	2,011	1,142
58	SLC38A3	2,384	0,963
59	RBP1	2,037	1,221
60	C9orf16	2,032	1,321
61	TRPV6	2,022	1,005
62	PRPH2	2,074	0,951
63	PPP3R2	2,061	0,913
64	ZNF573	2,107	0,976
65	CDKN1C	2,345	1,302

Table 23: Genes in Increasing over time category.

No.	Gene	Fold_Day3/6_Day9	Fold_Day9_Day14/Day21
1	ARHGAP11B	0,34	0,435
2	TFRC	0,302	0,387
3	CENPF	0,446	0,399
4	NETO2	0,379	0,407
5	UCHL5	0,337	0,496
6	UGT1A1	0,441	0,361
7	RPL39	0,338	0,492
8	FTL	0,321	0,322
9	HIST1H2AE	0,291	0,366
10	STAU1	0,424	0,452
11	BCLAF1	0,377	0,496
12	HNRNPD	0,445	0,485
13	CACYBP	0,27	0,426
14	RPL10A	0,422	0,481
15	RPS26.2	0,392	0,322
16	HACD2	0,345	0,462
17	NPIPB4	0,362	0,494
18	ANLN	0,47	0,431
19	PHIP	0,463	0,491
20	NIFK	0,262	0,491
21	CBX3	0,265	0,493
22	UBXN4	0,335	0,464
23	ANP32B	0,304	0,412
24	RAB13	0,413	0,452
25	NPIPB11	0,476	0,437
26	UFC1	0,483	0,491
27	VPS26A	0,412	0,469
28	MGST3	0,429	0,463
29	MYO5B	0,498	0,491
30	SMARCA5	0,438	0,416
31	BSG	0,392	0,434
32	SMC3	0,336	0,444
33	NPIPB4.1	0,225	0,488
34	HMGB2	0,297	0,496
35	MGST1	0,202	0,488
36	MYO1D	0,441	0,482
37	COPS3	0,409	0,496
38	NOA1	0,499	0,486
39	SSB	0,388	0,441
40	TOP2B	0,396	0,455
41	MRPL42	0,285	0,478
42	NPIPB3	0,327	0,488
43	ATRAID	0,407	0,478
44	PLEKHA1	0,424	0,488
45	ACOT13	0,406	0,447

46	SMOC2	0,489	0,4
47	HIST1H4C	0,225	0,439
48	ERO1A	0,474	0,368
49	IFITM1	0,287	0,482
50	ABCE1	0,494	0,487
51	GAGE12I	0,331	0,498
52	LUC7L3	0,299	0,377
53	RPS2	0,294	0,49
54	QARS	0,486	0,497
55	SLC38A2	0,329	0,476
56	HIST2H2AB	0,432	0,383
57	HIST1H2AI	0,139	0,471
58	ELOVL5	0,336	0,359
59	HNRNPDL	0,39	0,48
60	ZFAND1	0,483	0,495
61	PIK3R1	0,48	0,452
62	TMEM45B	0,452	0,486
63	GARS	0,494	0,481
64	NPIPB8	0,472	0,473
65	DDX21	0,346	0,497
66	HIST1H4E	0,256	0,462
67	HIST1H4J	0,259	0,393

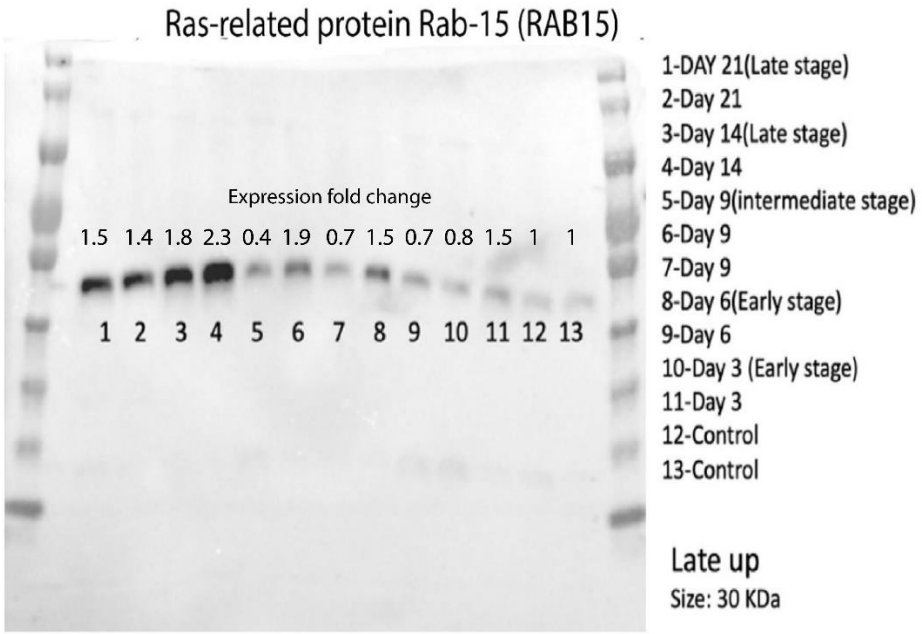

Figure 32: Western blot for RAB15 expression at protein level at different stages of LS174T tumor growth. Bands were analysed by Image J by comparing in vivo samples with control.

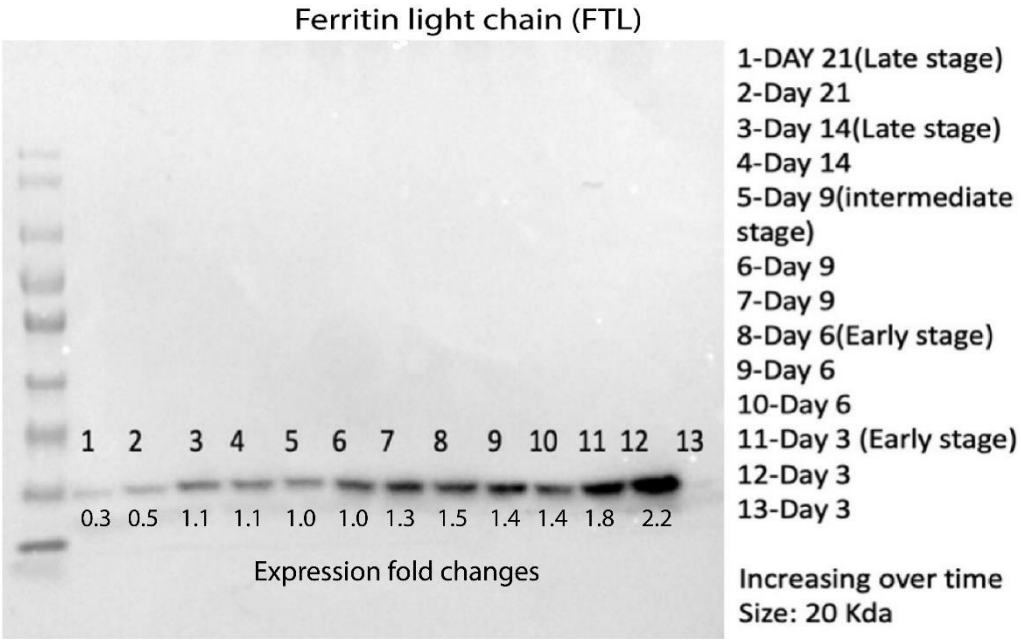

Figure 33: Western blot for FTL expression at protein level at different stages of LS174T tumor growth. Bands were analysed by Image J by comparing in vivo samples with control.

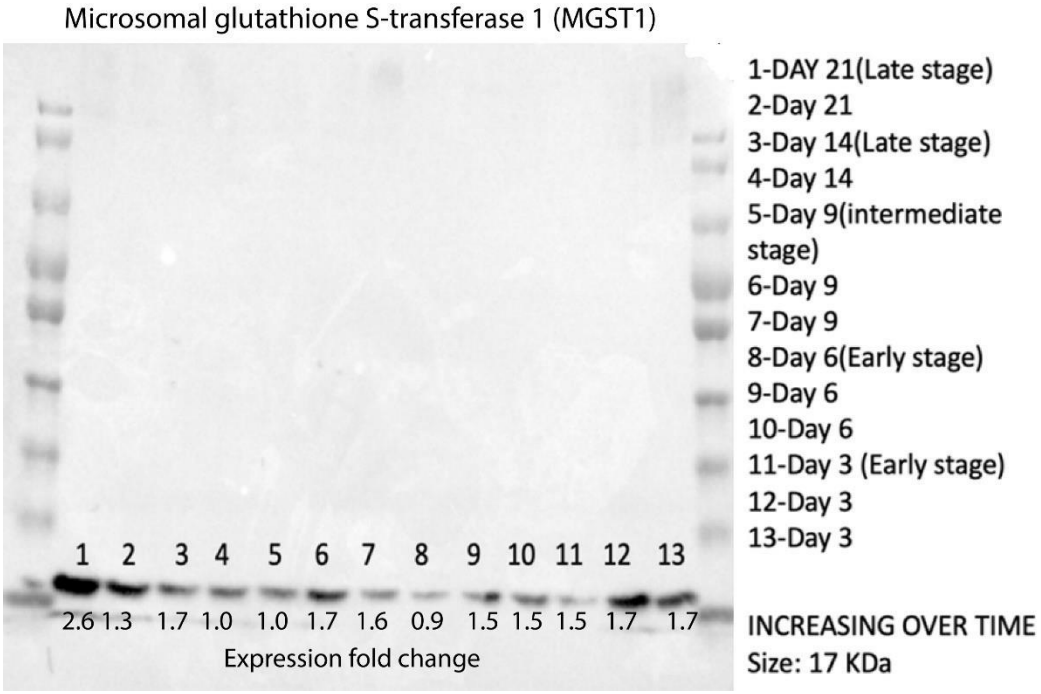

Figure 34: Western blot for MGST1 expression at protein level at different stages of LS174T tumor growth. Bands were analysed by Image J by comparing in vivo samples with control.

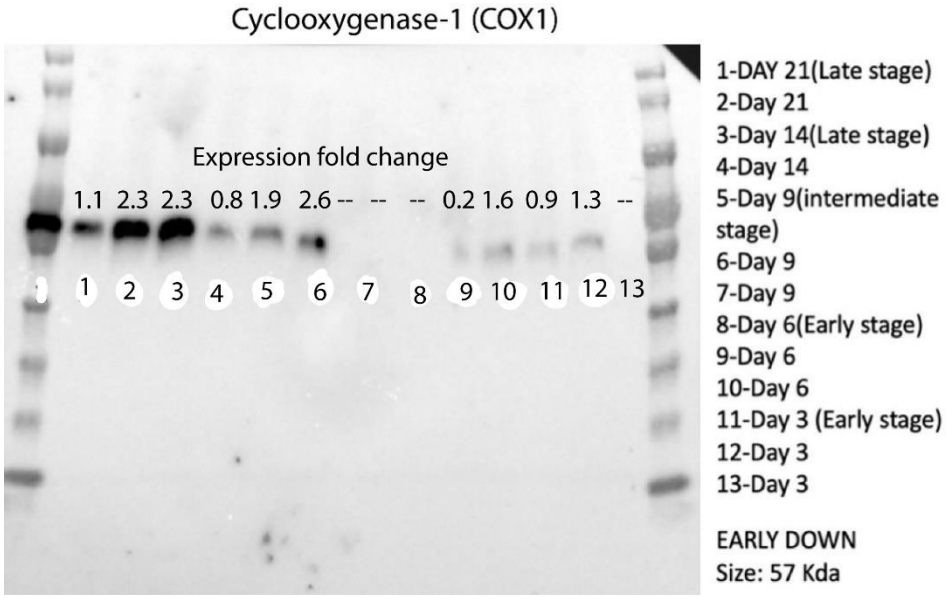

Figure 35: Western blot for COX1 expression at protein level at different stages of LS174T tumor growth. Bands were analysed by Image J by comparing in vivo samples with control.

CURRICULUM VITAE

Personal profile

Name, Surname:	Kazemi, Seyedeh Maryam
Date of Birth:	10.03.1990
Place of Birth:	Shahrekord-Iran
Citizenship:	Iranian
Marital Status:	Married since 2017
Contact information:	E-mail: Kazemimaryam9068@gmail.com
Address:	Im Neuenheimer Feld 674 69120 Heidelberg

Personal experience

2022-March 2024	Researcher in GenCC company (part-time) -Heidelberg
2016-2017	Scientific representative of biotechnology companies-Iran
2015-2017	Executive manager of the National Conference on Health Marketing-Iran

Education

2018-till now	PhD student at the German Cancer Research Center (DKFZ)-Heidelberg university Topic of PhD thesis: “Gene expression of human LS174T colorectal cancer cells implanted into the large bowel and liver of nude rats. “
2013-2017	Diploma of postgraduate studies in “cellular and molecular biology-Genetics“at Azad university, Tehran medical branch-Iran
2009-2013	Bachelor in “cellular and molecular biology-Genetics “at Isfahan University, Faculty of Science-Iran
9/2008-8/2009	Pre-university in mathematics-Isfahan, Iran
9/2005-8/2008	High school and Abitur certificate in the branch of mathematics in Isfahan, Iran

Publications

KAZEMI, S. M., ESMAIELI-BANDBONI, A., VEISI MALEKSHAHI, Z., SHAHBAZ SARDOOD, M., HASHEMI, M., MAJIDZADEH, K., KADKHODAZADEH, M., ESMAILI, R. & NEGAHDARI, B. 2022. **Vitamin D receptor gene polymorphisms and risk of breast cancer in Iranian women.** *Ann Med Surg (Lond),* 73, 103150.

GHANAVAT, M., SHAHROUZIAN, M., DERIS ZAYERI, Z., BANIHASHEMI, **S., KAZEMI, S. M.** & SAKI, N. 2021**. Digging deeper through glucose metabolism and its regulators in cancer and metastasis**. *Life Sci,* 264, 118603.

HUANG, H., ZEPP, M., GEORGES, R. B., JARAHIAN, **M., KAZEMI, M**., EYOL, E. & BERGER, M. R. 2020. **The CCR5 antagonist maraviroc causes remission of pancreatic cancer liver metastasis in nude rats based on cell cycle inhibition and apoptosis induction.** *Cancer Lett,* 474, 82-93.

EBRAHIMIFAR, M., HASANZADEGAN ROUDSARI, M., **KAZEMI, S. M.,** EBRAHIMI SHAHMABADI, H., KANAANI, L., ALAVI, S. A. & IZADI VASFI, M. 2017. **Enhancing Effects of Curcumin on Cytotoxicity of Paclitaxel, Methotrexate and Vincristine in Gastric Cancer Cells.** *Asian Pac J Cancer Prev,* 18, 65-68.

KANAANI, L., EBRAHIMI FAR, M., **KAZEMI, S. M.,** CHOUPANI, E., MAZLOUMI TABRIZI, M., EBRAHIMI SHAHMABADI, H. & AKBARZADEH KHIYAVI, A. 2017**. General Characteristics and Cytotoxic Effects of Nano-Poly (Butyl Cyanoacrylate) Containing Carboplatin on Ovarian Cancer Cells.** *Asian Pac J Cancer Prev,* 18, 87-91.

MOHAMADI, N., **KAZEMI, S. M**., MOHAMMADIAN, M., TOOFANI MILANI, A., MORADI, Y., YASEMI, M., EBRAHIMI FAR, M., MAZLOUMI TABRIZI, M., EBRAHIMI SHAHMABADI, H. & AKBARZADEH KHIYAVI, A. 2017. **Toxicity of Cisplatin-Loaded Poly Butyl Cyanoacrylate Nanoparticles in a Brain Cancer Cell Line: Anionic Polymerization Results.** *Asian Pac J Cancer Prev,* 18, 629-632.

Conferences

Poster presentation at "**IPSCC conference 2022**"-International PhD student cancer conference, June 2022

"**Second International Congress on Reproduction** "-ISERB Iranian Society of Embryology and Reproductive Biology. May 2016
"**Liver injury and hepatic regeneration; adult hepatocytes or hepatic stem cells**

Cutting Edge" Seminar, Department of Stem Cell and Developmental Biology, Royan Institute, Nov 2015.
"**Sperm Biology and reproduction**"-Royan Research Center, Isfahan. Aug 2015.

Experimental skills

In vitro part of study

DNA extraction, cDNA synthesis, mRNA and microRNA extraction, Quantitative real-time PCR, protein extraction,PCR, Cell lysate preparation, Western blot analysis, Cell culture adherent and suspension cells, Cell cycle assay, Hoechst 33342 staining, Synthesis of cDNA, Cell proliferation assay, Apopotosis assays, HPLC, Elisa and MTT assay

In vivo part of study

FELASA - B animal handling certificate, Building liver metastasis model of colorectal cancer in nude rats, flow cytometry, Organ harvesting, Tumor assessment, intra peritonea injection, tumor collection, liver collection, liver and tumor weighting.

Software

ImageJ, Graph Pad Prism 6, FlowJo, Endnote, Inkscape Illustrator, Ingenuity Pathway Analysis, LaTeX, IVIS Imaging system, MicroArray Analysis.

Other skills

Full proficiency in managing conferences and symposiums. Semi-specialized skills in Lab and Clinic management. Semi-specialized skills in Company management.

Language skills:

Persian: Mother tongue

English: very good (written and spoken)

German: good (written and spoken)

PERSONAL CONTRIBUTION

I performed all in vitro experiments including cell culture, transfection of cells, RNA extraction, DNA extraction, RT-PCR, and western blot. Chip array experiments were done by the respective Microarray Core Facility of the DKFZ.
For animal experiments, with assistance of Dr. Eyol, I performed anesthesia as well as tumor cells' implantation into liver and large bowel of nude rats, imaging, harvesting, liver perfusion, and tumor cell re-isolation.
For the statistical evaluation of chip array data I got technical assistance for the R program from Dr. Theresa Kordaß. For further analysis, I used the Ingenuity Pathway Analysis.

ACKNOWLEDGMENTS

Foremost, I extend my heartfelt gratitude to the Almighty for His abundant blessings that guided me through the successful completion of my project.

I am deeply thankful to my supervisors, **Prof. Dr. Martin R Berger**, and **Priv. -Doz. Dr Hassan Adwan**, for introducing the research topic, his unwavering patience, motivation, extensive knowledge, continuous support, and our enriching scientific discussions. His guidance has been instrumental throughout my research and thesis writing, shaping my critical thinking as a scientist and as an individual.

Special appreciation goes to my colleague and friend, Dr. Theresa Kordaß, for her insightful advice, continuous support, encouragement, and invaluable suggestions during the thesis revision.

Gratitude also to former research members of G401 unit at dkfz, including Dr. Michael Zepp, Dr. Ergul Eyol, Dr. Rania Georges, Dr. Doaa Ali, Dr. Huying Huang, and Dr. Nadine Sami Banna, just to name a few for their efforts and assistance in my animal studies. Special mention to my colleagues Nadine and Huiying for their ongoing advice and support.

I am grateful to Prof. Dr. Stefan Eichmüller, Elke, Luisa, and all my colleagues in the dkfz D210 group for their support of my PhD after retirement-related closure of the G401 unit.

Heartfelt thanks to my supportive friends Sara, Mohammadreza, Anahita, Pariroo, Najmeh Razieh, Narges, Roonak, Sina, Mario, Hashem, Naser, Ali, Armina, Eli, Alia, who have been steadfast companions from the beginning to the end of this thesis.

Special gratitude to my Instagram team members for their unwavering support and encouragement.

A warm thank you to my dear friend Neda for her constant inspiration, support, love, and invaluable wisdom.

I extend my deepest appreciation to my sister Mahshad for her unwavering support and continuous encouragement, especially during the challenging years of the pandemic.

My gratitude knows no bounds for my parents, whose relentless encouragement has shaped my personal and scientific growth. I dedicate this milestone to them, acknowledging that words fall short to express my gratitude for their selfless love and support.

Last but not least, I am profoundly grateful to my loving and supportive husband, Amin. His love and sacrifices have been my driving force, and I dedicate this milestone to him. Without him, none of this would have been possible.

Thank you.

Maryam Kazemi

EIDESSTATTLICHE ERKLÄRUNG

zum Antrag auf Zulassung zur Promotion gemäß PromO „Dr.sc.hum.“

AFFIDAVIT

1. Ich habe an keiner anderen Stelle einen Antrag auf Zulassung zur Promotion gestellt oder bereits einen Doktortitel auf der Grundlage des vorgelegten Studienabschlusses erworben und mich auch nicht einer Doktorprüfung erfolglos unterzogen (dies schließt äquivalente Verfahren bzw. Titel ausserhalb Deutschlands ein). *I have not applied anywhere else for a doctoral degree nor have I obtained a doctoral title on the basis of my presented studies or failed a doctoral examination (this includes similar procedures and titles in countries other than Germany).*

2. Die an der Medizinischen Fakultät der Universität Heidelberg zur Promotion eingereichte Arbeit mit dem Titel: *This thesis, submitted to the Medical Faculty of the University of Heidelberg is entitled:* ***Gene expression of human LS174T colorectal cancer cells implanted into the large bowel and liver of nude rats.***

in der Klinik/am Institut für ***Deutsches Krebsforschungszentrum***
in the clinic/at the institute of
unter Anleitung von (Doktorvater/ -mutter) ***. Dr. Hassan Adwan***
under the supervision of (name of official supervisor)
habe ich selbst verfasst und bei der Abfassung der Arbeit keine anderen als die in der Abhandlung aufgeführten Hilfsmittel benutzt. *I have written this thesis independently and I have not used any sources other than indicated in the thesis.*

3. Die Arbeit oder Teile davon habe ich bislang an keiner Hochschule des In- oder Auslands als Bestandteil einer Prüfungs- oder Qualifikationsleistung vorgelegt. *I have not yet presented this thesis or parts thereof to a university as part of an examination or degree.*

4. Die Dissertation wurde ohne Hinzuziehung einer kommerziellen Promotionsberatung erstellt. *This thesis was written without the assistance of any kind of commercial doctoral consulting agency.*

5. Mit der Veröffentlichung meines Lebenslaufes im Rahmen des Promotionsverfahrens (Dissertation) bin ich einverstanden. *I agree to the publication of my CV as part of my thesis.*

6. Ich komme der Veröffentlichungspflicht gemäß § 13 PromO nach und stimme der Veröffentlichung der Zusammenfassung meiner Dissertation im Internet unter Angabe meines Namens und des Studienabschlusses zu.

I will fulfill the publication requirement according to § 13 of the doctoral regulations and respectively agree to the publication of the summary of my thesis on the internet, quoting my name and the type of degree conferred.

7. Die Bedeutung der eidesstattlichen Erklärung und die strafrechtlichen Folgen einer unrichtigen oder unvollständigen eidesstattlichen Erklärung sind mir bekannt. *I am aware of the importance of a sworn affidavit and the prosecution in case of a false or incomplete affidavit.*

Ich versichere an Eides statt, dass ich nach bestem Wissen die reine Wahrheit erklärt und nichts verschwiegen habe.

I declare in lieu of oath that to the best of my knowledge, all the declarations are true and that I have not concealed anything.

Heidelberg, 18.07.2024

Ort und Datum / *place and date* Unterschrift / *signature*